

REPORT DOCUMENTATION PAGE				Form Approved OMB No. 0704-0188	
Public reporting burden for this collection of information is estimated to average 1 hour per response, including the time for reviewing instructions, searching existing data sources, gathering and maintaining the data needed, and completing and reviewing this collection of information. Send comments regarding this burden estimate or any other aspect of this collection of information, including suggestions for reducing this burden to Department of Defense, Washington Headquarters Services, Directorate for Information Operations and Reports (0704-0188), 1215 Jefferson Davis Highway, Suite 1204, Arlington, VA 22202-4302. Respondents should be aware that notwithstanding any other provision of law, no person shall be subject to any penalty for failing to comply with a collection of information if it does not display a currently valid OMB control number. <b>PLEASE DO NOT RETURN YOUR FORM TO THE ABOVE ADDRESS.</b>					
1. REPORT DATE (DD-MM-YYYY) 26-11-2008		2. REPORT TYPE Annual Report		3. DATES COVERED (From - To)	
4. TITLE AND SUBTITLE  Transition Delay in a Hypervelocity Boundary Layer using Nonequilibrium CO <sub>2</sub> Injection				5a. CONTRACT NUMBER	
				5b. GRANT NUMBER	
				5c. PROGRAM ELEMENT NUMBER	
6. AUTHOR(S) Amy Kar-Wei Beierholm, S.J. Laurence, J. Jewell (Graduate Aerospace Labs, Cal Tech); I. Leyva (AFRL/RZSA)				5d. PROJECT NUMBER	
				5e. TASK NUMBER	
				5f. WORK UNIT NUMBER 23070725	
7. PERFORMING ORGANIZATION NAME(S) AND ADDRESS(ES)  Air Force Research Laboratory (AFMC) AFRL/RZSA 10 E. Saturn Blvd. Edwards AFB CA 93524-7680				8. PERFORMING ORGANIZATION REPORT NUMBER  AFRL-RZ-ED-TP-2008-569	
9. SPONSORING / MONITORING AGENCY NAME(S) AND ADDRESS(ES)  Air Force Research Laboratory (AFMC) AFRL/RZS 5 Pollux Drive Edwards AFB CA 93524-7048				10. SPONSOR/MONITOR'S ACRONYM(S)	
				11. SPONSOR/MONITOR'S NUMBER(S) AFRL-RZ-ED-TP-2008-569	
12. DISTRIBUTION / AVAILABILITY STATEMENT  Approved for public release; distribution unlimited (PA #08469A).					
13. SUPPLEMENTARY NOTES AFOSR Annual Report					
14. ABSTRACT A new technique to delay transition to turbulence in hypervelocity air flows is introduced and investigated in this work. The main motivation for such a technique is the pressing need to reduce aerodynamic heating rates on hypersonic vehicles. Turbulent heat transfer rates can be an order of magnitude higher than laminar rates at hypersonic Mach numbers. Hence, schemes to delay transition to turbulence could provide an important means to reduce the heating rates on hypersonic vehicles. The technique presented here makes use of the recently discovered behavior of high-enthalpy nonequilibrium CO <sub>2</sub> . Seven injector geometries were built in which the injection angle, the number of orifices and the diameter of the orifices were varied. Five experimental series were conducted.					
15. SUBJECT TERMS					
16. SECURITY CLASSIFICATION OF:			17. LIMITATION OF ABSTRACT  SAR	18. NUMBER OF PAGES  133	19a. NAME OF RESPONSIBLE PERSON Dr. Ivett Leyva
a. REPORT Unclassified	b. ABSTRACT Unclassified	c. THIS PAGE Unclassified			19b. TELEPHONE NUMBER (include area code) N/A

# Transition Delay in a Hypervelocity Boundary Layer using Nonequilibrium CO<sub>2</sub> Injection

Amy Kar-Wei Beierholm<sup>1</sup>, I. Leyva<sup>2</sup>, S.J. Laurence<sup>1</sup>, J. Jewell<sup>1</sup>  
and H.G. Hornung<sup>1</sup>

<sup>1</sup>Graduate Aerospace Laboratories  
California Institute of Technology  
Pasadena, CA 91125

<sup>2</sup>Combustion Devices Group  
Air Force Research Laboratory/RZSA  
Edwards Air Force Base, CA 93524

This report was prepared for the Air Force Office of Scientific Research, USAF, under grant/contract number F49620-IHOUSE07E0000; Principal Investigator: Ivett Leyva.

October 28, 2008

GALCIT Report FM 2008.001

Distribution A: Approved for public release; distribution unlimited



# Acknowledgements

The body of this report is based on the thesis for the degree of Aeronautical Engineer of Amy Kar-Wei Beierholm. Financial support for this work was provided in part by the Air Force Office of Scientific Research, USAF, under grant/contract number F49620-IHOUSE07E0000. The authors are grateful to Dr. John Schmisser for his continued support throughout this project. The views and conclusions contained herein are those of the authors and should not be interpreted as necessarily representing the official policies or endorsements, either expressed or implied, of the Air Force Office of Scientific Research or the U.S. Government.



# Executive Summary

A new technique to delay transition to turbulence in hypervelocity air flows is introduced and investigated in this work. The main motivation for such a technique is the pressing need to reduce aerodynamic heating rates on hypersonic vehicles. Turbulent heat transfer rates can be an order of magnitude higher than laminar rates at hypersonic Mach numbers. Hence, schemes to delay transition to turbulence could provide an important means to reduce the heating rates on hypersonic vehicles.

The technique presented here makes use of the recently discovered behavior of high-enthalpy nonequilibrium  $\text{CO}_2$ . Experimental and computational data show that for the same stagnation enthalpy, the transition Reynolds number is larger for  $\text{CO}_2$  flows than for either air or  $\text{N}_2$  flows. The explanation for this phenomenon lies in the fact that when  $\text{CO}_2$  is in vibrational and chemical nonequilibrium, these relaxation processes absorb energy from the acoustic disturbances whose growth in the boundary layer is responsible for transition in hypervelocity flows (i.e., the second or Mack mode). In light of this behaviour, the injection of  $\text{CO}_2$  into the boundary layer of interest is explored as a transition-delaying technique in this work. The particular injection geometry investigated consists of a series of round orifices located at the upstream end of the test model. The test model is a 5 degree half angle cone. This geometry was chosen due to the wealth of previous information available with which the transition Reynolds number can be compared. Seven injector geometries were built in which the injection angle, the number of orifices and the diameter of the orifices were varied.

Five experimental series were conducted. Initial experiments used mixtures of  $\text{CO}_2/\text{N}_2$  as the test gas, rather than introducing  $\text{CO}_2$  directly to the boundary layer of the cone. This allowed the effect of the presence of varying amounts of  $\text{CO}_2$  on transition to be isolated from any specific injection scheme. *The obtained results demonstrated that the addition of  $\text{CO}_2$ , even as a minor component of the test mixture, significantly delays the onset of*

*transition.* For example, in the case of 60%N<sub>2</sub>/40%CO<sub>2</sub> by mole fraction, the value of the transition Reynolds number was more than double that of the case with 100% N<sub>2</sub>. A similar effect was noted in several experiments using mixtures of air and CO<sub>2</sub> as the test gas. Several runs were then performed in 100% air to determine a baseline condition for injection experiments. The requirement for this condition was for transition to occur near the mid-point of the cone, so that any adjustment to the transition location due to injection would be easily observed. Finally, tests were carried out with the purpose of visualizing the injection process to provide confirmation that the triggering of the injection system was appropriate to provide adequate CO<sub>2</sub> by the time of the arrival of the main test flow. *The timing of the CO<sub>2</sub> injection was successfully verified and it was established that the flow of CO<sub>2</sub> begins approximately 100 ms before the main flow arrives.*

As this project has progressed, a switch has been made from an old instrumented cone used by previous researchers, which was adequate to launch the project, to a new cone model having approximately four times the number of thermocouples. The thermocouples are now uniformly distributed in the circumferential and axial directions. This will allow us to pinpoint the onset of transition more accurately. Also, based on the results obtained thus far, a new injector tip has been designed and built, having approximately twice as many holes as previous ones. This will allow lower injection pressures to be used for the same mass flow rate.

# List of Figures

1.1	Relation between transition Reynolds number calculated at reference conditions and stagnation enthalpy. Open symbols indicate most fully laminar flows. Reproduced from [1] . . . . .	3
1.2	Relation between the transition Reynolds number, calculated at reference conditions, and the stagnation enthalpy, for air, $N_2$ and $CO_2$ shots in T5 (cold tunnel data is included for reference). Open symbols indicate most fully laminar flows. Reproduced from [1] . . . . .	4
1.3	Amplification rates for reacting and nonreacting disturbances in a reacting mean flow of (left) air (Shot 1162) and (right) carbon dioxide (Shot 1150). Figures reproduced from [14] . . . . .	5
1.4	Sound absorption rate per wavelength as a function of frequency for $N_2$ , air and $CO_2$ . Reproduced from [10]. . . . .	6
2.1	Schematic of the T5 hypervelocity shock tunnel. . . . .	7
2.2	The slender cone model used in the current experiments. . . . .	10
2.3	Schematic diagram showing the locations of the thermocouples on a developed view of the smooth half of the cone model. The azimuthal lines are drawn at 12.7 mm (0.5 in) intervals with the second line located at 165 mm (6.5 in). The first line shows the location of the interface between the cone tip and the injector/mid-section. All distances given are along the cone surface. . . . .	11
2.4	Schematic and photograph of the injection system. . . . .	12

# Contents

<b>Acknowledgements</b>	<b>iii</b>
<b>Executive Summary</b>	<b>v</b>
<b>Contents</b>	<b>x</b>
<b>List of Figures</b>	<b>xiii</b>
<b>List of Tables</b>	<b>xvi</b>
<b>1 Introduction</b>	<b>1</b>
1.1 Motivation . . . . .	2
1.2 Relevant Previous Work . . . . .	2
<b>2 Experimental Setup</b>	<b>7</b>
2.1 The GALCIT T5 Hypervelocity Shock Tunnel . . . . .	7
2.2 The Cone Model . . . . .	9
2.3 The Injection System . . . . .	10
2.3.1 Injector tip design . . . . .	14
2.3.2 Injection timing . . . . .	16
2.3.2.1 Operational amplifier . . . . .	18
2.3.2.2 Timing circuit . . . . .	18
2.3.2.3 Relay . . . . .	19
2.4 Diffusion calculation . . . . .	19
2.5 Injection mass flux calculations . . . . .	22
2.5.1 Required injection mass flux in the cone boundary layer . . . . .	22
2.5.2 Description of injection system components . . . . .	23

2.5.3	The Fanno flow relations . . . . .	24
2.5.4	Area changes . . . . .	25
2.5.5	Initial calculation . . . . .	25
2.5.6	Refined calculation . . . . .	27
2.6	Injection timing experiments . . . . .	29
2.6.1	Injection without main flow . . . . .	30
2.6.2	Low-enthalpy tests . . . . .	32
<b>3</b>	<b>Analysis</b>	<b>35</b>
3.1	T5 measurements . . . . .	35
3.2	Post-processing of Shock Tube Measurements . . . . .	36
3.3	Nozzle expansion . . . . .	37
3.3.1	Stagnation Conditions to Throat . . . . .	37
3.3.2	Expansion Through the Nozzle . . . . .	38
3.3.3	NENZF . . . . .	41
3.3.4	Nozzle Flow Matlab/Cantera Script . . . . .	42
3.4	Taylor-MacColl . . . . .	43
3.5	Viscosity . . . . .	43
3.6	St vs $Re^*$ . . . . .	44
3.6.1	The laminar case . . . . .	45
3.6.2	The turbulent case . . . . .	46
<b>4</b>	<b>Results and discussion</b>	<b>48</b>
4.1	Results of present experiments . . . . .	48
4.1.1	$N_2/CO_2$ mixtures . . . . .	48
4.1.2	Air and air/ $CO_2$ mixtures . . . . .	50
4.1.3	Injection experiments . . . . .	51
4.1.4	Injection visualization . . . . .	54
4.2	Future Work . . . . .	55
4.3	Conclusions . . . . .	56
<b>A</b>	<b>Run Conditions and Data Plots</b>	<b>59</b>
A.1	Series 1 Experiments - Seeded $N_2$ Flows . . . . .	59

A.2	Series 2 Experiments - Calibration in Air . . . . .	61
A.3	Series 3 Experiments - Seeded Air Flows . . . . .	63
A.4	Series 4 Experiments - High Enthalpy Injection . . . . .	65
<b>B</b>	<b>Matlab Scripts</b>	<b>67</b>
B.0.1	Xscriptnozflow.m . . . . .	67
B.0.2	nozflowfun.m . . . . .	67
B.0.3	isenfun.m . . . . .	72
B.0.4	nonideal_eq_soundspeed.m . . . . .	72
B.0.5	nonideal_soundspeed.m . . . . .	73
B.0.6	oneDflow.m . . . . .	73
B.0.7	areafun.m . . . . .	75
B.0.8	NASA2Chemkin.m . . . . .	76
B.0.9	Viscosity Files . . . . .	82
B.1	Input/Output Data Files . . . . .	83
B.1.1	Nozzle Geometry Files . . . . .	83
B.1.2	Nozzle Flow I/O Files . . . . .	85
B.1.3	Viscosity Input File . . . . .	91
<b>C</b>	<b>Reaction Mechanisms</b>	<b>95</b>
C.1	Micheltree 94 . . . . .	95
C.1.1	Mixed Gases . . . . .	95
C.1.2	Carbon Dioxide . . . . .	96
C.2	Various Sources - Carbon Dioxide . . . . .	96
<b>D</b>	<b>Thermofit data</b>	<b>99</b>
<b>E</b>	<b>Checklists</b>	<b>101</b>
E.1	High Enthalpy Shots . . . . .	101
E.2	Low Enthalpy Shots . . . . .	105
E.3	Checklist data . . . . .	109
E.3.1	Series 1 . . . . .	109
E.3.2	Series 2 . . . . .	109
E.3.3	Series 3 . . . . .	110

E.3.4	Series 4 . . . . .	111
E.3.5	Series 5 . . . . .	111

<b>References</b>		<b>113</b>
-------------------	--	------------

# Chapter 1

## Introduction

A novel method for delaying transition in hypervelocity flows of air by injecting CO<sub>2</sub> into the boundary layer of interest is investigated in this work. Experimental and numerical data show that when pure CO<sub>2</sub> is in vibrational and chemical non-equilibrium, these relaxation processes absorb energy from acoustic disturbances whose growth is responsible for transition in high enthalpy flows [9; 10; 13; 14]. This is an inviscid instability mode (second or Mack mode [16]) associated with wave-like disturbances that are trapped within the boundary layer. In contrast, the first mode, dominant in low-speed flows, is a viscous mode associated with Tollmien-Schlichting waves [21]. By absorbing energy at the same frequencies as the acoustic disturbances, nonequilibrium CO<sub>2</sub> delays transition in hypervelocity flows as compared to, in particular, N<sub>2</sub> and air.

In the present investigation, several injection pieces have been designed, built and incorporated into an injection system for an existing slender cone model. Several series of experiments have been performed in the T5 hypervelocity shock tunnel at Caltech using this cone model. Exploratory testing was carried out to determine the effect of adding an initial component of CO<sub>2</sub> to the test gas for both air and N<sub>2</sub> flows, with delayed transition observed in both cases. Further testing was performed to identify a suitable baseline condition in air for the injection experiments: the requirement for this condition was that transition occurred approximately midway along the surface of the cone. A limited number of injection tests were then performed, but questionable instrumentation readings meant that no firm conclusions could be drawn from these. Finally, visualizations of the injected flow were made with a high speed digital camera to verify that the timing of injection was appropriate for the requirements of the project, i.e, that adequate injection flow would be established by the time of arrival of the main flow in the test section during a shot.

2.5	Schematic of the injection components within the cone model: (top) the upstream end of the cone, which holds the cone tip injector; (below) the downstream end of the cone, showing the flange which holds the rigid metal tube for transporting the CO <sub>2</sub> . Note that the test configuration differed slightly from that shown. . . . .	13
2.6	Schematic and drawings of the cone tip injector piece. . . . .	17
2.7	Operational amplifier. . . . .	18
2.8	Timing circuit diagram. . . . .	19
2.9	Relay circuit diagram. . . . .	20
2.10	Run tank pressure trace from shot 2448, together with the profile obtained from the present calculation . . . . .	29
2.11	Schlieren visualizations from injection tests: (top) injection into ambient air with an initial run tank pressure of 149 psi; (bottom) injection into evacuated T5 dump tank with an initial run tank pressure of 439 psi. In each case, the time from triggering is, from left to right: 70, 183, and 300 ms. . . . .	30
2.12	Run tank pressure traces from shot 2448 and from an ambient injection test. Both the original test signal and a scaled/shifted version are plotted: the latter is scaled on the pressure axis so that the initial pressures match, and shifted on the time axis (by 182 ms) so that the initial parts of the profiles overlap. .	32
2.13	The run tank pressure trace from an ambient injection test, with voltage traces from two microsensors attached to the ball valve, showing the timing of the valve opening. $t=0$ corresponds to the trigger signal being sent to the injection system. Schlieren images from various points in the injection sequence are shown: (top left) $t=30$ ms, opening of the valve; (top right) $t=62$ ms, startup of the injection flow at the cone surface; (bottom left) $t=183$ ms, beginning of test time if main flow were present; (bottom right) $t=300$ ms, injection flow at a later time. . . . .	33
2.14	Schlieren visualisations from low enthalpy shots with various run tank pressures: (top left) 361 psi; (top right) 162 psi; (middle left) 50 psi; (middle right) 16 psi; (bottom) no injection. . . . .	34

4.1	Typical heat flux trace for a transitional flow. Shot 2332, $P_0=51.2$ MPa, $h_0=10.9$ MJ/kg, $N_2$ mole fraction=0.95, $CO_2$ mole fraction=0.05 . . . . .	49
4.2	Results from series 1 experiments: the effect of $CO_2$ mole fraction on $Re_{tr}^*$ on a freestream otherwise consisting of $N_2$ for a $5^\circ$ slender cone. . . . .	50
4.3	Heat transfer profiles with different mixtures of $CO_2$ /air as the test gas: (top left) 0% mole fraction $CO_2$ ; (top right) 20% mole fraction $CO_2$ ; (bottom) 70% mole fraction $CO_2$ . . . . .	52
4.4	The configuration for the injection experiments of Series 4: (left) photograph of injector tip #1 installed in the cone model; (right) schematic of the flow path of the injector tip. . . . .	53
4.5	Normalized heat flux vs $Re$ for Shot 2446, in which $CO_2$ was injected with injector tip #1. . . . .	53
4.6	Flow visualization of $CO_2$ injection from injector tip 1 into ambient air with an initial run tank pressure of 398 psi: (left) flow at 73 ms after trigger; (right) flow at 78 ms after trigger. . . . .	54
4.7	New cone with 80 thermocouple locations (as yet uninstalled): (left) overall view; (right) blow-up view detailing several of the thermocouple orifices. . . .	55
4.8	Schematic of the new injector tip (Injector 5) to be tested in the next set of experiments. . . . .	56
A.1	Heat flux profiles from series 1 experiments. . . . .	60
A.2	Heat flux profiles from series 2 experiments. . . . .	62
A.3	Heat flux profiles from series 3 experiments. . . . .	64
A.4	Heat flux profiles from series 4 experiments. . . . .	65



# List of Tables

2.1	Injector tip parameters. . . . .	16
2.2	Parameters used in diffusion computations, see Anderson [3], Table 16.2 . . .	21
2.3	Additional parameters used in diffusion calculations [3] . . . . .	22
2.4	Flow conditions at various points along the injection system . . . . .	27
3.1	ESTC Parameters of Interest. . . . .	36
3.2	Cont'd ESTC Parameters of Interest. . . . .	37
3.3	NENZF Parameters of Interest. . . . .	42
A.1	Series 1 run conditions. Baseline and seeded flow. . . . .	59
A.2	Series 2 run conditions. . . . .	61
A.3	Series 3 run conditions. . . . .	63
A.4	Series 4 run conditions. $CO_2$ injection in high enthalpy air flow. . . . .	65
C.1	$CO_2$ - $N_2$ Mechanism: 8 species, 12 reactions . . . . .	95
C.2	Arrhenius parameters for each reaction. . . . .	96
C.3	$CO_2$ Mechanism: 5 species, 6 reactions . . . . .	96
C.4	Arrhenius parameters for each reaction from fort.8.new. . . . .	97
D.1	NENZF thermofit data . . . . .	100
E.1	Series 1 Checklist data . . . . .	109
E.2	Series 1 Checklist data (cont'd) . . . . .	109
E.3	Series 2 Checklist data . . . . .	109
E.4	Series 2 Checklist data (cont'd) . . . . .	110
E.5	Series 3 Checklist data . . . . .	110
E.6	Series 3 Checklist data (cont'd) . . . . .	110

E.7	Series 4 Checklist data . . . . .	111
E.8	Series 4 Checklist data (cont'd) . . . . .	111
E.9	Series 5 Checklist data . . . . .	111
E.10	Series 5 Checklist data (cont'd) . . . . .	111

## 1.1 Motivation

Before engineers can reliably design devices to survive flight through or into an atmosphere at hypersonic speeds, they must somehow provide for, avoid, or otherwise accommodate the enormous heat-transfer rates to the vehicle engendered by such flight speeds.

–*William H. Dorrance, 1962.*[3]

The main justification for this work is the pressing need to reduce aerodynamic heating rates on hypersonic vehicles, including the configurations being studied for Rocket Based Combined Cycle (RBCC) propulsion. As a simple approximation, hypersonic aerodynamic heating grows as the cube of the free-stream velocity and linearly with the free-stream density [2]. Furthermore, turbulent heat transfer rates can be an order of magnitude higher than laminar rates for hypersonic Mach numbers [12]. Hence, for high velocities, heating loads become an important, if not the dominant, consideration in the design of hypersonic vehicles [2]. A reduction in heating loads means less thermal protection needed and hence less structural mass, or conversely greater payload for a given thrust. While one might not have control over the free-stream velocity for a given application, heating rates could hypothetically be reduced by keeping the boundary layer laminar over larger portions of the vehicle using schemes such as the one proposed here.

## 1.2 Relevant Previous Work

Hornung et al. [13] summarized the progress made over a decade at the T5 reflected shock tunnel at Caltech on the subject of transition and transition control. The first relevant study was performed by Germain [11], who investigated transition in hypervelocity boundary layers on a  $5^\circ$  slender cone instrumented with thermocouples. Heat flux profiles were obtained and the transition location was estimated in each case from the point at which a rapid rise in heating was observed. The model was tested in air and  $N_2$  with total flow enthalpies ranging from 5 to 15 MJ/kg. The data obtained from this study is shown in figure 1.1.

These results were extended by Adam [1] to include experiments with  $CO_2$  as the test

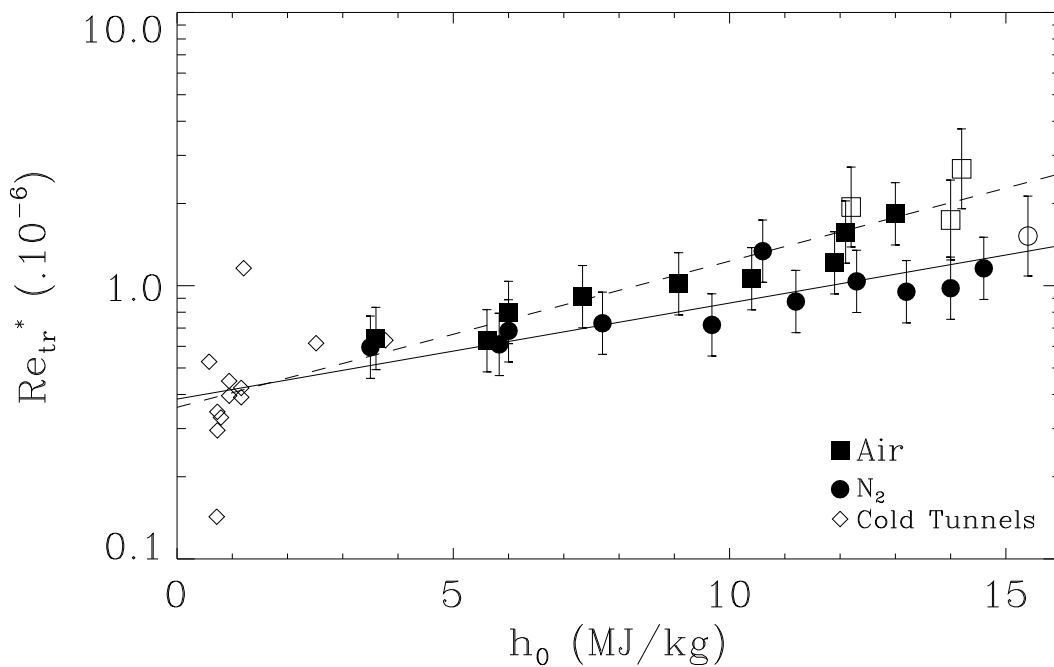


Figure 1.1: Relation between transition Reynolds number calculated at reference conditions and stagnation enthalpy. Open symbols indicate most fully laminar flows. Reproduced from [1]

gas using the same cone model. The range of flow enthalpies was 4-10 MJ/kg. Figure 1.2 compiles the transition data from all air,  $N_2$  and  $CO_2$  experiments. The open symbols correspond to cases in which the flow was laminar to the end of the cone. Figures 1.1 and 1.2 both include data from cold hypersonic facilities, obtained from DiCristina [6] and Demetriades [5]. In these figures  $Re_{tr}^*$  is the reference transition Reynolds number based on the distance from the cone tip to the transition location, measured along the surface of the cone (rather than the axial distance). The flow properties are evaluated at the Eckert's reference temperature [8]. Figure 1.2 demonstrates that the value of  $Re_{tr}^*$  for  $CO_2$  flows is typically four times larger than those for flows of either air or  $N_2$  at the same total enthalpy. This phenomenon is unique and serves as the basis for this study.

These experimental trends were confirmed by Johnson et al. [14] who used a linear stability analysis to compute  $Re_{tr}^*$  in  $CO_2$ , air, and  $N_2$  flows. These authors concluded that the low dissociation energies and large number of vibrational modes of the  $CO_2$  molecule absorb energy from the acoustic disturbances in the boundary layer and thus delay transi-

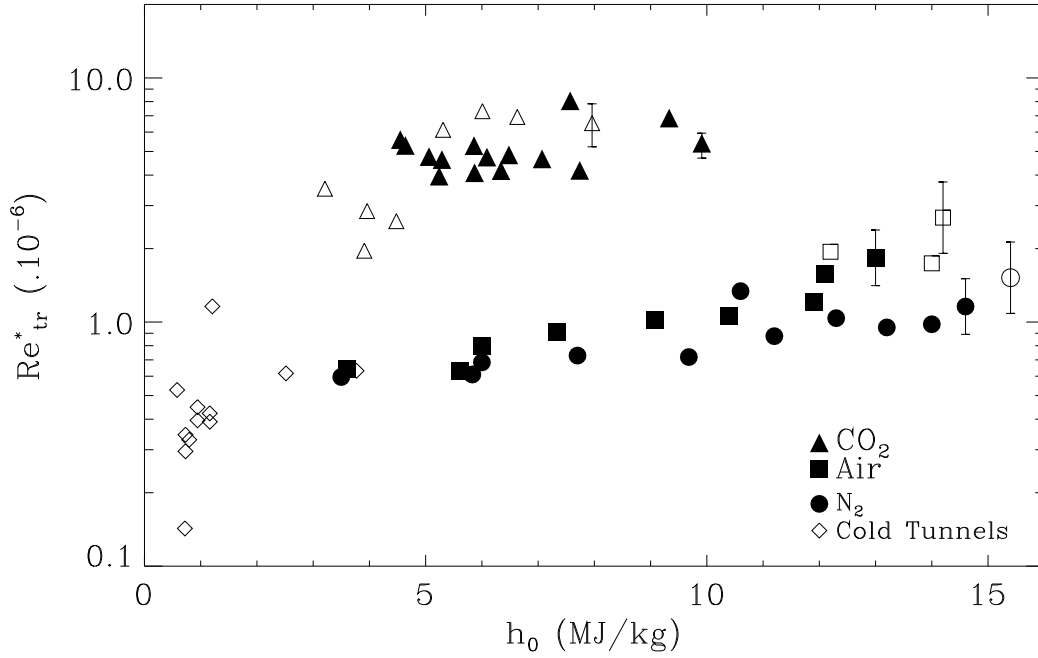


Figure 1.2: Relation between the transition Reynolds number, calculated at reference conditions, and the stagnation enthalpy, for air,  $N_2$  and  $CO_2$  shots in T5 (cold tunnel data is included for reference). Open symbols indicate most fully laminar flows. Reproduced from [1]

tion. Figure 1.3 compares the amplification rates for reacting and nonreacting disturbances in reacting mean flows of air and  $CO_2$ . The figure illustrates that in the case of  $CO_2$  flows, reacting disturbances are damped considerably in comparison to nonreacting disturbances for most frequencies, while for air the disturbances are similar whether or not they are reacting. Even though transition is a non-linear phenomenon, Johnson et al. note that the frequency of the most amplified disturbance found by linear analysis is the same as in the non-linear regime. Also, the linear amplification step is the slowest of the steps leading to transition [20]. Therefore, linear analysis can be used to give an order of magnitude estimate of the growth rate and dominant frequencies of the acoustic disturbances in the boundary layer.

Fujii et al. [9; 10] studied the effects of relaxing processes on transition in high enthalpy flows over swept cylinders (sweep angles:  $45^\circ$  and  $60^\circ$ ). In this work, the sound absorption rate per wavelength resulting from finite rate relaxation processes was computed for  $N_2$ ,  $CO_2$ , and air using an inviscid linear stability analysis. These absorption rates were then

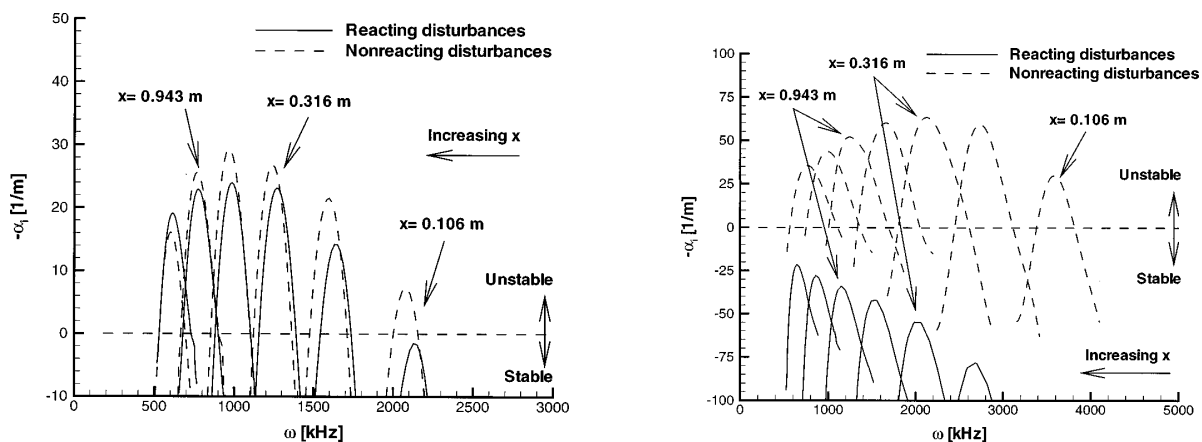
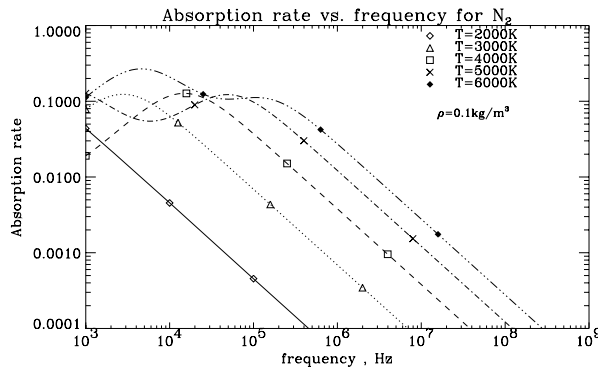
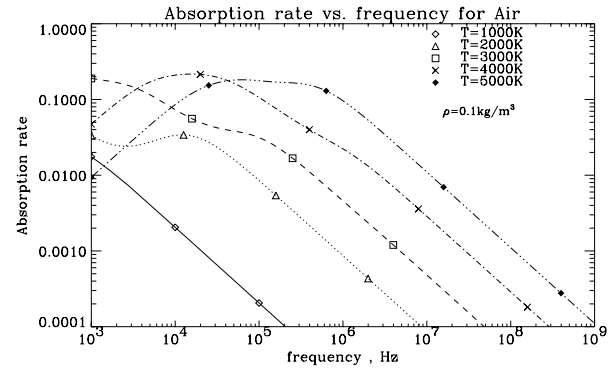


Figure 1.3: Amplification rates for reacting and nonreacting disturbances in a reacting mean flow of (left) air (Shot 1162) and (right) carbon dioxide (Shot 1150). Figures reproduced from [14]

compared with the growth rate of wave disturbances in the boundary layer. Figure 1.4 shows that for  $\text{CO}_2$ , the sound absorption rates are greater than the amplification rates for acoustic disturbances in the frequency range (1-10 MHz) where the acoustic disturbances are greatest. From this, we might expect the relaxation processes to lead to significant acoustic damping in  $\text{CO}_2$ . In comparison, for the case of air, the sound absorption rates peak much before the acoustic amplification rates become significant and nonequilibrium processes would thus not be expected to lead to transition delay. The experimental data of these authors showed good agreement with the numerical predictions.

(a)  $N_2$ 

(b) Air

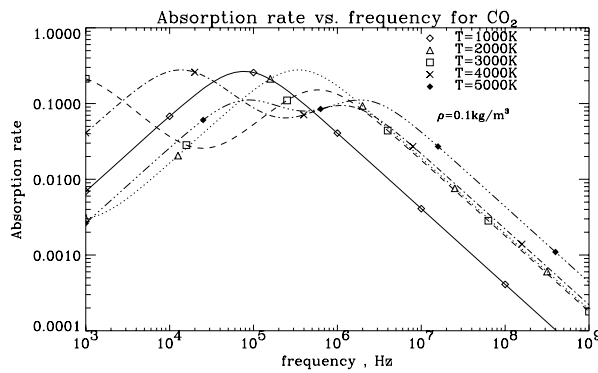
(c)  $CO_2$ 

Figure 1.4: Sound absorption rate per wavelength as a function of frequency for  $N_2$ , air and  $CO_2$ . Reproduced from [10].

## Chapter 2

# Experimental Setup

### 2.1 The GALCIT T5 Hypervelocity Shock Tunnel

The facility used in all experiments in the current study was the T5 hypervelocity shock tunnel. It is the fifth in a series of free-piston driven, reflected shock tunnels built by R.J. Stalker, H.G. Hornung and colleagues. The T5 facility consists of four major components: the secondary air reservoir (2R), the compression tube (CT), the shock tube (ST), and the test section/dump tank. The first three of these components are illustrated in figure 2.1.

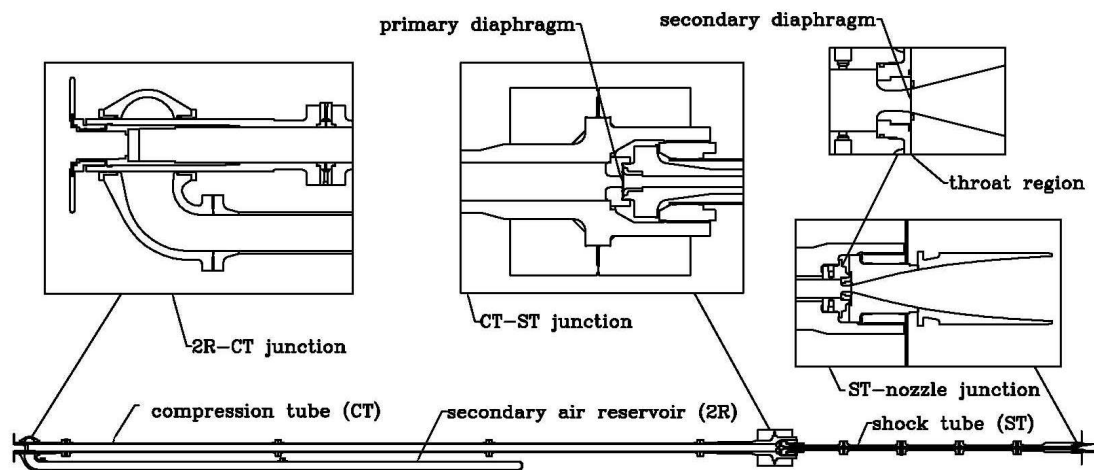


Figure 2.1: Schematic of the T5 hypervelocity shock tunnel.

Two types of experiments were performed during this study: in the majority of shots the facility was run under normal operating conditions, but a few shots were performed at low-enthalpy (LE) conditions, in which T5 was essentially run as a large Ludwieg tube. Under normal conditions, a heavy (120 kg) piston is driven down the CT by the release of

high-pressure air from the 2R. For the experiments in the present series, the initial pressure in the 2R was between 800 and 1150 psi, while the light gas mixture in the CT, typically 85% He and 15% Ar, was initially at an absolute pressure of 98 to 116 kPa. The CT gas is compressed adiabatically by the advance of the piston until the pressure at the primary diaphragm, located at the junction of the CT and ST, reaches a sufficiently high pressure that the diaphragm bursts. In the present shots, the primary diaphragm consisted of a 0.187 to 0.270-inch thick stainless steel plate etched with a X-shaped groove, between 0.042" and 0.073" deep, to control the burst pressure. Burst typically occurred at between 75 and 110 MPa. The test gas in the ST was either air or  $N_2$ , at an initial absolute pressure of between 76 and 117 kPa. The burst of the primary diaphragm produces a shock wave that travels the length of the ST and reflects from the end wall, producing stagnation conditions at the end of the ST, which serves as reservoir. The incident shock also bursts the secondary diaphragm, consisting of a 0.002" mylar membrane located at the ST-nozzle junction. The test gas then expands through the nozzle, flowing into the test section and finally into the dump tank. The test section and dump tank are initially evacuated, separated from the ST by the secondary diaphragm. Startup of the flow in the test section typically takes 1 ms from the time of arrival of the incident shock at the nozzle throat; the test time is of the order of 1-2 ms. In all experiments, a contoured nozzle of area ratio 100 was used.

Unfortunately, midway through these experimental series the facility compressor broke down, meaning that sufficiently high 2R pressures to run the facility under normal conditions were unattainable for a period of approximately six months. The decision was made to continue testing under low enthalpy conditions, with the principal aim of obtaining visualizations of flow injection. In the LE configuration, the primary diaphragm was removed, meaning the CT and ST were at the same initial pressure, typically 122 kPa. The piston was again driven by a compressed gas from the 2R, but at a much lower initial pressure than under normal conditions. For the present experiments, the 2R gas was  $N_2$ , supplied by bottles ( $N_2$  was found to be more readily available than air); three to four bottles were required to fill to the desired pressure of 170 psi. The secondary diaphragm was still used in this configuration, now serving as the main diaphragm. Two mylar membranes were used to obtain the desired burst pressure of approximately 2 MPa. Other details of the operation are the same as in the normal configuration: see Kaneshige [15] for a more complete description of the LE configuration. It should be noted that Kaneshige built a special nozzle throat

for his experiments, whereas in the present case the standard 30 mm contoured throat was used.

The T5 facility is instrumented with various diagnostic tools. Two LVDTs are used to measure the recoils of the 2R and CT. An accelerometer is attached to the CT, and was in the past used as part of the laser-timing system; in the current experiments the signal from this accelerometer was used to trigger injection. Pressure transducers are located at various points within the facility. Two are located at the primary diaphragm station, and are used to determine the burst pressure. Pressure transducers placed along the length of the ST mark the arrival times of the incident shock; these arrival times and the known distance between the pressure transducers are used to determine the shock speed, which is used to calculate the stagnation enthalpy in the reservoir. Two further pressure transducers are located just ahead of the end wall of the ST, and are used both to determine the reservoir pressure of the test gas and to trigger the T5 data acquisition system.

The T5 data acquisition system (DAS) is in two parts. The older DSP-based system is used to record facility data, as well as providing approximately 30 channels for model data. The newer NI-based system provides an additional 48 channels. Both systems record at 200 MHz.

The T5 optical setup is a typical Z-arrangement schlieren system. A high-speed digital camera allows the recording of a sequence of images during the test time; this is used in conjunction with either a continuous white light source or a spark-gap source.

## 2.2 The Cone Model

The model employed in the current experiments was the slender cone used in a number of previous experimental studies in T5, including those of Germain [11], Adam [1], and Rasheed [19]. It is a slender,  $5^\circ$  half-angle cone of approximately 1 m in length and is composed of three sections: a sharp tip made of molybdenum (to withstand the high heat fluxes), a mid-section, and the main body. A schematic of the model is shown in figure 2.2. Given the long, slender nature of this body, it was important to ensure that the flow exiting the T5 nozzle was parallel, hence the use of the contoured nozzle. Also, to ensure that the expansion wave emanating from the nozzle edge did not affect the flow upstream of any of the thermocouples located on the surface of the model, the cone was positioned so that the

cone tip intruded slightly into the nozzle.

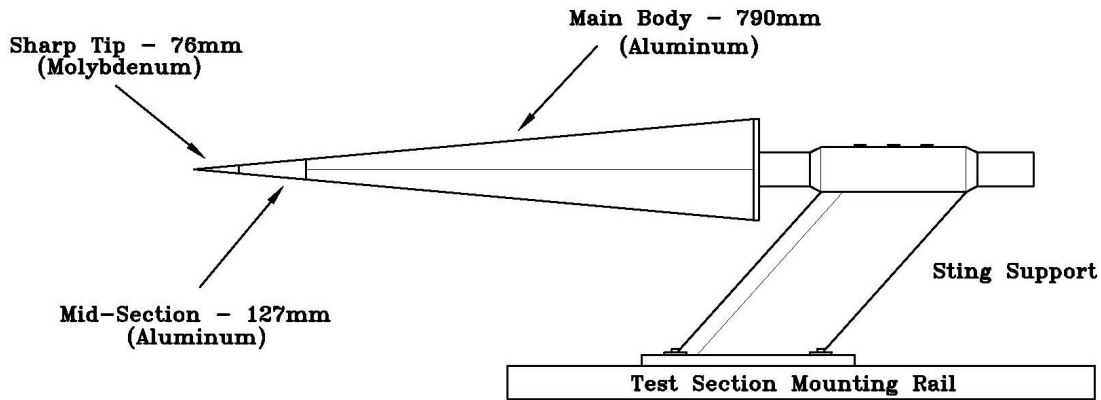


Figure 2.2: The slender cone model used in the current experiments.

For part of the present experimental series, an injection system was added to the cone model. The modifications to the cone model itself included a rigid tube running down the centerline, as well as an injector piece replacing the solid aluminum mid-section shown in figure 2.2. Further details of the injection system are given in section 2.3. Aside from these modifications, the current model configuration is that of Rasheed, who added a sleeve over the cone to divide it into smooth and porous half-conical sections, each with 27 thermocouples. A layout of the thermocouple positions on the smooth side, together with tabulated values of the axial coordinates, is shown in figure 2.3. For the present experiments, only the readings of the thermocouples on the smooth side were of interest; unfortunately, it was found that several of the thermocouples had sustained damage, and only 21 were operational.

## 2.3 The Injection System

A schematic of the injection system is shown in figure 2.4, together with a photograph of the components outside the test section. The injector is fed from a high-pressure run tank, which is filled from a CO<sub>2</sub> bottle (and then disconnected) prior to the shot. The tank is a high-pressure model of approximately 5-gallon capacity, and is monitored by both a digital pressure gauge and a Kulite pressure transducer, the latter connected to the T5 DAS to allow recording of the changing pressure during the tank discharge. The run tank leads to

Thermocouple	Angle	Distance		Thermocouple	Angle	Distance	
		in	mm			in	mm
1	90	10.05	255.3	15	70	22.05	560.1
2	80	11.05	280.7	16	60	23.05	585.5
3	100	11.55	293.4	17	40	24.05	610.9
4	90	12.55	318.8	18	50	25.05	636.3
5	80	13.55	344.2	19	90	26.05	661.7
6	70	14.55	369.6	20	100	26.55	674.4
7	60	15.55	395.0	21	110	27.55	699.8
8	90	16.05	407.7	22	120	28.55	725.2
9	100	17.05	433.1	23	130	29.55	750.6
10	110	18.05	458.5	24	140	30.55	776.0
11	120	19.05	483.9	25	90	31.55	801.4
12	130	20.05	509.3	26	80	32.05	814.1
13	90	20.55	522.0	27	70	33.05	839.5
14	80	21.05	534.7	28	60	34.05	864.9

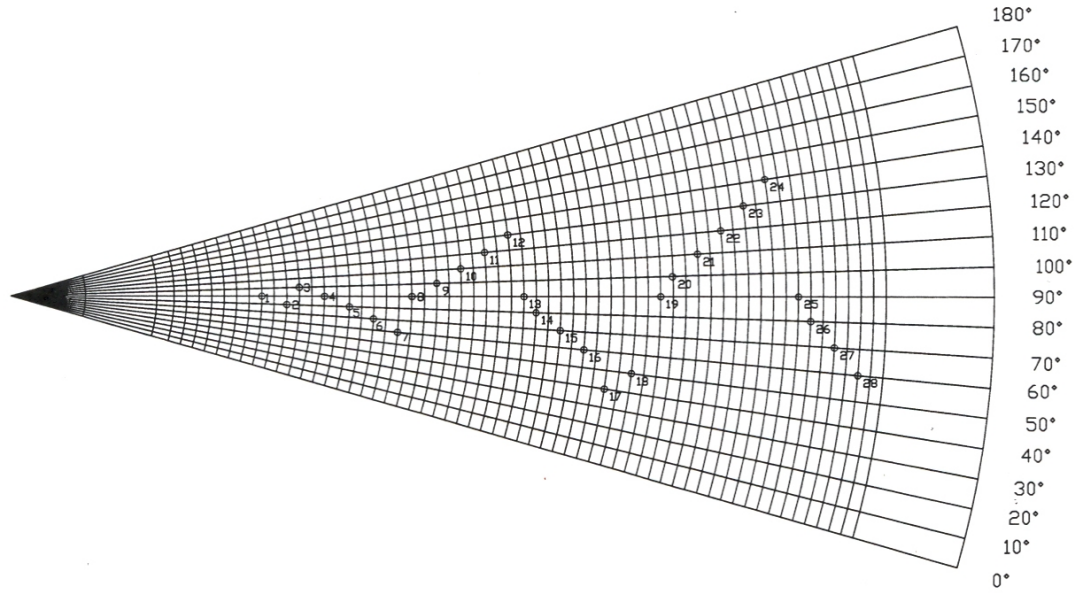


Figure 2.3: Schematic diagram showing the locations of the thermocouples on a developed view of the smooth half of the cone model. The azimuthal lines are drawn at 12.7 mm (0.5 in) intervals with the second line located at 165 mm (6.5 in). The first line shows the location of the interface between the cone tip and the injector/mid-section. All distances given are along the cone surface.

the cone model via a series of flexible metal hoses and rigid tubing, described in more detail in section 2.5. An actuated ball valve, controlled in turn by a solenoid valve, lies along the flow path and controls the timing of the injection initiation. In experiments, the system was triggered from a signal generated by an accelerometer attached to the CT, allowing sufficient time for the injection flow to be established before the arrival of the main flow in the test section.

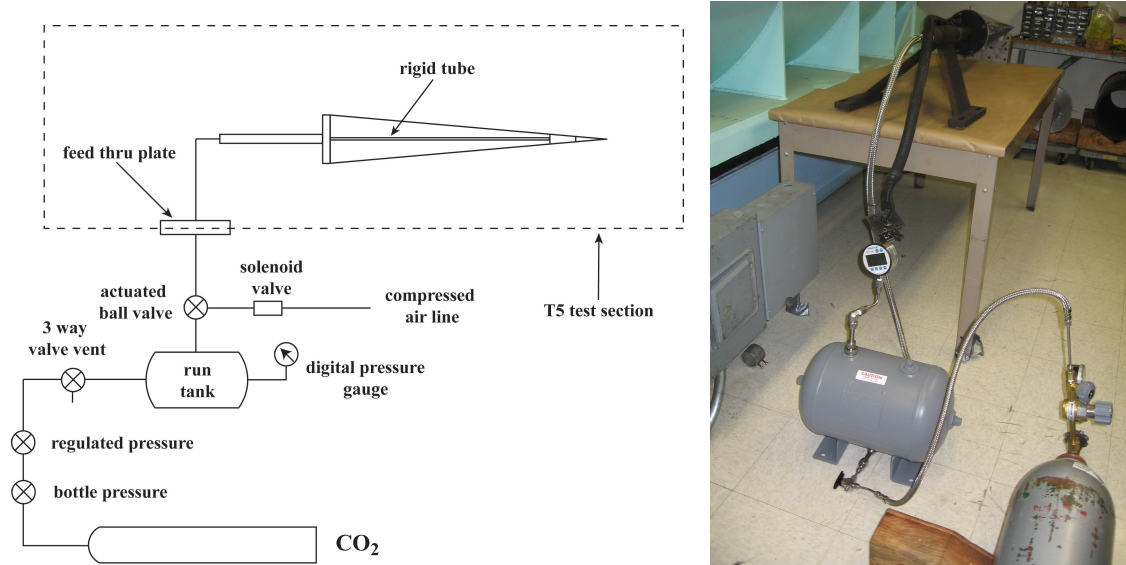
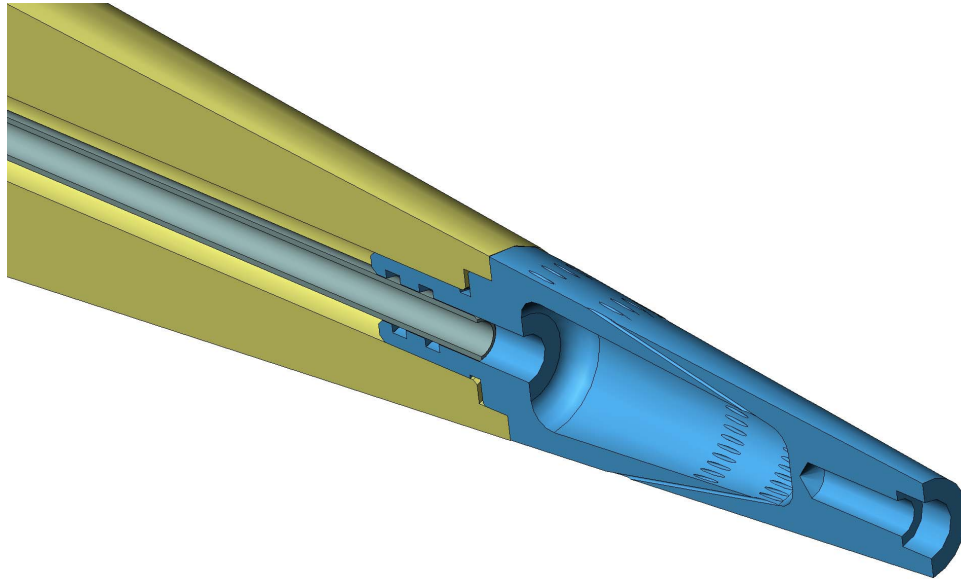


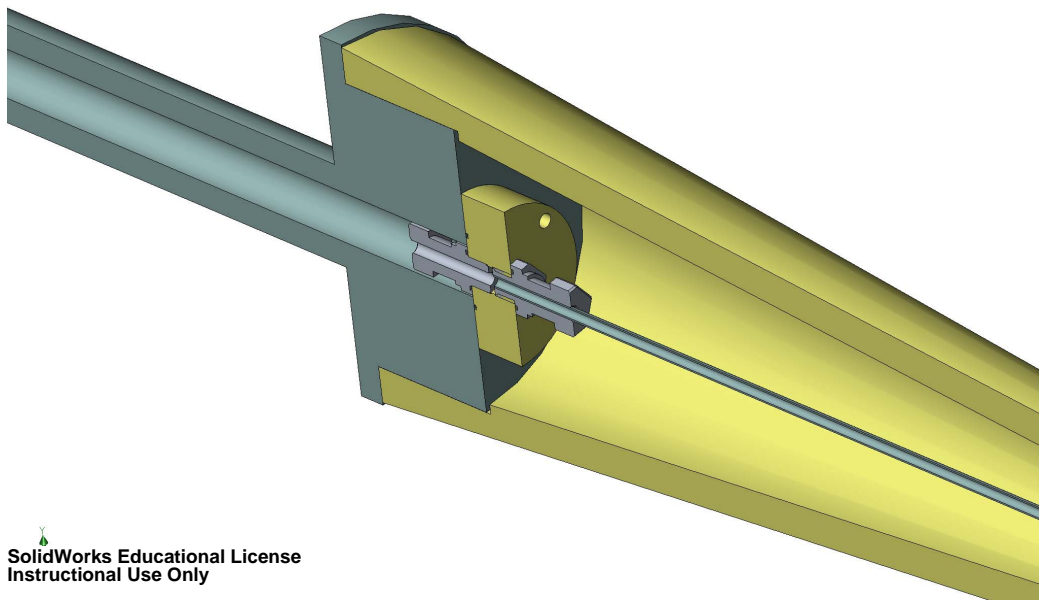
Figure 2.4: Schematic and photograph of the injection system.

Drawings of the final part of the flow path within the cone model can be found in figure 2.5. This was an earlier design, however, and the configuration was modified partway through testing, so this should only be used as a rough guide.<sup>1</sup> All injector tips were designed such that the flow would choke at the injector holes. However, due to an error in manufacturing, the holes in the tip used in all experiments described here (tip #1) were of larger diameter than designed. The minimum area thus occurred at the 1/4-inch tubing leading to the plenum from which the injector holes were fed (see figure 2.5). It is thus assumed in mass flow calculations that the sonic point was located at the end of this tubing, immediately before the plenum. The injector tip, containing the plenum and injection holes, is described in the following section.

<sup>1</sup>All Solidworks drawings shown in this chapter were produced by Bahram Valiferdowsi.



 SolidWorks Educational License  
Instructional Use Only



 SolidWorks Educational License  
Instructional Use Only

Figure 2.5: Schematic of the injection components within the cone model: (top) the upstream end of the cone, which holds the cone tip injector; (below) the downstream end of the cone, showing the flange which holds the rigid metal tube for transporting the  $\text{CO}_2$ . Note that the test configuration differed slightly from that shown.

### 2.3.1 Injector tip design

The injector tip took the place of the cone mid-section piece shown in figure 2.2, and, as such, the design of this piece was limited by the constraints that this external geometry placed upon it. Even within these constraints, however, there were many factors that needed to be considered within the design. A review of the literature revealed that relevant work has focused principally on injecting gases onto turbine blades for cooling or film cooling, and no reference could be found to injecting gases into hypervelocity boundary layers. Design inspiration was thus taken from previous work in film cooling [4].

Thin-film cooling is employed in gas turbines because, by cooling the blades, it is possible to run the turbine at higher temperature and, therefore, higher efficiency. In thin film cooling, the object is to inject a thin, uniform layer of gas that covers as much of the blade as possible for uniform cooling. While the current application also requires a thin layer of gas, the needs are somewhat different. Instead of a complete blanket of  $\text{CO}_2$  adhering to the cone surface, the requirement is for the gas to mix thoroughly into the test gas boundary layer as quickly as possible in order that the temperature of the injected  $\text{CO}_2$  (initially at room temperature,  $\approx 300\text{ K}$ ) is raised to a value close to that of the test gas in the boundary layer ( $\approx 2000\text{ K}$ ), thereby exciting the vibrational modes and causing dissociation. Only under these circumstances can the injected gas be expected to have a transition-suppressing effect.

The first design decision was whether to employ holes or slots. Early efforts in thin-film blade cooling concentrated on slots, as these produced 2-D sheet-like jets which were well suited to the requirements of this application. In the current application, however, the use of holes seemed to hold several key advantages, both in the ease of manufacturing and in that the injected gas in this case would be mixed more rapidly into the existing boundary layer.

Having decided upon holes, the relevant design parameters were the size and arrangement of holes on the injector surface, and the hole shaping and exit angle. The aim was to produce a minimal disturbance to the boundary layer while injecting a sufficient mass flow of  $\text{CO}_2$ , with adequate coverage, for the transition-delaying effects to become apparent. The standard in thin-film cooling of turbine blades is to design the holes with as shallow an exit angle as possible and with a spacing of at least two hole diameters between adjacent

holes [4]. The present design follows this convention. The geometry of the injector tip dictated that the minimum exit angle for a straight hole tunnel was  $11^\circ$  for one row of holes or  $12^\circ$  for two. The circumferential spacing was at least 2 hole diameters in all cases; for configurations with two rows of holes, the axial spacing between rows was 2.5 to 5 hole diameters, and the rows were staggered with respect to one another.

A further consideration was the ratio of the length of the hole-tunnel to the hole diameter,  $L/D$ . By minimizing this value, total pressure losses due to friction would be kept to a minimum. In the literature, the value of  $L/D$  typically ranges from 1 to 10 [4]. To minimize the injection angle while ensuring adequate strength of the injector tip, a somewhat larger value was necessary in the current configuration. The tunnel length was typically 25 mm while the hole diameter was 0.5 mm, resulting in a  $L/D$  ratio of approximately 50.

Recently, a major advance in thin-film cooling has been the incorporation of shaping into the exit hole to improve blade surface coverage [4]. Such shaping has not been adopted in the current configuration, but could possibly be used in the future to improve the tangency of the flow (axial shaping is envisaged, rather than the lateral fanning that is typically employed to improve injection coverage).

The position of injection was also a compromise. Injection near the cone tip would provide increased time for the injected gas to mix with the test gas and reach nonequilibrium conditions. Injecting further downstream, where the boundary layer is thicker, would decrease the likelihood of the injected flow blowing off the boundary layer. In the end, the former of these considerations, together with the geometry constraints provided by the existing model, led to the selection of an injection position near the cone tip.

The injector tip was designed such that the injected flow would choke at the exit holes, in order that the injection conditions could be easily calculated. The injection flow rate would be controlled through adjusting the initial pressure in the  $\text{CO}_2$  run tank. Approximate calculations of the required and supplied mass flow rates in the present configuration are provided in section 2.5.

Because of the uncertainty in both the optimal design for the injector tip and the optimal manufacturing method, a number of tips were constructed, with the intention that several of these would be tested to determine the best compromise. The important parameters of these tips are listed in table 2.1.

The original mid-section was made from aluminum. The first version of the cone tip

Table 2.1: Injector tip parameters.

Injector tip no.	manufac- tured by:	avg hole size [ <i>inch</i> ]	number of rows	angle [ <i>deg</i> ]	image nos.	comments
1	Solid Conc	0.0258	2	12		insert
1b	Scicon	blocked	1	12		solid metal
2	Scicon	0.0163	1	12		nickel plated; insert
3	Solid Conc	0.0310	2	12		
4	Solid Conc	blocked	2	12		
5	Scicon	0.0350	1	12		nickel plated
6	Scicon	0.0271	1	11		nickel plated
7	Scicon	0.0171	2	12		
8	Solid Conc	0.0301	1	11		white

injector was made by rapid prototyping a high impact plastic. The second version was also made by rapid prototyping, but a metal powder was used. The second tip was discarded since the holes could not be resolved and the surface was extremely rough. The added cost of drilling holes at an angle and machining the surface to give it a smooth finish made it economically unviable. The third version was made again by rapid prototyping a high impact plastic, but it was then nickel plated to protect it from the high heat flux. The metal coating was on the order of  $10\text{ }\mu\text{m}$ , but since the maximum temperature rise experienced by the thermocouples is  $30\text{ K}$  for a test time of  $4\text{ ms}$ , it was calculated that the penetration depth would be sufficiently small that this metal coating would be adequate to protect the plastic. Visual inspection of the coating after a high enthalpy shot confirmed this.

The injector tip (#1) that was used in all relevant experiments described in this study (i.e. series 4 and 5; for other series the original solid midsection was used) is shown in figure 2.6. This tip was expected to provide injection conditions closest to those desired, so, given the limited testing time, only this tip was tested. The internal geometry of the tip may be seen in the drawings: a short section of pipe opens into a hollowed out plenum, that leads to the surface of the cone by way of two rows of 36 holes, spaced  $10^\circ$  apart with the rows staggered from each other by  $5^\circ$ . The hole path is at a  $12^\circ$  angle (in the same sense as the half-angle of the cone) and each hole has a diameter of  $0.5\text{ mm}$ .

### 2.3.2 Injection timing

Controlling the timing of the injection was an important consideration, as there was a significant startup time from triggering to the establishment of quasi-steady injected flow

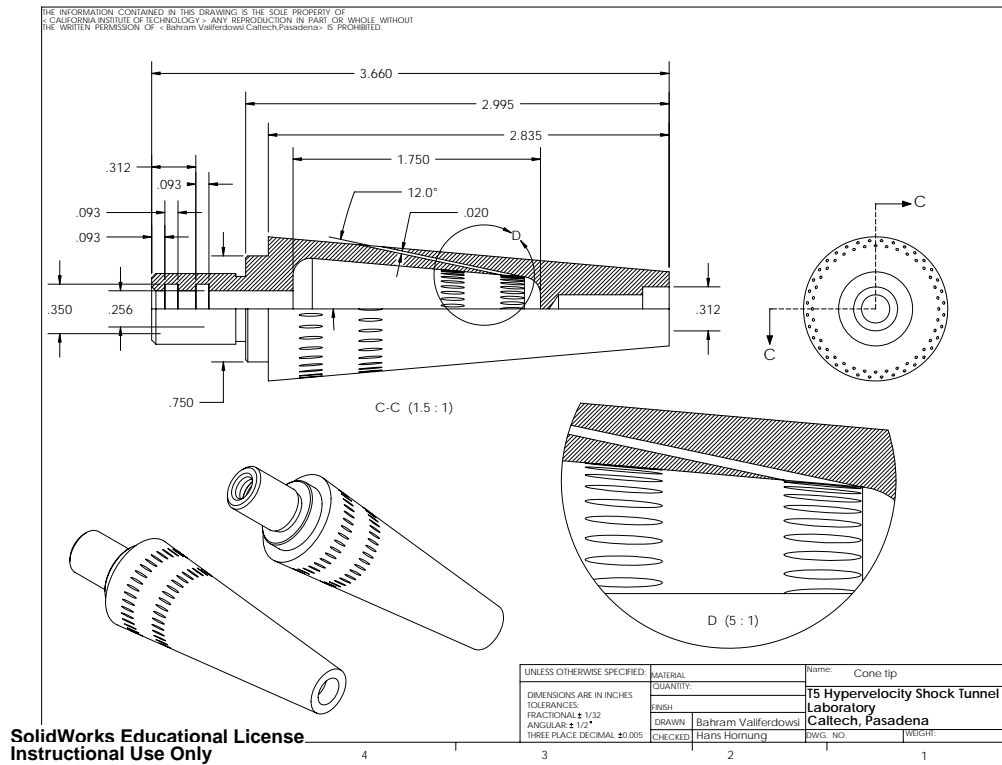


Figure 2.6: Schematic and drawings of the cone tip injector piece.

at the surface of the cone. Initiation of the injection was controlled by an actuated ball valve, located a small distance down the flow line from the run tank. This ball valve was in turn controlled by a solenoid valve. Both valves normally resided in the closed position: when the solenoid valve received a 12-volt trigger signal, it opened to allow compressed air to pass through and actuate the ball valve. The solenoid stayed opened until the 12-volt signal ceased; when it closed, the compressed air supply was cut off and the spring action of the ball valve returned it to its original position. Because this spring action opposed the opening of the valve, the opening time was somewhat longer than the closing time, and there was some concern that the ball valve would not open fast enough for the  $\text{CO}_2$  to reach the surface of the cone by the onset of the test flow. For this reason, it was decided to trigger the injection by the earliest signal produced during the shot: that of the accelerometer attached to the CT.

Several electronic components were designed as part of the triggering system: these are described in the following subsections.

### 2.3.2.1 Operational amplifier

The signal coming from the accelerometer was very weak (around  $40\text{ mV}$ ), so it was necessary to amplify this signal. Originally it was input directly to the operational amplifier circuit shown in figure 2.7. However, there was an impedance mismatch which altered the input signal. It was therefore necessary to bring the accelerometer signal to a delay generator and use the TTL output from that to input to the op amp. The delay generator was set at zero delay and the  $\sim 3\text{ volt}$  TTL output pulse was then amplified to trigger the timing circuit shown in figure 2.8. This op amp doubles the TTL amplitude, which is more than the voltage necessary to trigger the timing circuit.

A large ( $1\text{M}\Omega$ ) resistor,  $R_3$ , was placed to draw down the voltage once the pulse ended, otherwise the op amp would continue to output the amplified TTL pulse until the power supply was switched off. This resistor can be seen in figure 2.7.

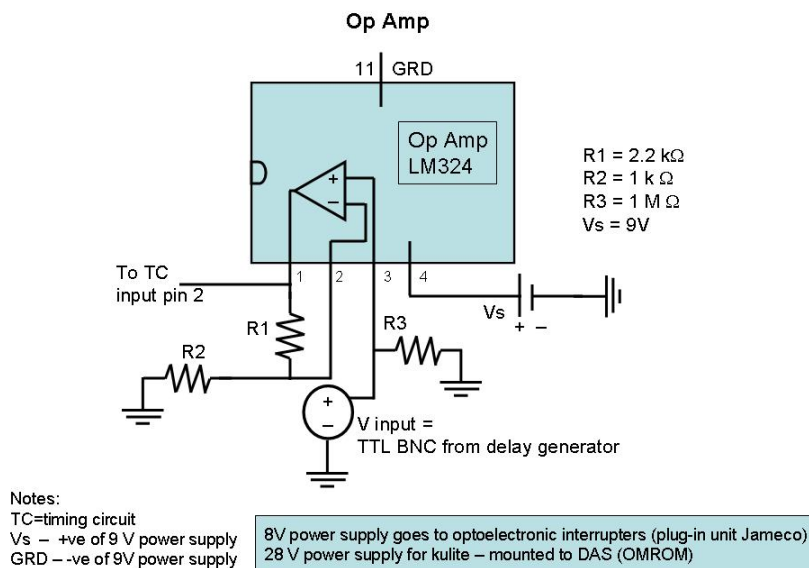


Figure 2.7: Operational amplifier.

### 2.3.2.2 Timing circuit

The timing circuit shown in figure 2.8 takes the output from the op amp, in this case the amplified TTL pulse, generates a delay and then outputs a pulse of amplitude  $\sim 6\text{ volts}$  and the desired duration. The delay is determined by the time constant  $\tau_1 = R_1 \times C_1$ .



The purpose of the relay in figure 2.9 is to close the circuit between the power supply and the solenoid valve which controls the flow of compressed air that actuates the ball valve. When the solenoid valve opens, the compressed air rushes through and turns the ball valve by 90 deg. Once the relay stops receiving an input voltage, it breaks the circuit, causing the solenoid valve to close, thereby cutting off the compressed air supply to the actuated ball valve. The ball valve is controlled by a quick return actuator, which uses an internal spring to rotate the ball valve by  $-90$  deg and close the supply from the run tank.

One concern is that the injected CO<sub>2</sub> would not fully mix with the air boundary layer over the length of the cone. Considering only mass diffusion and no convective or vorticity-driven

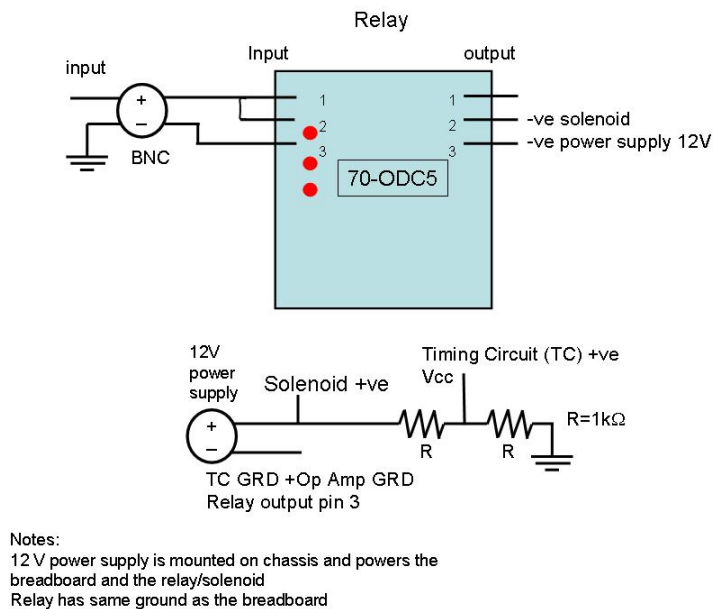


Figure 2.9: Relay circuit diagram.

mixing, it can be shown that the two gases would fully mix before the end of the cone. The effect of these other mechanisms would further aid the mixing of the two gases.

The following diffusion calculation follows Anderson[3] pages 696-699. Based on kinetic theory, the general diffusion equation is

$$D_{AB} = K'_D \frac{\sqrt{T^3}}{P \sigma}$$

where  $D_{AB}$  is the binary diffusion coefficient (or diffusivity) for species A into B,  $\sigma$  is the collision cross section, and  $K'_D$  is a constant[3].

More specifically, from Fick's law (equation 2.1[3; 7]),  $D_{AB}$  is given by

$$j_A = -\rho D_{AB} \nabla c_A \quad (2.1)$$

$$D_{AB} = 0.0018583 \frac{\sqrt{T^3 \left( \frac{1}{M_A} + \frac{1}{M_B} \right)}}{P d_{AB}^2 \Omega_{D,AB}} \quad (2.2)$$

where  $j_A$  is the mass flux of species A in mass per second per unit area,  $c_A$  is the mass fraction of A and  $M_i$  is the molecular weight of species i[3].  $D_{AB}$  is given in units of  $[cm^2/s]$ , T in [K], P in [atm], and  $d_{AB}$  in  $[\text{\AA}]$ [3]. Refer to Table 16.1[3] for tabulated values

of  $\Omega_{D,AB}$  as a function of  $k_1 T / \varepsilon_{AB}$ . Here,  $\varepsilon/k_1$  and  $d$  are the Lennard-Jones parameters which represent the characteristic energy of interaction and the characteristic molecular diameter respectively[3].  $\varepsilon_{AB}$  and  $d_{AB}$  can be approximated by

$$\begin{aligned}\varepsilon_{AB} &= \sqrt{\varepsilon_A \varepsilon_B} \\ d_{AB} &\sim \frac{1}{2} (d_A + d_B)\end{aligned}$$

From Table 16.2[3],

Table 2.2: Parameters used in diffusion computations, see Anderson [3], Table 16.2

Gas	Molecular Weight	Lennard-Jones Parameters	
	$M$	$\sigma$	$\varepsilon/k_1$
	[g/mol]	[Å]	[K]
air	28.97	3.617	97.0
$N_2$	28.02	3.681	91.5
$CO_2$	44.01	3.996	190

$$\begin{aligned}\frac{\varepsilon_{AB}}{k_1} &= \sqrt{\frac{\varepsilon_A}{k_1} \frac{\varepsilon_B}{k_1}} = \sqrt{97.0 \times 190} = 135.8 \\ d_{AB} &\sim \frac{1}{2} (3.617 + 3.996) = 3.807\end{aligned}$$

Assume that the temperature is 0.7 of the stagnation temperature, which is typically around 3000 K. A pressure of 0.25 atm is typical at the edge of the boundary layer. Using  $T=2000$  K,

$$\frac{T}{\varepsilon_{AB}/k_1} = \frac{2000}{135.8} = 14.73$$

This is used to find the value for  $\Omega_{D,AB}$  in Table 2.3[3]. Values are given for  $Tk_1/\varepsilon = 10$  and 20. Interpolating between these values,

Substituting these values into Equation 2.2, the diffusivity is then

$$\begin{aligned}D_{AB} &= 0.0018583 \frac{\sqrt{2000^3 \left( \frac{1}{28.97} + \frac{1}{44.01} \right)}}{0.25 \times (3.807^2) \times 0.7056} \\ &= 15.55 \text{ cm}^2/\text{s} = 0.001555 \text{ m}^2/\text{s}\end{aligned}$$

Table 2.3: Additional parameters used in diffusion calculations [3]

$k_1 T / \varepsilon$ or $k_1 T / \varepsilon_{AB}$	$\Omega_\mu = \Omega_k$ for viscosity and thermal conductivity	$\Omega_{D,AB}$ for mass diffusivity
10	0.8242	0.7424
14.73	0.7859	0.7056
20	0.7432	0.6640

Taking a reference speed of  $U_{ref} = 4000$  m/s at half the expected boundary layer thickness, the distance of interest,  $t_{BL}$ , is 0.0005 m. The diffusion distance,  $x_{diff}$ , is then

$$x_{diff} = \frac{t_{BL}^2 \times U_{ref}}{D_{AB}} = \frac{0.0005^2 \times 4000}{0.001555} = 0.643 \text{ m}$$

Thus, through diffusion alone, the injected CO<sub>2</sub> should be fully mixed by 64 cm along the surface of the cone. Since there will be convective mixing in addition to mass diffusion, the two gases should be fully mixed around halfway along the surface of the cone.

## 2.5 Injection mass flux calculations

In this section, estimates are made of both the injection flow rate necessary to supply an adequate amount of CO<sub>2</sub> to the cone boundary layer and the mass flow rate provided by the current injection system. The latter is based on the geometry of the injection components and the known pressure in the run tank.

### 2.5.1 Required injection mass flux in the cone boundary layer

The following simple calculation gives an indication of the injected CO<sub>2</sub> mass flow rate necessary to produce a significant effect on the transition Reynolds number.

The target condition for the injection experiments is that of Shot 675, for which it has been calculated [1] that the flow velocity and density at the edge of the boundary layer,  $u_e$  and  $\rho_e$ , are 4208 m/s and 0.0786 kg/m<sup>3</sup>, respectively. Within the boundary layer, the velocity will decrease towards the cone surface while the density will increase (as the cone temperature is lower than that of the flow), but to a first approximation, we assume that their product remains constant. According to the boundary layer calculations of Adam [1], at a cone diameter of  $d_{cone} = 5$  cm (roughly 10 cm downstream of the injection point), the

boundary layer thickness,  $\delta$ , will be approximately 1 mm. According to these assumptions then, the mass flux within the boundary layer at this position will be given by:

$$\dot{m}_{bl} = u_e \rho_e \frac{\pi}{4} [(d_{cone} + 2\delta)^2 - d_{cone}^2] \quad (2.3)$$

$$= 0.053 \text{ kg/s.} \quad (2.4)$$

Since the amount of injected CO<sub>2</sub> that would be necessary to lead to a significant delay in transition is not certain, let us simply assume that an mass flow rate equal to the boundary layer mass flux at this point would be required. An injection mass flow rate of 0.053 kg/s is certainly feasible with the current injection system. If we further assume that the transition Reynolds number scales linearly with the fraction of CO<sub>2</sub> in the boundary layer, it is possible to estimate the expected  $Re_{tr}^*$  in this case. From previous experiments [13], the transition Reynolds number for  $h_0 \approx 10 \text{ MJ/kg}$  increases from  $\sim 1 \times 10^6$  for 100% air to  $\sim 5 \times 10^6$  for 100% CO<sub>2</sub>. For equal amounts of air and CO<sub>2</sub> then, a value of  $Re_{tr}^* \sim 3 \times 10^6$  is obtained.

### 2.5.2 Description of injection system components

To estimate the mass flow rate in the injection system, a complete description of the physical components of the system is first necessary. The components were as follows. Leading from the run tank to the ball valve is  $\sim 5''$  long, 1/2-inch (0.4'' ID) rigid pipe. From the valve to the feed-through plate is a 90° bend fitting, of 0.4'' ID, with a total length of  $\sim 4''$ , followed by a 10'' long 1/2-inch rigid pipe (0.4'' ID) connected to a 36'' long, 1/4-inch flexible metal hose. According to the manufacturer (Swagelok), this hose has a minimum internal diameter of 0.19''. From the feed-through plate to the model, there is first a 90° bend fitting, of 0.4'' ID, with a total length of  $\sim 5''$ , followed by a 48'' long 1/2-inch flexible metal hose, with a quoted minimum ID of 0.4''. Attached to either end of this hose is a 3 1/2'' long, 0.4'' ID fitting. The hose leads to a 23'' long, 0.4'' ID rigid tube, situated inside the model, which contracts to a 6'' long, 1/4-inch (0.17'' ID) rigid section leading to the injector plenum.

For the calculation, the flow path is modelled as a series of straight pipes and area changes. The flow through each pipe section is assumed to follow the Fanno relations, while the flow through the area changes is assumed to take place under isentropic conditions. Such a treatment ignores the total pressure losses induced at both the ball valve and the two 90° bends in the flow path, but these are expected to be small relative to the losses

caused by friction in the large L/D pipe sections in the current configuration.

### 2.5.3 The Fanno flow relations

A discussion of Fanno flow may be found in almost any textbook on compressible flow: the summary in this section follows Shapiro [22]. Fanno flow refers to the steady adiabatic flow of fluid through a constant-area pipe with friction. The frictional effects are characterized through a coefficient of friction,  $f$ , defined as

$$f = \frac{\tau_w}{\rho u^2/2}, \quad (2.5)$$

where  $\tau_w$  is the wall shearing stress. It may be shown that in Fanno flow, whether the flow is subsonic or supersonic, the Mach number always tends to unity. If the length of the pipe is larger than a critical length,  $L_{max}/D$  (here normalized by the pipe diameter), at which  $M=1$ , choking will occur. For a perfect gas, this critical length can be related to the initial Mach number,  $M$ , as

$$4\bar{f}\frac{L_{max}}{D} = \frac{1-M^2}{\gamma M^2} + \frac{\gamma+1}{2\gamma} \log \left( \frac{\gamma+1}{2} \frac{M^2}{1 + \frac{\gamma-1}{2}M^2} \right), \quad (2.6)$$

where  $\bar{f}$  is the mean friction coefficient with respect to pipe length. Other flow quantities may also be obtained, and are usually presented in terms of their values at the point at which the Mach number reaches unity, denote by a star. Of interest here are the density, velocity, temperature, and sound speed:

$$\frac{\rho}{\rho^*} = \frac{u^*}{u} = \frac{1}{M} \left[ \frac{2}{\gamma+1} \left( 1 + \frac{\gamma-1}{2}M^2 \right) \right]^{1/2} \quad (2.7)$$

$$\frac{T}{T^*} = \frac{a^2}{a^{*2}} = \frac{\gamma+1}{2 \left( 1 + \frac{\gamma-1}{2}M^2 \right)}. \quad (2.8)$$

The value of the friction coefficient depends on a number of factors, in particular whether the flow is laminar or turbulent, the Reynolds number of the flow, and the roughness of the pipe. A representative value for high Reynolds number flows is 0.0025. A complete discussion of the behaviour of the friction coefficient under different flow regimes may be

found in Schlichting [21], who uses a slightly different parameter,  $\lambda$ , defined as

$$\lambda = \frac{\tau_w}{\rho u^2/8}. \quad (2.9)$$

It follows immediately that  $\lambda=4f$ . For smooth pipes, as will be assumed the case here, a relation has been derived from experimental data with Reynolds numbers of up to  $3.4 \times 10^6$ , as follows:

$$\frac{1}{\sqrt{\lambda}} = 2.0 \log(Re\sqrt{\lambda}) - 0.8. \quad (2.10)$$

this relation is known as Prandtl's universal law of friction for smooth pipes.

#### 2.5.4 Area changes

Flow between area changes is assumed to take place under isentropic conditions, so the standard isentropic flow relations hold:

$$\frac{A}{A^*} = \frac{1}{M} \left[ \frac{2}{\gamma+1} \left( 1 + \frac{\gamma-1}{2} M^2 \right) \right]^{\frac{\gamma+1}{2(\gamma-1)}}, \quad (2.11)$$

as well as:

$$\frac{T}{T_0} = \frac{a^2}{a_0^2} = \left( 1 + \frac{\gamma-1}{2} M^2 \right)^{-1} \quad (2.12)$$

$$\frac{\rho}{\rho_0} = \left( 1 + \frac{\gamma-1}{2} M^2 \right)^{-1/(\gamma-1)}. \quad (2.13)$$

The respective quantities here are referenced either to the sonic values, denoted by an asterisk, or the stagnation conditions, denoted by a zero subscript.

#### 2.5.5 Initial calculation

An initial calculation was made using a constant value of  $f=0.0025$  in equation 2.6. The flow was assumed to choke at the end of the 1/4-inch rigid pipe leading into the injector plenum, meaning there were 8 locations at which the flow conditions had to be calculated. Following the flow path from the run tank to the injector plenum, with the internal geometry between each consecutive pair indicated, these were as follows:

1. Downstream junction of the run tank and 1/2-inch pipe

- 0.4"ID pipe of length 19",  $L/D=47.5$
- 2. Upstream junction of the 1/2-inch pipe and 1/4-inch hosing  
→ Area change,  $A_3/A_2=0.2256$
- 3. Downstream junction of the 1/2-inch pipe and 1/4-inch hosing  
→ 0.19"ID hose of length 36",  $L/D=189$
- 4. Upstream junction of the 1/4-inch hosing and 1/2-inch pipe  
→ Area change,  $A_5/A_4=4.432$
- 5. Downstream junction of the 1/4-inch hosing and 1/2-inch pipe  
→ 0.4"ID pipe/hose of length 83",  $L/D=208$
- 6. Upstream junction of the 1/2-inch pipe and 1/4-inch pipe  
→ Area change,  $A_7/A_6=0.214$
- 7. Downstream junction of the 1/2-inch pipe and 1/4-inch pipe  
→ 0.185" pipe of length 6",  $L/D=32$
- 8. Exit of 1/4-inch pipe into plenum

Using the assumed condition of  $M=1$  at location 8, equations 2.6 and 2.11 were used to calculate the Mach number at every location back through the system. The expansion in the run tank takes place under adiabatic conditions, with no work done either on or by the gas, so this expansion will to a good approximation be isothermal. Using the known reservoir conditions and equations 2.7, 2.8, 2.12, and 2.13, the other flow quantities of interest can then be traced back forward through the system to the location of choking.

Table 2.4 lists the flow quantities of interest calculated by this method. The density depends on the run tank pressure and so is expressed at each station as a fraction of the run tank density (note that  $\rho_0$  in the relevant column refers to this run tank density rather than the stagnation value at that point in the system); the other flow quantities may be considered independent of the run tank pressure. Values of  $\gamma=1.3$  and  $R=189 \text{ J/kgK}$  were assumed for  $\text{CO}_2$ .

Using the conditions at location 1 (at which the area is  $8.11 \times 10^{-5} \text{ m}^2$ ), the mass flow rate,  $\dot{m}=\rho VA$ , can be easily calculated. Given that the quantities  $T_0$  and  $p_0$  are known

Location	$M$	$T$ (K)	$a$ (m/s)	$V$ (m/s)	$\rho/\rho_0$
0	0	298	271	0	1
1	0.083	298	270	22	0.997
2	0.083	298	270	22	0.995
3	0.402	291	267	108	0.922
4	0.588	283	264	155	0.639
5	0.110	298	270	30	0.751
6	0.112	298	270	30	0.738
7	0.663	280	262	174	0.600
8	1	259	252	252	0.410

Table 2.4: Flow conditions at various points along the injection system

directly, and that  $T_1 \approx T_0$  and  $p_1 \approx p_0$ , it is useful to write the mass flux as

$$\dot{m} \approx p_0 M_1 A_1 \sqrt{\frac{\gamma}{RT_0}}. \quad (2.14)$$

Then, if  $p_0 = 300$  psi ( $= 2.07 \times 10^6$  Pa), a mass flux of  $\dot{m} \approx 0.067$  kg/m<sup>3</sup> is obtained.

Using table 2.4 and the known system geometry, we may also estimate the time for the fluid to pass from the run tank through to the injector plenum as 0.098 s, meaning that the total flow time from run tank to injection tips, once the flow is fully established, is of the order of 0.1 s. This compares with the time taken for a sound wave to propagate this distance of approximately 0.014 s (under stationary flow conditions).

### 2.5.6 Refined calculation

In the previous calculation, a friction coefficient of 0.0025 was assumed in all pipe sections. Using the results of this calculation, together with equation 2.10, a more accurate determination of this friction coefficient is possible. Assuming a run tank pressure of  $\sim 300$  psi, and thus a density of  $\rho_0 \sim 36$  kg/m<sup>3</sup>, together with a viscosity of  $\mu = 1.38 \times 10^{-5}$  (suitable for CO<sub>2</sub> at 273 K), an average Reynolds number between locations 7 and 8 of approximately  $1.2 \times 10^6$  is obtained. Solving equation 2.10 graphically gives  $\lambda = 2.25 \times 10^{-3}$ , from which  $f = 0.56 \times 10^{-3}$ . Repeating the calculation from the previous subsection with this value of  $f$  throughout, a Mach number at location 1 of  $M_1 = 0.1085$  results. Substituting this into equation 2.14 with the other values as before ( $p_0 = 300$  psi) now yields  $\dot{m} \approx 0.087$  kg/m<sup>3</sup>.

This calculation may be tested in the following manner. According to the above assumptions, the run tank temperature,  $T_0$ , is constant, and so differentiating the ideal gas

equation,  $p_0 = \rho_0 RT_0$ , the rate of change of the run tank pressure is

$$\frac{dp_0}{dt} = RT_0 \frac{d\rho_0}{dt}. \quad (2.15)$$

As  $d\rho_0/dt = -\dot{m}/V_0$ , where  $V_0$  is the run tank volume, we thus have

$$\frac{dp_0}{dt} = -RT_0 \frac{\dot{m}}{V_0} \quad (2.16)$$

$$\approx -M_1 \sqrt{\gamma RT_0} \frac{A_1}{V_0} p_0, \quad (2.17)$$

where we have made use of equation 2.14. This differential equation may be easily solved to yield:

$$p_0(t) = p_0(t_0) \exp(-M_1 \sqrt{\gamma RT_0} \frac{A_1}{V_0} (t - t_0)). \quad (2.18)$$

We thus see that the characteristic time,  $\tau$ , for the run tank pressure drop, i.e., that time required to drop to  $1/e$  of its original value, is  $(M_1 \sqrt{\gamma RT_0} \frac{A_1}{V_0})^{-1}$ . For  $V_0 = 0.0189 \text{ m}^3$  (5 gallons),  $M_1 = 0.1085$ , and the other quantities as before,  $\tau = 7.95 \text{ s}$ .

In figure 2.10, the measured run tank pressure from shot 2448 is plotted together with the theoretical profile given by equation 2.18. The run tank pressure transducer signal was recorded on a channel of each of the two T5 data acquisition systems: on the new NI system, the signal was recorded over a period of 5 s, and thus shows an appreciable drop in  $p_0$ ; on the old DSP system, only a brief 20 ms window was recorded, and this reading is thus only useful for determining the tank pressure during the test time. Actually, as may be seen, there is some difference in the two readings, with the DSP signal indicating a pressure approximately 10 psi higher. In fact, the initial pressure reading from the digital pressure gage was also different from the initial Kulite transducer reading, at 229 psi. These discrepancies were not investigated further, but do add a further degree of uncertainty to the mass flow rate calculation.

The longer-term measured run tank profile shows a sharp initial drop in pressure as the injection flow starts up. This startup period appears to extend slightly past  $t=0$  and then a relatively steady drop in pressure is established. A further examination of the injection startup period is made in section 2.6. The reference point,  $t_0$ , in equation 2.18 is chosen as  $t_0 = 50 \text{ ms}$ , and the resulting theoretical curve is shown. The theoretical and measured profiles are almost indistinguishable for a period of approximately 2 s, suggesting that the

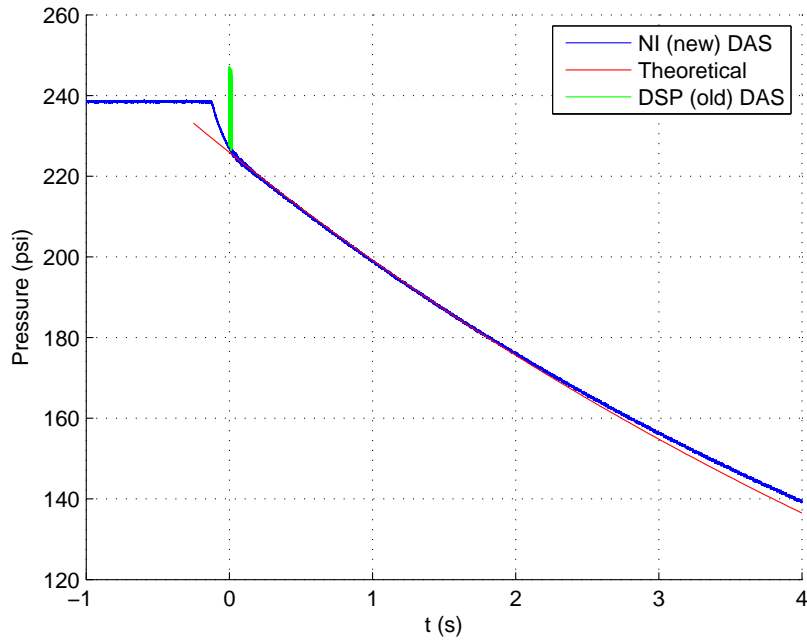


Figure 2.10: Run tank pressure trace from shot 2448, together with the profile obtained from the present calculation

present calculation gives a good indication of the mass flow rate during this time. However, the theoretical curve diverges from the measured trace at earlier times. This divergence is only slight at  $t=0$ , but still suggests that the injection flow has yet to be fully established at this time. The actual mass flux during the test time may thus be slightly higher than the above calculation indicates.

## 2.6 Injection timing experiments

One of the most pressing concerns regarding the injection system was whether the startup would be sufficiently quick that there would be adequate injection at the cone surface by the time of arrival of the main test flow. A number of experiments involving visualization of the injected flow were thus performed in order to gain information about the injection timing.

### 2.6.1 Injection without main flow

The first series of tests involved visualizing the injection process without flow in the test section while recording the unsteady run tank pressure over a period of several seconds, with the data acquisition and injection triggered by the same signal (generated by tapping the accelerometer on the CT). As such a run tank profile had been obtained during shot 2448 (see figure 2.10), test and shot profiles could be correlated to estimate the extent of the injected flow during the test time of the shot. Two sets of tests were performed: in the first set, the injection was into ambient air; in the second, the injection was into the evacuated dump tank. For the first series, as the cone tip protruded from the front of the test section, the dump tank was simply moved into a position so that the injector tip was within the line-of-sight of the optical system; for the second, the cone was moved back in the test section so that the injector tip was in line with the windows. Figure 2.11 shows schlieren images obtained during two test runs: the first sequence shows injection into ambient air, the second injection into the dump tank vacuum. The initial run tank pressure and time elapsed after triggering in each image are indicated in the caption.

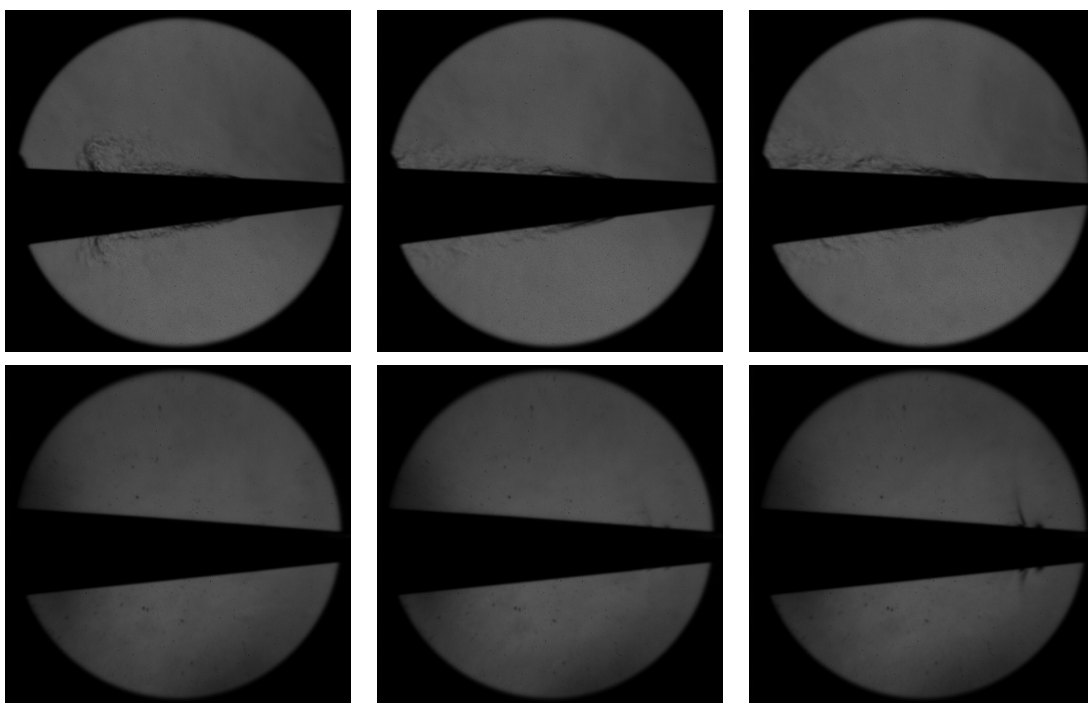


Figure 2.11: Schlieren visualizations from injection tests: (top) injection into ambient air with an initial run tank pressure of 149 psi; (bottom) injection into evacuated T5 dump tank with an initial run tank pressure of 439 psi. In each case, the time from triggering is, from left to right: 70, 183, and 300 ms.

While the injected gas is very much apparent in the ambient injection, in the vacuum injection, even with the higher run tank pressure, the flow features are very difficult to discern. Expansion fans are barely visible at the injection tips in the last image of the sequence, but the startup of the flow is impossible to estimate from these images. The images obtained from the ambient injection tests were thus used as a guide. The first appearance of injected flow in these tests was typically visible at around 60 ms after triggering. Visually, the flow is fairly well established within 100 ms of this first appearance, although a slight broadening of the injected layer continues after this time.

The run tank pressure was also recorded during these experiments, and the obtained traces could be compared with that recorded during shot 2448. In figure 2.12 the shot 2448 trace is shown together with the test profile at the initial run tank pressure closest to that of the shot. Two versions of the latter signal are shown: the first is the original signal, while the second has been scaled on the pressure axis so that the initial pressure matches that of the shot, and the time axis has been shifted so that the initial parts of the profiles overlap. The best match was found for a shift of 182 ms, indicating that the delay between the accelerometer signal trigger and the triggering of the data-acquisition system by the reservoir transducers in the shot was approximately 182 ms (with the test time beginning approximately 1 ms after the triggering of the DAS). This is important information, as it enables us to return to the injection images and estimate to what extent the injected flow had been established at the time of arrival of the main flow in the test section in the shot.

In figure 2.13, the run tank pressure trace from the test shown in figure 2.12 is again plotted, this time with schlieren images showing the state of the injected flow at several relevant times. Also included on this plot are the voltage signals from two photomicrosensors attached to the ball valve, showing the timing of the valve opening. The injected flow at the estimated beginning of the test time, at  $t=183$  ms, is shown. The flow at this point is fairly well established, with only a slight broadening of the injected layer occurring afterwards. If anything, the startup under vacuum conditions would be quicker than under the ambient conditions considered here, due to the stronger shocks propagating down the system in the former case. These tests thus show that the injection system developed here is indeed suitable for the requirements of the experiments.

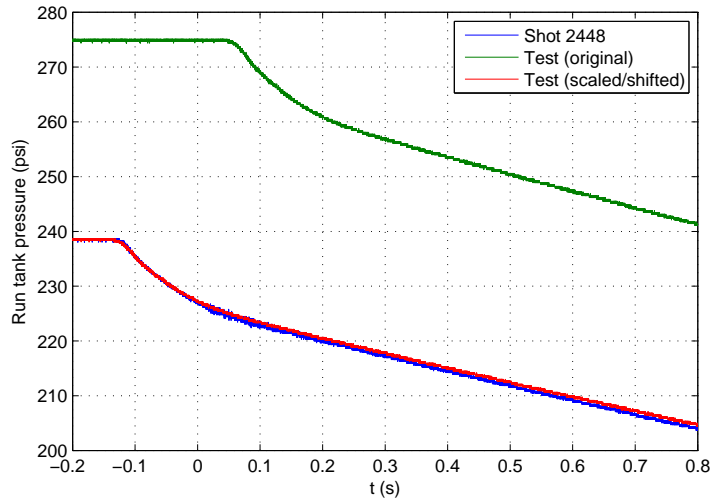


Figure 2.12: Run tank pressure traces from shot 2448 and from an ambient injection test. Both the original test signal and a scaled/shifted version are plotted: the latter is scaled on the pressure axis so that the initial pressures match, and shifted on the time axis (by 182 ms) so that the initial parts of the profiles overlap.

### 2.6.2 Low-enthalpy tests

Finally, a series of low-enthalpy experiments were run in the facility, in the configuration outlined in section 2.1 of this chapter. As the time from piston launch to flow arrival in the test section is different in low-enthalpy experiments to operation under normal conditions, these experiments could not be used as a realistic test for the injection timing. The intent was rather to visualize injection under conditions in which the main test section flow was present. In figure 2.14, visualizations from five low enthalpy shots with different run tank pressures are shown: run tank pressures ranged from 361 to 16 psi, and one shot was performed without injection. As may be seen, for these low-enthalpy cases, the injected gas quickly extends out past the conical shock. The stagnation pressure in these low-enthalpy shots is only of the order of 2 MPa, whereas in a normal shot, this number would be closer to 50 MPa. Thus, a significantly higher mass flux would be present in the main test stream under normal conditions, which would cause the injected flow to “hug” the cone more closely. Also, to further decrease the exit angle of the injected flow, a new tip has been designed and built. This tip, discussed further in section 4.2, has four rows of holes, allowing the same injected mass flux for a lower run tank, and thus injector tip, pressure.

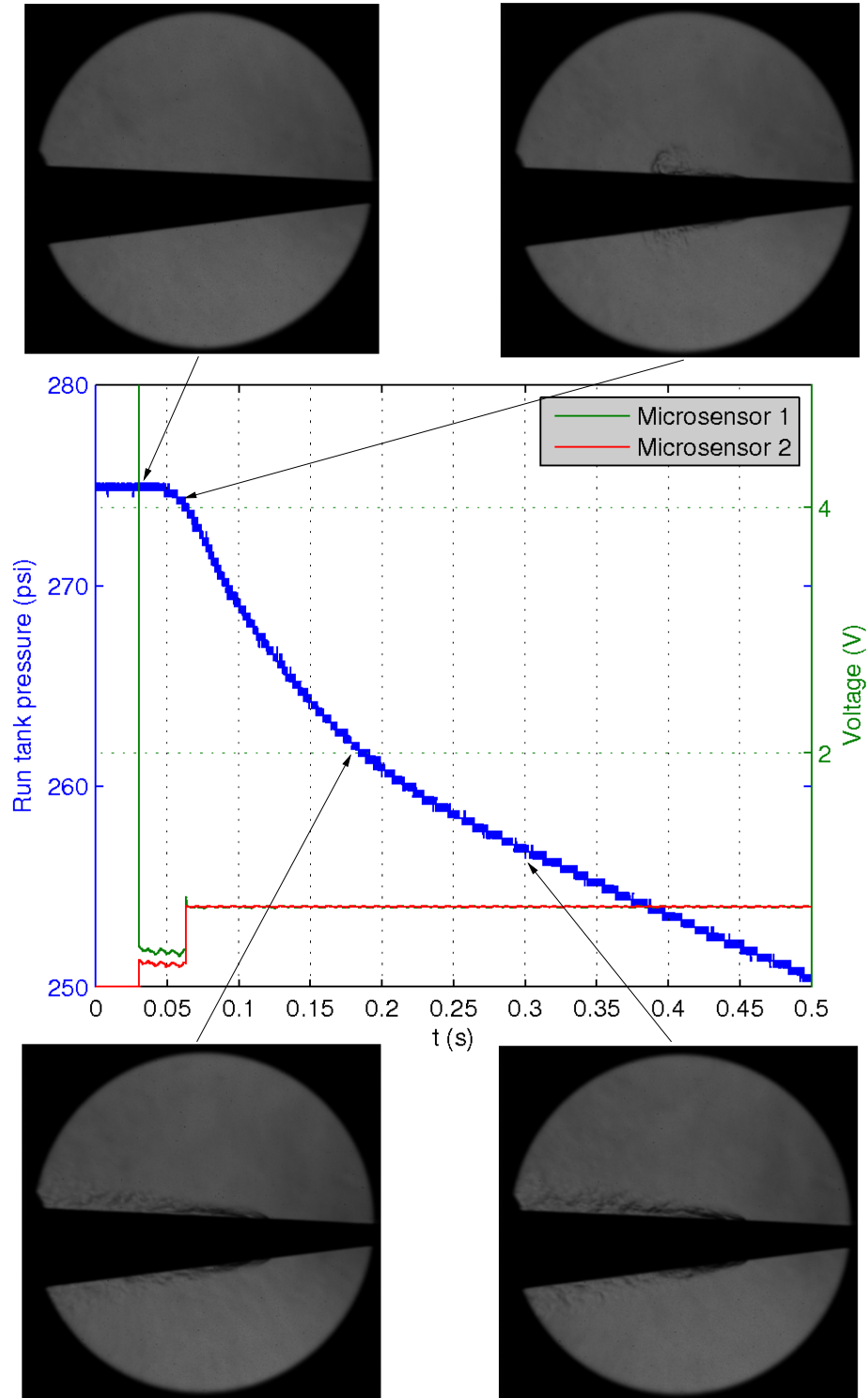


Figure 2.13: The run tank pressure trace from an ambient injection test, with voltage traces from two microsensors attached to the ball valve, showing the timing of the valve opening.  $t=0$  corresponds to the trigger signal being sent to the injection system. Schlieren images from various points in the injection sequence are shown: (top left)  $t=30$  ms, opening of the valve; (top right)  $t=62$  ms, startup of the injection flow at the cone surface; (bottom left)  $t=183$  ms, beginning of test time if main flow were present; (bottom right)  $t=300$  ms, injection flow at a later time.

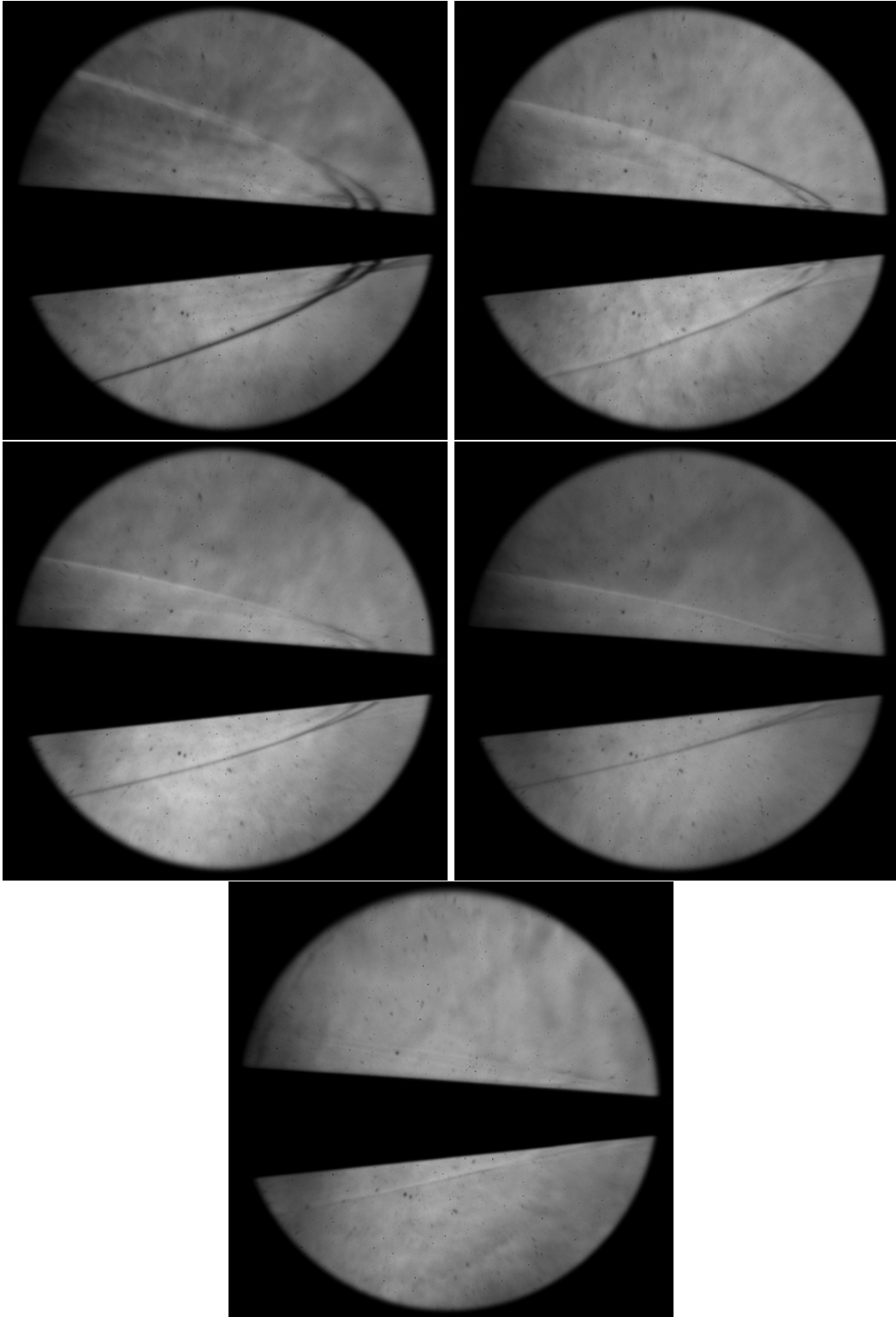


Figure 2.14: Schlieren visualisations from low enthalpy shots with various run tank pressures: (top left) 361 psi; (top right) 162 psi; (middle left) 50 psi; (middle right) 16 psi; (bottom) no injection.

## Chapter 3

# Analysis

This chapter follows the analysis procedure from the experiment through to calculating the transition Reynolds number.

### 3.1 T5 measurements

During the experiment, the shock tube initial pressure ( $P_i$ ), the ambient temperature ( $T_{amb}$ ), and the run tank pressure are recorded as part of the checklist procedure. After the experiment, the run tank pressure is noted again. These quantities are used in postprocessing the recorded data. Data files from the old DAS (Data Acquisition System) can be found on the GALCIT server in `/home/hyper/T5/das/shot/T5/xxxx/`, where `xxxx` is the 4 digit shot number. Data files from the new DAS are transferred to the GALCIT server and copied to this folder.

Two PCB piezo-electric pressure transducers mounted at points along the shock tube and two more mounted at the reservoir near the end allow measurements of the shock speed and the stagnation pressure to be made. The passing shock is recorded by these transducers as a sharp rise in pressure. From the time interval between the passage of the shock past the first and second transducer, and from the time interval between the passage of the shock past the second transducer and the two reservoir pressure transducers near the end wall of the tube, the shock speed is calculated. The two transducers near the shock tube end give the reservoir pressure. Together with knowledge of the pre-shock state of the gas, this is sufficient information to calculate the reservoir state, as described below.

### 3.2 Post-processing of Shock Tube Measurements

Using the pressure transducer data, the program T5\_data\_proc.m calculates the shock speed ( $U_s$ ) in the shock tube and measures the stagnation pressure ( $P_0$ ) at the end of the shock tube. The version of T5\_data\_proc.m used for the CO<sub>2</sub> injection experiments<sup>1</sup> can be found on the GALCIT server in /home/hyper/T5/das/data\_proc.amy. From this folder, open Matlab Version 6<sup>2</sup> and run T5\_data\_proc.

In most of the range of T5 operation, the incident shock causes gases such as nitrogen, oxygen, and carbon dioxide to become vibrationally excited and partially dissociated. In almost all parts of the range the vibrational and dissociational relaxation distances are negligibly small, so the assumption that the gas outside of a thin shock is everywhere in equilibrium holds. We first calculate the conditions after the incident shock using the initial state of the gas, the shock speed, and the equilibrium properties of the gas using ESTC (Equilibrium Shock Tube Calculation), a program written by M. McIntosh (Ph. D. thesis, Australian National University, 1971). The same program is used to calculate the conditions after the reflected shock. The pressure after the reflected shock differs from the measured reservoir pressure, unless the shock tube is operated in perfectly tailored-interface conditions. To determine the reservoir conditions, ESTC assumes that the process transforming the gas from the reflected-shock state to the measured reservoir pressure is isentropic. The ESTC calculation thus gives the complete thermodynamic state of the reservoir gas.

The quantities  $T_{amb}$ ,  $P_i$ ,  $U_s$ , and  $P_0$  are then input into ESTC. At the end of the T5 shock tube, the gases are shocked with both the incident and reflected waves, so the program calculates the thermodynamic and chemical properties for twice shocked gases. The input file is fort.8. The parameters of interest are:

Table 3.1: ESTC Parameters of Interest.

<i>parameter</i>	<i>meaning</i>	$N_2$	$CO_2$	<i>air</i>	<i>mixtures</i>
IRUN	shot#	2331	2333,35,36;2444-45	2433-40,46-49	2332,34,37;2441-43
ISC	# elements	1	2	2	3
ISS	# species	2	5	5	8

<sup>1</sup>The more general version can be found on the GALCIT server in /home/hyper/T5/das/data\_processing

<sup>2</sup>Some modifications need to be made before it will run in more recent versions of Matlab

Table 3.2: Cont'd ESTC Parameters of Interest.

<i>parameter</i>		<i>comments</i>
IC	0	# ions, excluding E-
NFIT	1	thermofit cards: 1 used, 0 none used
KHO	1	harmonic oscillator cards: 1 used, 0 none used
CTMXX	5000	temp [K] where switch is made from harmonic oscillator to thermofit data
BZERO	0	constant used in imperfect gas correction
THETA	0	wedge angle; 0 for vertical wall
IGJ	1	thermofit data available for species J
IGJ	2	only thermofit (no harmonic oscillator) data for species J; use for CO <sub>2</sub>

From the output, the stagnation temperature ( $T_0$ ), stagnation enthalpy ( $h_0$ )<sup>3</sup>, and stagnation composition are used in the next step.

### 3.3 Nozzle expansion

There are two programs that calculate the flow conditions after nozzle expansion. Either NENZF or Xscriptnozflow.m, the nozzle flow expansion script which is written in Matlab and uses Cantera, can be used.

#### 3.3.1 Stagnation Conditions to Throat

Starting from the stagnation conditions calculated in ESTC, an isentrope on the  $P - v$  diagram is followed to reach the sonic condition at the nozzle throat.

Given two thermodynamic properties of the initial reservoir condition, stagnation temperature ( $T_0$ ) and stagnation pressure ( $P_0$ ), and the molar concentrations of each species in the reservoir, all the thermodynamic properties are determined in Cantera. The program makes note of the specific volume ( $v_0$ ), stagnation enthalpy ( $h_0$ ), stagnation entropy ( $s_0$ ), and the soundspeed of the gas. Since we are considering the reservoir conditions, the fluid is taken as quiescent, i.e.  $u = 0$ .

<sup>3</sup>Please note that for CO<sub>2</sub> gas, 8.933; MJ/kg should be added to the value given by ESTC to compensate for the enthalpy of formation at STP. The enthalpy in this output is measured relative to molecular oxygen, which is assigned a heat of formation at STP of zero. For fluid mechanical purposes, however, it is convenient to think of the enthalpy relative to carbon dioxide.

### 3.3.2 Expansion Through the Nozzle

The following derivation obtains the differential equations for nozzle flow solved in Matlab code. Starting with the mass (3.1), momentum (3.2), energy (3.3) and species (3.4) equations,

$$\frac{1}{\rho} \frac{d\rho}{dx} + \frac{1}{U} \frac{dU}{dx} + \frac{1}{A} \frac{dA}{dx} = 0 \implies -\frac{1}{\rho} \frac{d\rho}{dx} = \frac{1}{U} \frac{dU}{dx} + \frac{1}{A} \frac{dA}{dx} \quad (3.1)$$

$$\rho U dU = -dP \implies \frac{dP}{dx} = -\rho U \frac{dU}{dx} \quad (3.2)$$

$$h + \frac{U^2}{2} = h_t \implies \frac{dh}{dx} = -U \frac{dU}{dx} \quad (3.3)$$

$$U \frac{dy_i}{dx} = \frac{1}{\rho} W_i \dot{\omega}_i \quad (3.4)$$

where  $y_i$  is the mass fraction of species  $i$  and  $\dot{\omega}_i$  is the production rate of species  $i$ .

For a mixture of species, specific heat and enthalpy are written as:

$$\begin{aligned} C_p &= \sum_{i=1}^k y_i C_{pi} = \left. \frac{\partial h}{\partial T} \right|_{y_i} \\ h &= \sum_{i=1}^k y_i h_i \implies \frac{\partial h}{\partial y_i} = h_i \\ dh &= \left. \frac{\partial h}{\partial T} \right|_{y_i} dT + \sum_{i=1}^k \frac{\partial h}{\partial y_i} dy_i \\ \frac{dh}{dx} &= C_p \frac{dT}{dx} + \sum_{i=1}^k h_i \frac{dy_i}{dx} \end{aligned} \quad (3.5)$$

Solve (3.5) for the temperature gradient and then use (3.3) to simplify.

$$\begin{aligned} \frac{dT}{dx} &= \frac{1}{C_p} \frac{dh}{dx} - \sum_{i=1}^k \frac{h_i}{C_p} \frac{dy_i}{dx} \\ &= -\frac{U}{C_p} \frac{dU}{dx} - \sum_{i=1}^k \frac{h_i}{C_p} \frac{dy_i}{dx} \end{aligned} \quad (3.6)$$

Prescribing an equation of state

$$P = \rho R T \implies \frac{1}{P} \frac{dP}{dx} = \frac{1}{\rho} \frac{d\rho}{dx} + \frac{1}{R} \frac{dR}{dx} + \frac{1}{T} \frac{dT}{dx} \quad (3.7)$$

Using the mass dependent gas constant expression

$$R = \frac{R_u}{W} \implies R_u = RW$$

where

$$W = \left( \sum_{i=1}^k \frac{y_i}{W_i} \right)^{-1} = \sum_{i=1}^k \chi_i W_i$$

and  $\chi_i$  is the mole fraction of species  $i$ . Then the gradient of the gas constant becomes:

$$\begin{aligned} \frac{dR}{dx} &= -\frac{R_u}{W^2} \frac{dW}{dx} \\ \frac{dW}{dx} &= -\sum_{i=1}^k \left( \sum_{i=1}^k \frac{y_i}{W_i} \right)^{-2} \frac{1}{W_i} \frac{dy_i}{dx} \\ &= -\sum_{i=1}^k \frac{W^2}{W_i} \frac{dy_i}{dx} \\ \frac{dR}{dx} &= \sum_{i=1}^k \frac{R_u}{W_i} \frac{dy_i}{dx} = R \sum_{i=1}^k \frac{W}{W_i} \frac{dy_i}{dx} \end{aligned}$$

Substitute this result into (3.7) and we have the following, which we subsequently solve for the temperature gradient and equate to (3.6).

$$\begin{aligned} \frac{1}{P} \frac{dP}{dx} &= \frac{1}{\rho} \frac{d\rho}{dx} + \sum_{i=1}^k \frac{W}{W_i} \frac{dy_i}{dx} + \frac{1}{T} \frac{dT}{dx} \\ \frac{dT}{dx} &= T \left[ \frac{1}{P} \frac{dP}{dx} - \frac{1}{\rho} \frac{d\rho}{dx} - \sum_{i=1}^k \frac{W}{W_i} \frac{dy_i}{dx} \right] \\ -\frac{U}{C_p} \frac{dU}{dx} - \sum_{i=1}^k \frac{h_i}{C_p} \frac{dy_i}{dx} &= T \left[ \frac{1}{P} \frac{dP}{dx} - \frac{1}{\rho} \frac{d\rho}{dx} - \sum_{i=1}^k \frac{W}{W_i} \frac{dy_i}{dx} \right] \end{aligned}$$

Divide this result by  $T$  and substitute (3.1) and (3.2) to the right hand side. Then

collect like terms and multiply by  $U$ .

$$\begin{aligned}
-\frac{U}{C_p T} \frac{dU}{dx} - \sum_{i=1}^k \frac{h_i}{C_p T} \frac{dy_i}{dx} &= -\frac{\rho U}{P} \frac{dU}{dx} + \frac{1}{U} \frac{dU}{dx} + \frac{1}{A} \frac{dA}{dx} - \sum_{i=1}^k \frac{W}{W_i} \frac{dy_i}{dx} \\
\frac{dU}{dx} \left[ -\frac{U}{C_p T} + \frac{\rho U}{P} - \frac{1}{U} \right] &= \frac{1}{A} \frac{dA}{dx} - \sum_{i=1}^k \left( \frac{W}{W_i} - \frac{h_i}{C_p T} \right) \frac{dy_i}{dx} \\
\frac{dU}{dx} \underbrace{\left[ -\frac{U^2}{C_p T} + \frac{\rho U^2}{P} - 1 \right]}_{\star} &= \frac{U}{A} \frac{dA}{dx} - \sum_{i=1}^k \left( \frac{W}{W_i} - \frac{h_i}{C_p T} \right) U \frac{dy_i}{dx} \tag{3.8}
\end{aligned}$$

$$\begin{aligned}
\star &\Rightarrow \underbrace{\left( \frac{\rho}{P} - \frac{1}{C_p T} \right)}_{\star\star} U^2 - 1; \\
\star\star &\Rightarrow \frac{1}{RT} - \frac{1}{C_p T} = \frac{1}{RT} \left( 1 - \frac{R}{C_p} \right) \\
&= \frac{1}{RT} \frac{1}{\gamma} = \frac{1}{a^2}; \\
\star &\Rightarrow \frac{U^2}{a^2} - 1 = - \underbrace{(1 - M^2)}_{\equiv \eta}
\end{aligned}$$

where  $\eta$  is defined as the sonic parameter. Substituting  $\eta$  back into (3.8), we obtain

$$\frac{dU}{dx} = -\frac{1}{\eta} \left[ \frac{U}{A} \frac{dA}{dx} - \sum_{i=1}^k \left( \frac{W}{W_i} - \frac{h_i}{C_p T} \right) U \frac{dy_i}{dx} \right]$$

which gives us the following set of differential equations to solve.

$$\begin{aligned}
\frac{dU}{dx} &= \frac{1}{\eta} \left[ \dot{\sigma} - \frac{U}{A} \frac{dA}{dx} \right] \\
\frac{dP}{dx} &= -\frac{\rho U}{\eta} \left[ \dot{\sigma} - \frac{U}{A} \frac{dA}{dx} \right] \\
\frac{d\rho}{dx} &= \frac{\rho}{U\eta} \left[ \dot{\sigma} - M^2 \frac{U}{A} \frac{dA}{dx} \right] \\
\frac{dy_i}{dx} &= \frac{W_i \dot{\omega}_i}{\rho U}
\end{aligned}$$

where the thermicity,  $\dot{\sigma}$ , is defined as:

$$\dot{\sigma} \equiv \sum_{i=1}^k \left( \frac{W}{W_i} - \frac{h_i}{C_p T} \right) U \frac{dy_i}{dx}$$

### 3.3.3 NENZF

Although the shock tube flow remains in equilibrium, the flow through the nozzle does not. While the gas is in equilibrium in the reservoir and through the throat, and even up to an area ratio of 3 or more, the chemical reaction rates become important as the gas density decreases in the nozzle expansion. Nozzle expansion is calculated with NENZF (Non-Equilibrium Nozzle Flow), a program developed by Lordi, Mates and Moselle (NASA CR-472, 1966). This is an inviscid quasi-one-dimensional flow code. The input information for this program consists of the temperature and pressure in the reservoir, the nozzle shape, the equilibrium gas properties, the chemical reactions that are active, and the reaction rate constants. Vibrational excitation may be set to be in equilibrium or frozen.

The most recent version of the NENZF executable is `nenzfh`. The original `nenzf.f` compiles using `f77` in the unix environment only. Modifications would have to be made to the Fortran script in order to run it in the linux environment. The other two existing Fortran scripts, `nenzfg.f` and `nenzfh.f`, compile using `f77` in linux. The executable `nenzfg` is similar to `nenzfh` with the exception that  $T_0$  and  $P_0$  are entered when prompted instead of entered in the input file. The input file in all cases (`nenzf`, `nenzfg`, and `nenzfh`) is `fort.8`, while the output file is `fort.9`. The input file must be in the same folder as the NENZF executable. The parameters of interest are summarized in the following table. IRUN, ISC, ISS, IC, NFIT, KHO, CTMXX, BZERO, and IGJ are the same as for ESTC. See Table 3.1 above.

The output quantities are given in the same units as the output of ESTC. The enthalpy is again referenced to an assigned value of zero for molecular oxygen, and the species concentrations are given in moles per gram of mixture. However these are also given as mole fractions at the very end for the free-stream gas composition. The two numbers called *St* and REYNOLDS *N* are the normalizing factor to produce the Stanton number from heat flux value, and the product of free-stream density and free-stream velocity. These are merely convenient numbers for determining Stanton and Reynolds numbers.

The NENZF outputs for all the shots are stored in a directory in the T5 computer and

Table 3.3: NENZF Parameters of Interest.

<i>parameter</i>		<i>comments</i>
ISR		Number of reactions - depends on mechanism model used.
NQS		
IUPD	0	Starting downstream of throat.
IUPD	1	Starting upstream of throat.
KKUR	1	Third body reactions used.
KKUR	0	No third body rxns used.
NAFIT	1	Fitted (e.g. contour) nozzle used.
NAFIT	0	Standard (e.g. conical) nozzle used.
CTAP	xxxx	Stagnation temperature in K.
PRESA	x.xxE+07	Stagnation pressure in Pa.
CXMAX		Maximum (non-dimensional) distance x.
CXMAX	100.0	Length of contour nozzle.
CXMAX	109.0	Length of conical nozzle.
SL	1.0	Characteristic length in cm, used to non-dimensionalize x.
CECHII		Check that there are ISR number of entries for CECHII.
ALPIJ		The first ISC number of rows of this matrix must represent the elements.

are available on demand.

NENZF output seemed to be incorrect for the contour nozzle geometry used to accommodate the slender cone in the test section, so an alternate program was used for these calculations. However, NENZF seemed to work for conical geometry.

### 3.3.4 Nozzle Flow Matlab/Cantera Script

For the Matlab script, we input  $T_0$ ,  $P_0$ , the test gas stagnation composition, the nozzle geometry (contour, conical or constant area), the gas mechanism (thermodata and reaction rates), and the length of the cone (i.e. the distance at which to stop the integration).

Xscriptnozflow.m is a short Matlab script containing a list of shot numbers which calls nozflowfun.m recursively until all the desired shots have been processed. This in turn calls the following non-Cantera subroutines: nozflowfun.m, oneDflow.m, areafun.m, non-ideal.eq\_soundspeed.m, nonideal\_soundspeed.m, and isenfun.m. These subroutines make use of subroutines that are included in the Cantera package: importPhase.m, set.m, pressure.m, density.m, temperature.m, entropy\_mass.m, enthalpy\_mass.m, moleFraction.m, cp\_mass.m, cv\_mass.m, nSpecies.m, massFractions.m, moleFractions.m, netProdRates.m, molecularWeights.m, and meanMolecularWeight.m.

The output file, which is in the form T5\_xxxx\_output.plt gives the initial stagnation

conditions, the sonic conditions at the throat, and the flow properties at the end of the nozzle.

### 3.4 Taylor-MacColl

After exiting the nozzle, the flow passes through a conical shock which sits at some angle from the surface of the cone. To find the flow properties at the edge of the boundary layer, the Taylor-MacColl solution is used to solve for flow conditions through conical shocks. First the ratio of specific heats, the freestream Mach number, the cone half-angle, and an initial guess of the conical shock angle are entered. For the cases in the present experiments, an initial guess of 12 or 13 degrees was usually sufficient. Once the program converges on a solution, the program prompts the user for the specific gas constant, the stagnation enthalpy (which was obtained from ESTC), the freestream temperature, and the freestream pressure. Here, freestream refers to the flow at the nozzle exit. The Taylor-MacColl program gives the flow properties at the edge. In order to calculate the Stanton and Reynolds numbers at each thermocouple, the only remaining properties needed are the boundary and edge viscosities. The assumption that the conical shock is a weak one allows for the use of the freestream composition as the edge composition.

### 3.5 Viscosity

Using the edge temperature and the freestream composition, the viscosity can be calculated. Wilke's Rule [27] is used for the viscosity of the mixed gases. A Matlab script was written by Eric Marineau for the mixing of  $Ar$ ,  $O_2$ , and  $N_2$  for air. This was modified by Ivett Leyva to include  $CO_2$  and its subspecies. The edge temperature is then used to calculate the reference temperature. The reference temperature for air,  $T^*$ , given by Eckert [8] is

$$\frac{T^*}{T_e} = 0.5 + 0.039M_e^2 + 0.5\frac{T_w}{T_e}, \quad (3.9)$$

where  $T_w$  is the wall temperature (taken to be  $T_{amb}$ , the ambient temperature) and the subscript  $e$  indicates the edge conditions.

Dorrance [7] showed that a more general expression could be derived from similarity

considerations as

$$\frac{T^*}{T_e} = 0.5 + \frac{\gamma - 1}{2} \frac{Pr}{6} M_e^2 + 0.5 \frac{T_w}{T_e} \quad (3.10)$$

where  $Pr_{lam}$  is given by  $\sqrt{\gamma}$  and  $Pr_{turb}$  is given by  $\sqrt[3]{\gamma}$ .

The viscosity is recalculated using the reference temperature so that the Stanton number vs the reference Reynolds number can be plotted. When both axes are on the log scale, a slope of -1/2 indicates a laminar boundary layer. A sharp jump indicates transition.

### 3.6 St vs Re\*

The discussion in this section follows that of Adam [1]. Similar material may also be found in the thesis of Germain [11], although a mistake appears in this work in equation 2.11b; the correct form is given by Adam in equation 4.14 (here equation 3.21). Refer to White [25] for a fuller treatment of this material.

It is desired to reduce the experimentally obtained heat transfer profiles to suitable nondimensional variables: the heat transfer rate is typically expressed as the Stanton number, whereas the distance along the cone surface is normalized into the Reynolds number. The Reynolds number is defined as

$$Re = \frac{\rho_e u_e x}{\mu_e}, \quad (3.11)$$

where  $x$  is the distance along the centerline from the cone tip, and the subscript  $e$  indicates that the fluid properties are to be evaluated at the edge of the boundary layer. The Stanton number is given by the following expression

$$St = \frac{\dot{q}(x)}{\rho_e u_e \left[ h_0 - \frac{1}{2} u_e^2 (1 - r) - C_p T_w \right]}, \quad (3.12)$$

where  $\dot{q}(x)$  is the heat transfer rate and  $r$  is the recovery factor. For laminar flows,  $r_{lam} = \sqrt{Pr}$ , and for turbulent flows,  $r_{turb} \approx Pr^{1/3}$ , where  $Pr$  is the Prandtl number.  $Pr$  is assumed to be constant, which is a reasonable approximation under the conditions of interest.

Theoretical or empirical expressions relating the Stanton number to the Reynolds number have been obtained for both laminar and turbulent boundary layers. These are discussed separately in the following.

### 3.6.1 The laminar case

For self-similar boundary layers at sufficiently high speeds, regardless of whether the flow is laminar or turbulent, the Renolds analogy postulates that the Stanton number may be related to the skin friction coefficient,  $C_f(x) = \tau_w(x)/\frac{1}{2}\rho_e U_e^2$ , where  $\tau_w(x)$  is the shear stress at the wall, as [25]

$$St \approx \frac{1}{2} C_f Pr^{-2/3}. \quad (3.13)$$

Thus, if an expression relating the skin friction coefficient to the Reynolds number can be found, this would give the desired  $Re$ - $St$  relationship.

For an incompressible two dimensional boundary layer in a zero pressure gradient, the classical Blasius flat plate solution may be solved numerically, allowing the incompressible skin friction coefficient to be obtained as

$$C_{f,inc}(x) = \frac{0.664}{\sqrt{Re_x}}. \quad (3.14)$$

If compressible effects are to be included, a correction factor must be introduced. The now-approximate expression then becomes

$$C_{f,comp}(x) = \frac{0.664}{\sqrt{Re_x}} \sqrt{C_w}, \quad (3.15)$$

where  $C_w = \rho_w \mu_w / \rho_e \mu_e$  is the Chapman-Rubesin parameter evaluated at the wall. While this expression is quite accurate for an adiabatic wall, for a hot or cold wall unfortunately it is not as good. This problem may be remedied, however, by employing the reference temperature of either Eckert or Dorrance, as discussed in the previous section and given in equations 3.9 and 3.10. Then, using  $C^* = \rho^* \mu^* / \rho_e \mu_e$ ,

$$C_{f,comp}(x) \approx \frac{0.664}{\sqrt{Re_x}} \sqrt{C^*}. \quad (3.16)$$

A final consideration is that the conical geometry of the case under consideration must be accounted for. This is done by making use of the Lees-illingworth transformation, which results in

$$C_{f,cone} = \sqrt{3} C_{f,plate}. \quad (3.17)$$

The desired  $St-Re$  relationship for the cone is thus

$$St \approx \frac{0.664}{2} \frac{\sqrt{3C^*}}{Pr^{2/3}\sqrt{Re_x}}. \quad (3.18)$$

### 3.6.2 The turbulent case

As in the laminar case, we begin with equation 3.13 as the basis for our desired  $St-Re$  relationship, again seeking to express the skin friction coefficient in terms of the Reynolds number. While no exact expression exists in the turbulent case, a good approximation for the incompressible turbulent skin friction on a flat plate is given by (see White [25]):

$$C_{f,inc} = \frac{0.455}{\log^2(0.06Re_x)}. \quad (3.19)$$

It is now desired to introduce a compressibility compression factor, equivalent to the Chapman-Rubesin parameter in the laminar case. This can only be done if it is assumed that the compressible turbulent boundary layer does not differ significantly in a qualitative manner from an incompressible one. According to the hypothesis of Morkovin [17], this holds if the density fluctuations are small, which holds for boundary layers at Mach numbers of up to around 5. It is typical to introduce to correction factors as:

$$C_{f,comp} = \frac{1}{F_c} C_{f,inc}(Re_x F_{Re}) \approx \frac{1}{F_c} \frac{0.455}{\log^2(0.06Re_x F_{Re})}, \quad (3.20)$$

where  $F_{Re}$  is the "stretching" factor, modifying the Reynolds number within the incompressible equation 3.19, and  $F_c$  is the correction factor for the resulting skin friction.

Two formulations for  $F_{Re}$  and  $F_c$  are considered: the first by van Driest [24], the second by White and Christoph [26]. The former is the more widely used. In both models,  $F_c$  is given by

$$F_c = \frac{T_{aw}/T_e - 1}{(\arcsin A + \arcsin B)^2}, \quad (3.21)$$

where  $T_{aw}$  is the adiabatic wall temperature defined as

$$\frac{T_{aw}}{T_e} = 1 + r_{turb} \frac{\gamma - 1}{2} M_e^2. \quad (3.22)$$

The parameters  $A$  and  $B$  are given by

$$A = \frac{2a^2 - b}{\sqrt{b^2 - 4a^2}}, \quad (3.23)$$

$$B = \frac{b}{\sqrt{b^2 - 4a^2}}, \quad (3.24)$$

where  $a$  and  $b$  are defined as

$$a = \left( \frac{\gamma - 1}{2} M_e^2 \frac{T_e}{T_w} \right)^{1/2}, \quad (3.25)$$

$$b = \frac{T_{aw}}{T_w} - 1. \quad (3.26)$$

The model differ in the specification of the stretching factor  $F_{Re}$ . In the van Driest model, commonly referred to as "van Driest II", this is given by

$$F_{Re} = \frac{1}{F_c} \frac{\mu_e}{\mu_w}, \quad (3.27)$$

whereas in White and Christoph's model, it takes the form

$$F_{Re} = \frac{1}{\sqrt{F_c}} \frac{\mu_e}{\mu_w} \sqrt{\frac{T_e}{T_w}}. \quad (3.28)$$

Allowance must finally be made for the fact that the flow is conical rather than over a flat plate. For turbulent conical flows, the transformations used in the laminar case are approximate, and yield a factor of approximately 1.10, in comparison to  $\sqrt{3}$  in laminar conical flow (van Driest [23]).

## Chapter 4

# Results and discussion

### 4.1 Results of present experiments

Over the last two years, five series of experiments relevant to the current study have been conducted. Tables of run conditions for each of these series, together with heat transfer profiles, where applicable, may be found in Appendix A.

#### 4.1.1 N<sub>2</sub>/CO<sub>2</sub> mixtures

The first series consisted of testing with mixtures of N<sub>2</sub> and CO<sub>2</sub> in various ratios as the test gas, with no injection. These runs serve as a baseline to assess the effect of adding CO<sub>2</sub> to delay boundary layer transition because CO<sub>2</sub> is not being introduced at the boundary layer and so the results are independent from any given injection scheme. The average  $p_0$  for these runs was 51 MPa and the average mixture  $h_0$  was 10.7 MJ/kg. The transition location for each shot was deduced from the heat transfer profile obtained along the length of the cone. Figure 4.1 shows a typical heat flux profile, and in this case the beginning of transition from laminar to turbulent flow in the boundary layer is seen. That the flow is initially laminar is shown by the good agreement between the experimental data and the theoretical prediction for laminar flow. Then, as the  $Re$  increases, a sharp increase in the heat flux is seen. The intersection between the laminar prediction line and a least-squares fit to these data can be used as a good approximation to the onset of transition. From this intersection,  $Re_{tr} = \rho_e U_e x_{tr} / \mu_e$  (where subscript  $e$  denotes the conditions at the edge of the boundary layer) can be determined.

The results of the experiments in Series 1 are shown in figure 4.2, in which the transition Reynolds number,  $Re^*$ , is plotted against the N<sub>2</sub> mole fraction of the test gas. The test

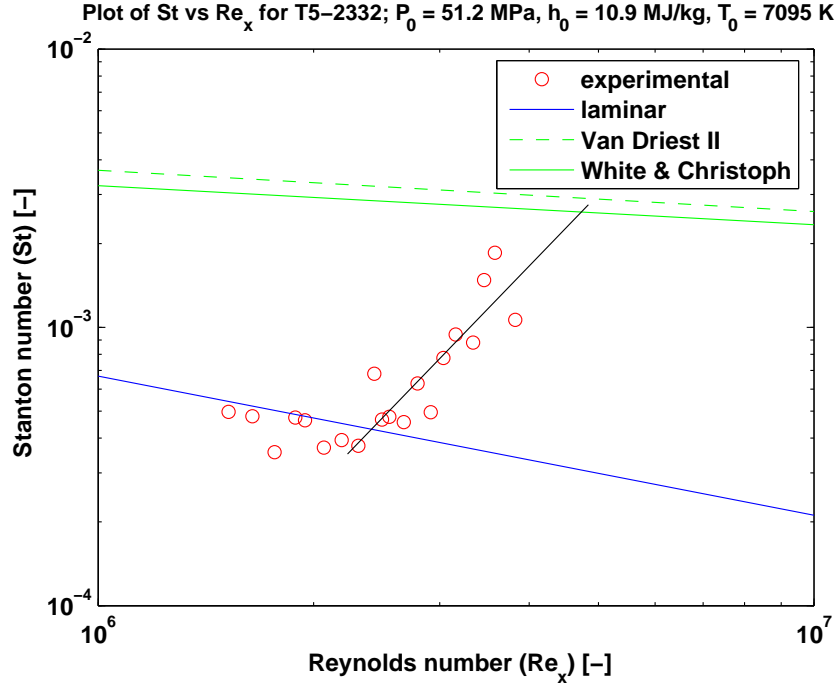


Figure 4.1: Typical heat flux trace for a transitional flow. Shot 2332,  $P_0=51.2$  MPa,  $h_0=10.9$  MJ/kg,  $N_2$  mole fraction=0.95,  $CO_2$  mole fraction=0.05

gas consists of mixtures of  $N_2$  and  $CO_2$ . Note that for this data, a switch has been made from the Reynolds number based on the edge conditions to  $Re_{tr}^* = \rho^* U_{e_{tr}} / \mu^*$ , where the density and viscosity are evaluated at the reference conditions denoted by the \* superscript (see section 3.5 and 3.6). The use of such conditions was shown by Eckert [8] to be more appropriate for discerning trends between different gases at different stagnation enthalpies. The results from these data are best read from right to left. For 100%  $N_2$ , the minimum value of  $Re_{tr}^*$  is obtained, but, as  $CO_2$  is added,  $Re_{tr}^*$  increases significantly, more than doubling by the time the  $N_2$  fraction is reduced to 60%. The data pertaining to 0% mole fraction  $N_2$  was inconclusive: although transition appeared to begin toward the end of the cone, there was not a clear trend. The data point plotted here signifies the minimum value that  $Re_{tr}^*$  could take, corresponding to the position of the last thermocouple. Previous experiments have been performed with either pure  $N_2$  or pure  $CO_2$  in which  $Re_{tr}^*$  was shown to be significantly larger for  $CO_2$  flows at a given  $h_0$ . However, this is the first time that experiments have been performed in the T5 facility with mixtures of  $CO_2/N_2$  in the free stream for the purpose of measuring transition locations. The data from these experiments shows that  $CO_2$  is effective in delaying the transition of the boundary layer from laminar

to turbulent flow when present as a component of the free-stream gas.

The results shown here employed the Wilke mixing rule [27] to compute mixture viscosities and the data for the viscosity of CO<sub>2</sub> obtained from Olynick et al. [18]. This result lends optimism to the effectiveness of the transition delay technique being investigated here.

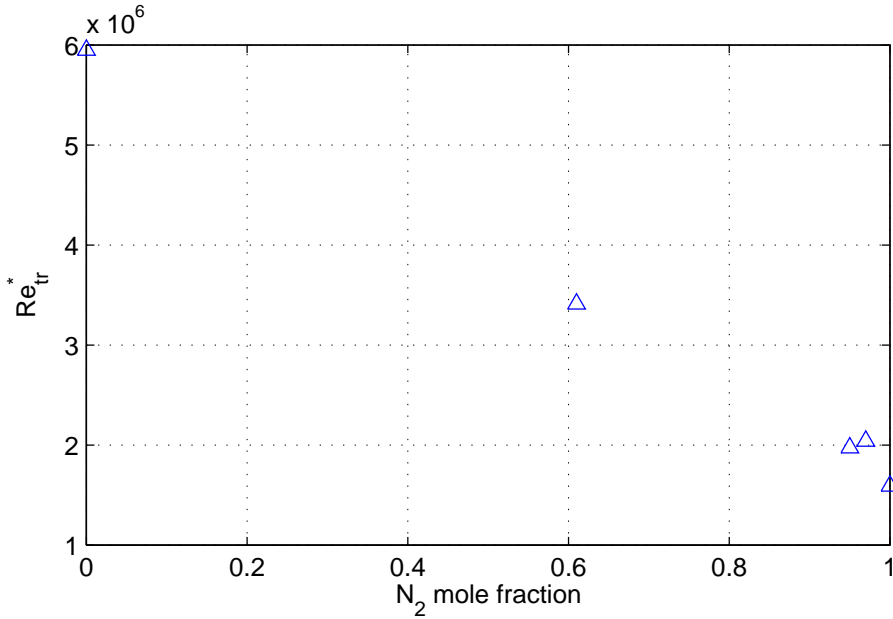


Figure 4.2: Results from series 1 experiments: the effect of CO<sub>2</sub> mole fraction on  $Re_{tr}^*$  on a freestream otherwise consisting of N<sub>2</sub> for a 5° slender cone.

#### 4.1.2 Air and air/CO<sub>2</sub> mixtures

While series 1 focused on mixtures of the test gas, in series 2 the aim was to find a pure air baseline condition in which the boundary layer transitioned somewhere near the middle of the cone, so that when CO<sub>2</sub> was added to the boundary layer via the injection system, the effect on the transition location could be easily seen. For this series the stagnation pressure was varied from 39 to 56 MPa, with the stagnation enthalpy falling between 8 and 11 MJ/kg. These ranges were chosen based on a previous condition run in T5 (shot 675  $h_0=10.5$  MJ/kg,  $p_0=58.5$  MPa), where transition occurred near the desired location. Based on the results from this series and the previous results from shot 675, it was decided to use  $p_0 \sim 54$  MPa and  $h_0 \sim 8$  MJ/kg as the target conditions for the injection experiments.

The series 3 experiments were similar to those of series 1, except air/CO<sub>2</sub> mixtures were

used in place of  $N_2/CO_2$  mixtures. In addition to allowing us to assess the effect of the presence of  $CO_2$  on boundary layer transition in air, this also enabled an assessment of any effects from the other elements in air besides  $N_2$ . Furthermore, such mixtures represent more practically realistic conditions, since if this technique were to be employed in a hypersonic vehicle, the freestream flow would be air. The percentage of  $CO_2$  in the free-stream was 0%, 20%, 40%, 70% and 100% by mass fraction, respectively, for the various experiments: *St-Re* plots from the first three of these are shown in figure 4.3. Comparing the first two cases, the presence of  $CO_2$  appears to delay the onset of transition, which agrees with the results obtained in Series 1 with  $N_2/CO_2$  mixtures. However, for the last two cases (70% and 100%  $CO_2$ ), the heat transfer plots were radically different: the heat fluxes were typically higher by an order of magnitude than expected from the theoretical laminar predictions but the profiles had slopes close to these predictions (see figure 4.3). Therefore, it is not clear whether these two cases are transitional or turbulent, or, in fact, whether this result is due to the thermocouples failing or malfunctioning due to excessive wear. Comparing the 100%  $CO_2$  profiles from series 1 and 3 suggests the latter possibility.

#### 4.1.3 Injection experiments

In series 4, for the first time,  $CO_2$  was introduced to the cone boundary layer through an injector tip. The baseline air condition determined from series 2 was run and  $CO_2$  was injected at different mass flow rates. The injector employed (injector tip #1) had 72 holes with diameters of 0.0258", and is shown in figure 4.4. Four runs were completed, all with  $h_0 \sim 6-7$  MJ/kg and  $p_0 \sim 46 - 56$  MPa. The reason these numbers differ slightly from the target condition is that the primary diaphragms used previously were no longer available, so this condition could not be exactly reproduced.

One of the obtained heat transfer profiles is shown in figure 4.5; the remainder may be found in Appendix A. As may be seen, the *St-Re* profiles for these experiments are all similar to one another, and also resemble the profiles from series 3 in which the  $CO_2$  fraction was 60% or above. The experimental Stanton numbers are significantly higher than the corresponding theoretical values, and the profiles typically show a slightly negative slope (according to the least-squares fits shown), although the large scatter in the data makes meaningful conclusions difficult to draw. The similarity of these profiles to the high- $CO_2$ -fraction experiments of series 3 may indicate one of two things: either that, despite the

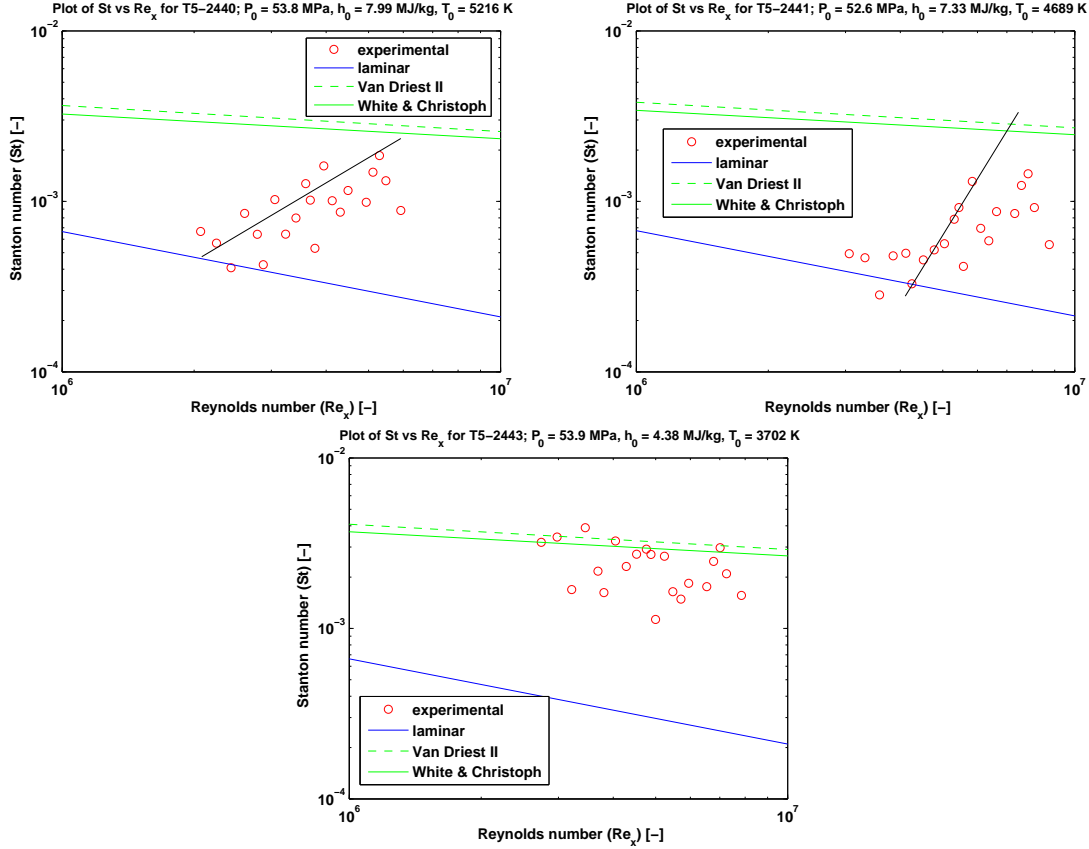


Figure 4.3: Heat transfer profiles with different mixtures of  $CO_2$ /air as the test gas: (top left) 0% mole fraction  $CO_2$ ; (top right) 20% mole fraction  $CO_2$ ; (bottom) 70% mole fraction  $CO_2$ .

fact that the main test gas is air and  $CO_2$  is being injected only over a small area close to the tip of the cone, the injected  $CO_2$  is dictating the behavior of the heat transfer over the surface of the cone, or, that the thermocouples were continuing to malfunction. If the former is true, and these are valid data, it may be possible to discern a further trend in the data, namely a trend towards an increasingly positive slope in the  $St-Re$  profile from shot 2446 to 2449. This corresponds to both decreasing stagnation pressure and increasing run tank pressure. Note, for example, that the least-squares fit gives a positive value for the profile slope for shot 2449, which corresponds to both the lowest  $p_0$  and the highest run tank pressure among the shots. This may indicate a trend towards transition at such conditions, though this would be counterintuitive since this shot had both the lowest overall  $Re$  and the largest flux of injected  $CO_2$ . Another possibility is that at higher injection rates, the injected gas is disrupting the boundary layer, causing an earlier transition to turbulence.

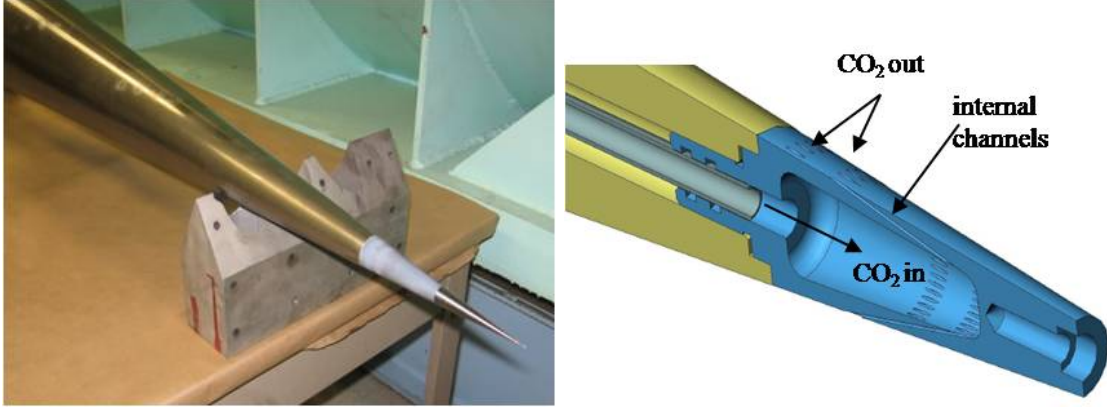


Figure 4.4: The configuration for the injection experiments of Series 4: (left) photograph of injector tip #1 installed in the cone model; (right) schematic of the flow path of the injector tip.

Again, however, the scatter in the data and the possibility of malfunctioning thermocouples prevent any firm conclusions being drawn.

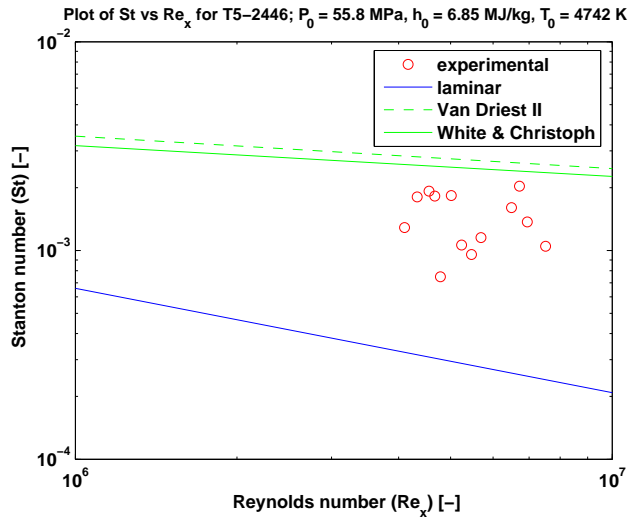


Figure 4.5: Normalized heat flux vs  $Re$  for Shot 2446, in which CO<sub>2</sub> was injected with injector tip #1.

With the possibility of faulty instrumentation in mind, at this point it was decided to switch to visualization of the CO<sub>2</sub> injection with the existing model while a new cone model was being designed and manufactured. The new model was to have more than four times the number of thermocouples of the existing model, allowing for much more detailed measurements.

#### 4.1.4 Injection visualization

In the last of these series of experiments, series 5, it was decided to focus on visualizing the injection flow and validating that the flow of  $\text{CO}_2$  would be established before the main test gas arrives at the cone. Uncertainty about the synchronization of the injection with the tunnel flow prompted us to investigate the timing by using a Phantom high-speed movie camera to determine the delay from the time of sending the trigger signal to the injector valve to the establishment of injected  $\text{CO}_2$  at the surface of the cone. By comparing run tank pressure traces from these tests and from shot 2448, it was found that this delay needed to be less than  $\sim 180$  ms. Further details of these experiments are given in section 2.6. Figure 4.6 shows the results from one test in which  $\text{CO}_2$  was injected into ambient air. These experiments demonstrated that the onset of  $\text{CO}_2$  injection at the surface of the cone occurred approximately 70 ms after the trigger signal. *The injection timing is thus compatible with the operation of the tunnel and this result confirms that the injection mechanism (valving time, trigger signal, etc.) that has been designed is suitable for this experiment.*

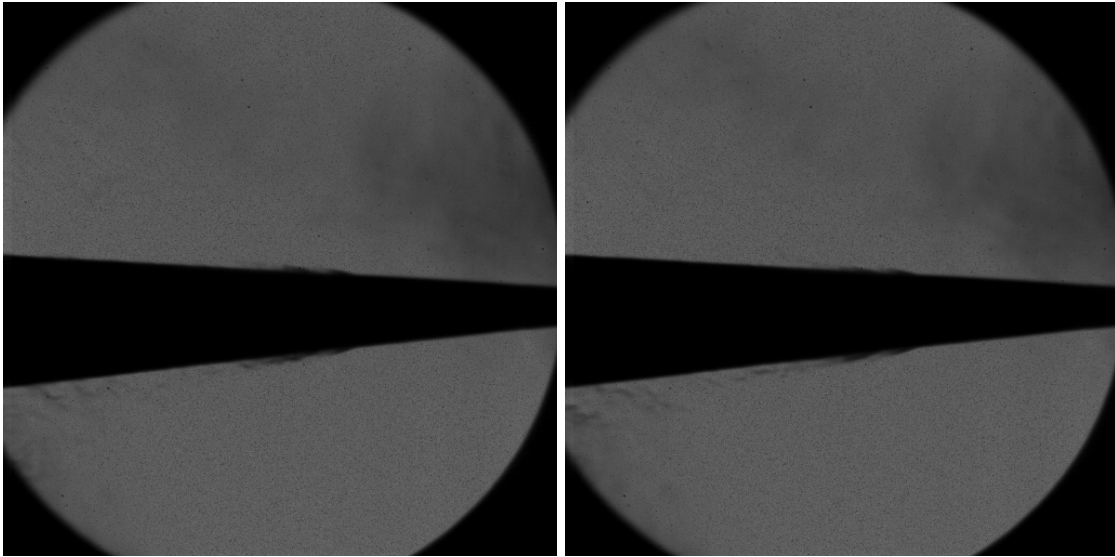


Figure 4.6: Flow visualization of  $\text{CO}_2$  injection from injector tip 1 into ambient air with an initial run tank pressure of 398 psi: (left) flow at 73 ms after trigger; (right) flow at 78 ms after trigger.

## 4.2 Future Work

With experience gained from the testing performed thus far, a new series of experiments is planned with important improvements to both the instrumentation and the injection method. The first improvement is the design and manufacture of a new cone, carrying significantly more instrumentation than the cone model described in this report. This older cone was used for the present experiments because, having been already built and successfully used in a past project, it represented no added cost to our limited budget. As discussed, this cone performed quite well in series 1 and 2 but the thermocouples may have started to show signs of aging in series 3 and 4. The new cone has, in fact, already been designed and built, and is currently being instrumented. Photographs of the main body are shown in figure 4.7. In addition to having 80 thermocouples in comparison to the 21 of the old cone, the new cone also has the thermocouples distributed uniformly in the circumferential direction as well as the longitudinal axis, whereas the old cone had usable thermocouples only on one half.



Figure 4.7: New cone with 80 thermocouple locations (as yet uninstalled): (left) overall view; (right) blow-up view detailing several of the thermocouple orifices.

The second improvement for the future series is a new injector tip, which has been designed and manufactured. This tip is longer than those previously used, allowing the accommodation of a larger number of holes, and thus an increased mass flow rate for the same run tank pressure. A schematic of the new design is shown in figure 4.8.

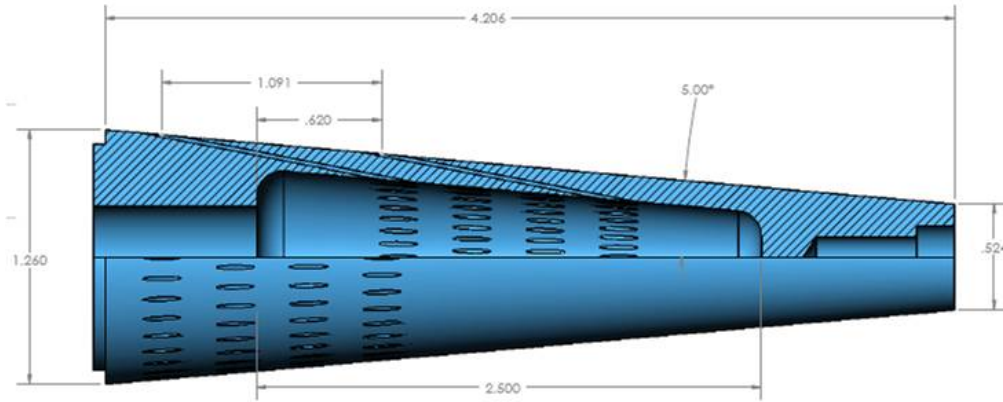


Figure 4.8: Schematic of the new injector tip (Injector 5) to be tested in the next set of experiments.

In the next series of experiments it is intended to start with the previously-determined baseline condition of  $P_0=54$  MPa,  $h_0=8$  MJ/kg with 100% air in the test gas and  $\text{CO}_2$  only being introduced via the injection tips. For this baseline condition, for which transition occurs on the downstream half of the cone when no injection is present, several  $\text{CO}_2$  mass flow rates (high, medium, low) will be tested with at least one old injector tip (fitted with an adapter section for the new cone) and the new injector tip. It is expected that a few calibration shots with no  $\text{CO}_2$  will be performed to check the thermocouples in the new cone, and to make sure previous conditions can be repeated. We expect to demonstrate delay of the boundary layer transition through varying of the  $\text{CO}_2$  mass flow rate introduced to the baseline condition.

### 4.3 Conclusions

In this project, a new technique to delay the transition in hypervelocity air flows by injecting  $\text{CO}_2$  into the boundary layer of interest has been proposed and investigated. The motivation for this idea comes from experimental and computational data that shows that for the same stagnation enthalpy, the transition Reynolds number,  $Re_{tr}^*$ , is larger for  $\text{CO}_2$  flows than for either air or  $\text{N}_2$  flows. The explanation for this phenomenon lies in the fact that when  $\text{CO}_2$  is in vibrational and chemical nonequilibrium, these relaxation processes absorb energy from the acoustic disturbances whose growth in the boundary layer is responsible for transition in hypervelocity flows (second or Mack mode).

Five experimental series have been conducted in this project to test this technique in high enthalpy flows over a  $5^\circ$  slender cone. This geometry was chosen due to the wealth of previous information available with which obtained  $Re_{tr}^*$  data can be compared. A side benefit of using this geometry was that an instrumented cone already existed and therefore allowed us to start this project with a limited budget. Initial experiments used mixtures of  $\text{CO}_2/\text{N}_2$  as the test gas, rather than introducing  $\text{CO}_2$  directly to the boundary layer of the cone. *The obtained results demonstrate that the addition of  $\text{CO}_2$  delays the onset of transition.* For example, in the case of 60% $\text{N}_2$ /40% $\text{CO}_2$  by mole fraction, the value of  $Re_{tr}^*$  was more than double in comparison to the case of 100%  $\text{N}_2$ . A similar effect was noted in several experiments using mixtures of air and  $\text{CO}_2$  as the test gas. Several runs were then performed in 100% air to determine a baseline condition for injection experiments: the requirement for this condition was that transition occurred near the mid-point of the cone, so that any adjustment of transition location due to injection would be easily observed. A small number of experiments were subsequently carried out with  $\text{CO}_2$  injection into an air freestream, but questionable thermocouple readings meant that no firm conclusions could be drawn from these. Finally, tests were carried out in which the injected flow was visualized, *providing confirmation that the triggering of the injection system is appropriately timed to provide adequate injected  $\text{CO}_2$  during the test time.* In fact, the  $\text{CO}_2$  flow starts approximately 100 ms before the main flow arrives, providing enough time for the injection flow to be fully established.

A new cone model has been constructed with 80 thermocouples uniformly distributed in the circumferential and axial directions. This compares with the older model that was restricted to 21 thermocouples located only on one side of the cone. A new injector tip has also been designed and built, having twice as many holes as, and approximately double the flow area of the previously used tip. This will allow lower injection pressures to be used for the same mass flow rate. The next test campaign is scheduled to be completed by the end of this year. The first focus of this campaign will be to quantify the effect of different injection conditions, for a given free-stream condition, on transition delay.



## Appendix A

# Run Conditions and Data Plots

This appendix contains the relevant run condition data from each of the experimental series, together with plots of the Stanton number (normalized heat flux) versus the Reynolds number for each relevant shot. In these plots, theoretical curves corresponding to laminar and turbulent heat transfer profiles (both the Van Driest II and White & Christoph turbulent models are shown) are plotted together with the experimental data, and a best-fit transition line is also indicated where relevant.

### A.1 Series 1 Experiments - Seeded N<sub>2</sub> Flows

In the Series 1 experiments, the N<sub>2</sub> test gas was seeded with varying fractions of CO<sub>2</sub>.

Table A.1: Series 1 run conditions. Baseline and seeded flow.

Shot No.	$P_0$ [MPa]	$T_0$ [K]	$h_0$ [MJ/kg]	[N <sub>2</sub> ] [mol/mol]	[CO <sub>2</sub> ] [mol/mol]
2331	52.2	7375	10.75	1.0000	0.0000
2332	51.2	7095	10.90	0.9500	0.0500
2333	50.0	4434	9.43	0.0000	1.0000
2334	50.1	5380	10.89	0.6111	0.3889
2335	37.6	3459	5.58	0.0000	1.0000
2336	37.2	3606	6.12	0.0000	1.0000
2337	51.2	7379	11.37	0.9676	0.0324

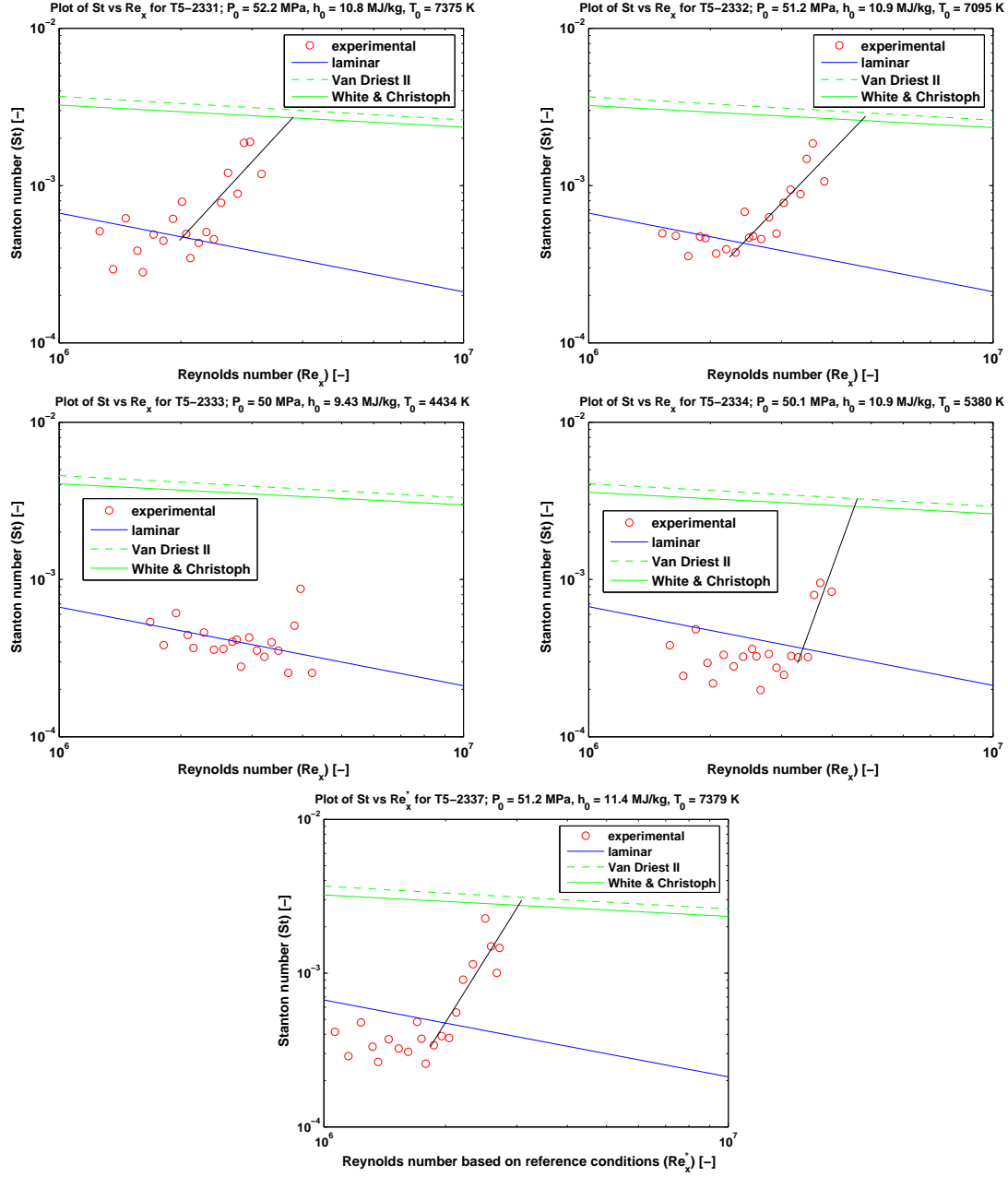


Figure A.1: Heat flux profiles from series 1 experiments.

## A.2 Series 2 Experiments - Calibration in Air

In Series 2, the test gas was air in all cases. A baseline condition was sought in which transition was observed to occur at approximately the midpoint of the cone.

Table A.2: Series 2 run conditions.

Shot No.	$P_0$ [MPa]	$T_0$ [K]	$h_0$ [MJ/kg]
2433	39.1	5305	8.34
2434	42.5	5538	8.87
2435	48.9	5843	9.53
2436	49.5	6069	10.07
2437	46.8	6567	11.33
2438	48.9	6069	10.08
2439	55.5	5715	9.15

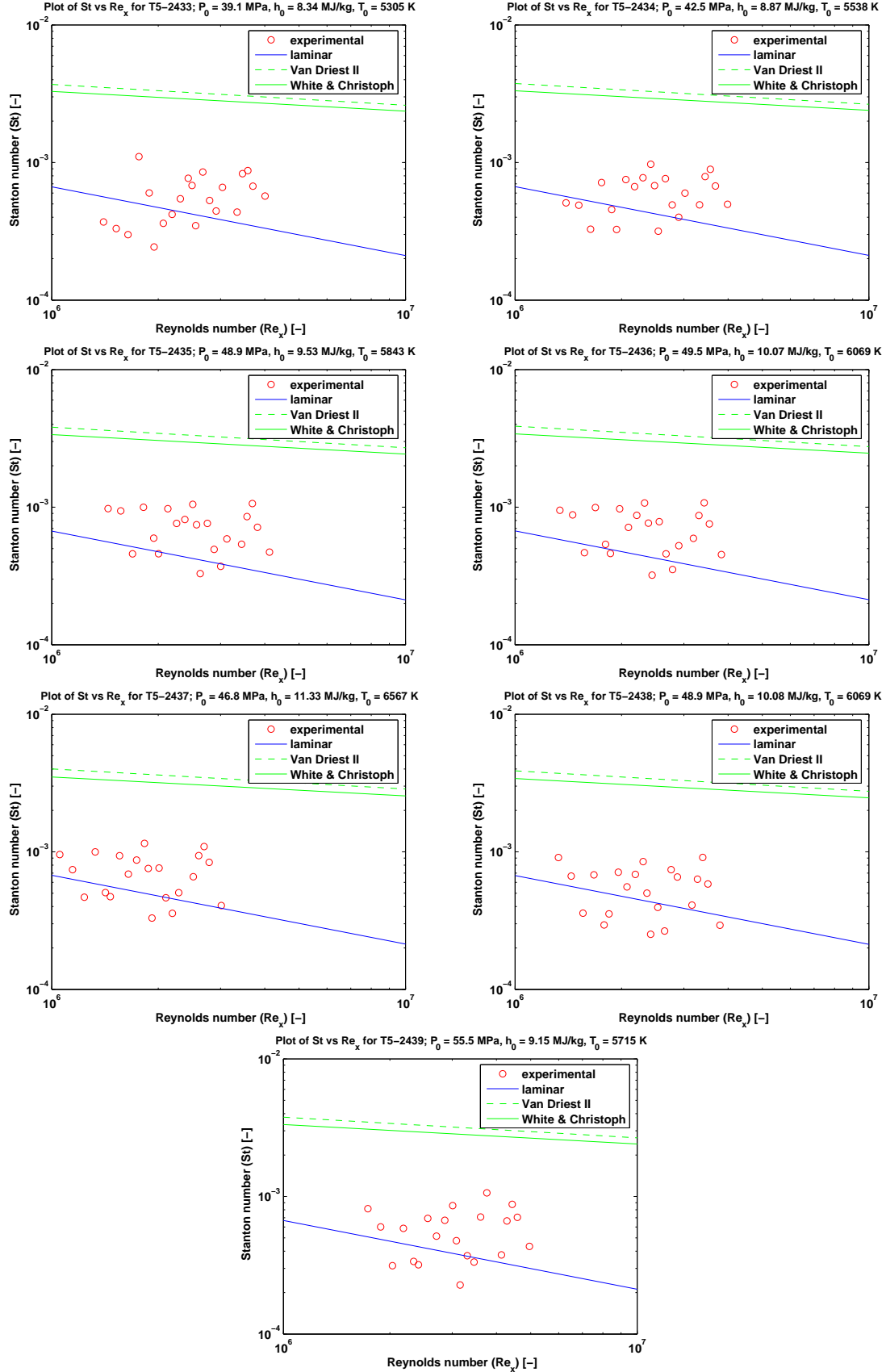


Figure A.2: Heat flux profiles from series 2 experiments.

### A.3 Series 3 Experiments - Seeded Air Flows

In series 3, the air test gas was seeded with varying fractions of  $\text{CO}_2$ . Shot 2440 was used as a baseline and  $\text{CO}_2$  was gradually introduced until the test gas was 100%  $\text{CO}_2$ .

Table A.3: Series 3 run conditions.

shot no.	$P_0$ [MPa]	$T_0$ [K]	$h_0$ [MJ/kg]	[air] [g/g]	[CO <sub>2</sub> ] [g/g]
2440	53.8	5216	7.99	1.0000	0.0000
2441	52.6	4689	7.33	0.8000	0.2000
2442	53.3	4250	7.18	0.6000	0.4000
2443	53.9	3702	4.38	0.3000	0.7000
2444	53.0	3616	5.99	0.0000	1.0000
2445	53.3	3782	6.61	0.0000	1.0000

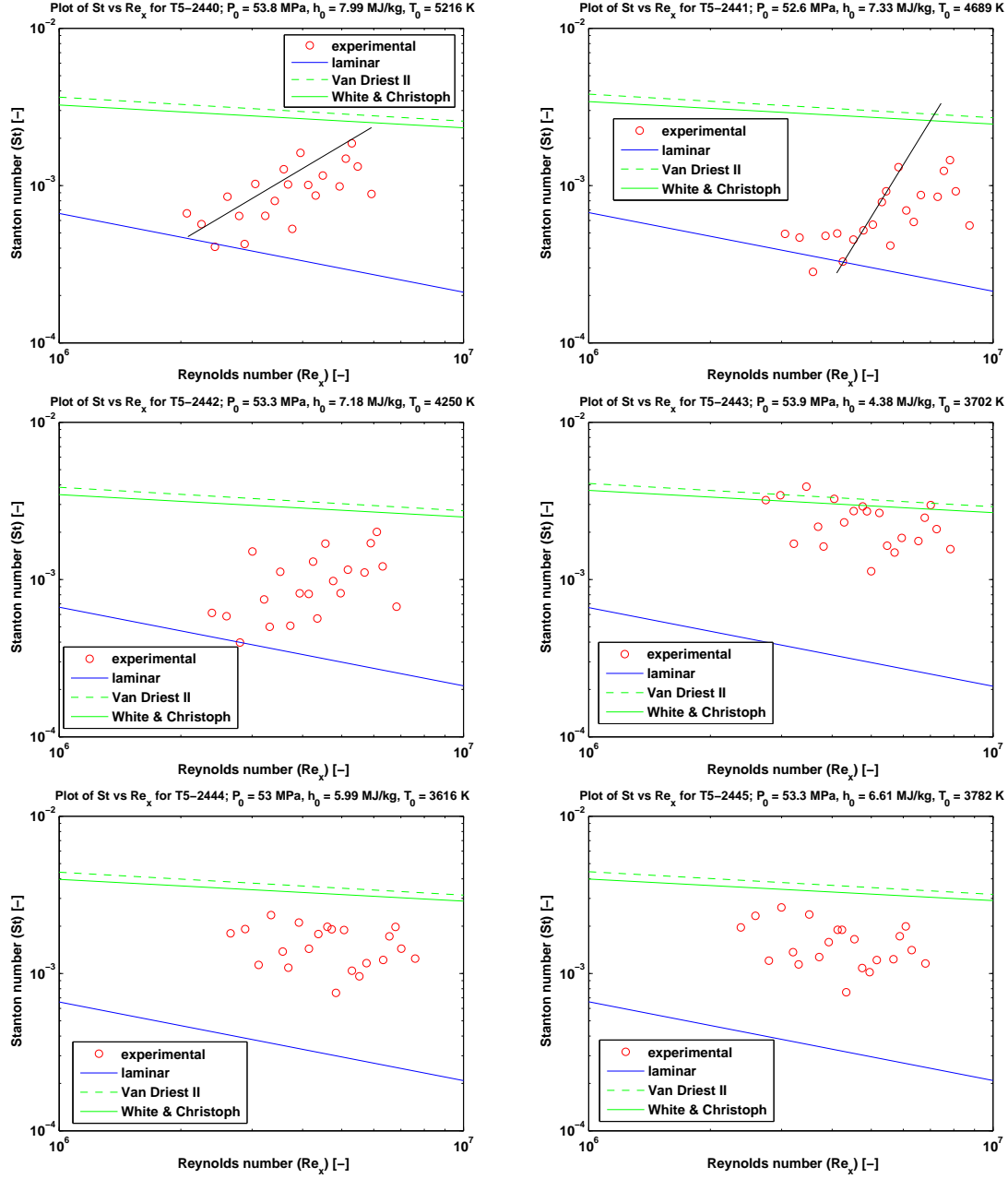


Figure A.3: Heat flux profiles from series 3 experiments.

## A.4 Series 4 Experiments - High Enthalpy Injection

In Series 4,  $\text{CO}_2$  was injected into the boundary layer of the cone in a test flow consisting of 100% air. The run tank pressure reading,  $P_{rt}$ , indicated below is the fill pressure as read from the digital gauge, and the (approximate) mass flow rate is calculated from this. This gauge was found to read slightly lower than the Kulite pressure transducer, and the initial value thus may be a good approximation to the actual tank pressure during the test time.

Table A.4: Series 4 run conditions.  $\text{CO}_2$  injection in high enthalpy air flow.

shot no.	$P_0$ [MPa]	$T_0$ [K]	$h_0$ [MJ/kg]	$p_{rt}$ [MPa]	$\dot{m}$ [kg/s]
2446	55.8	4742	6.85		
2447	50.5	4357	6.06	1.35	0.057
2448	48.4	4358	6.07	1.58	0.067
2449	45.7	4286	5.94	2.43	0.103

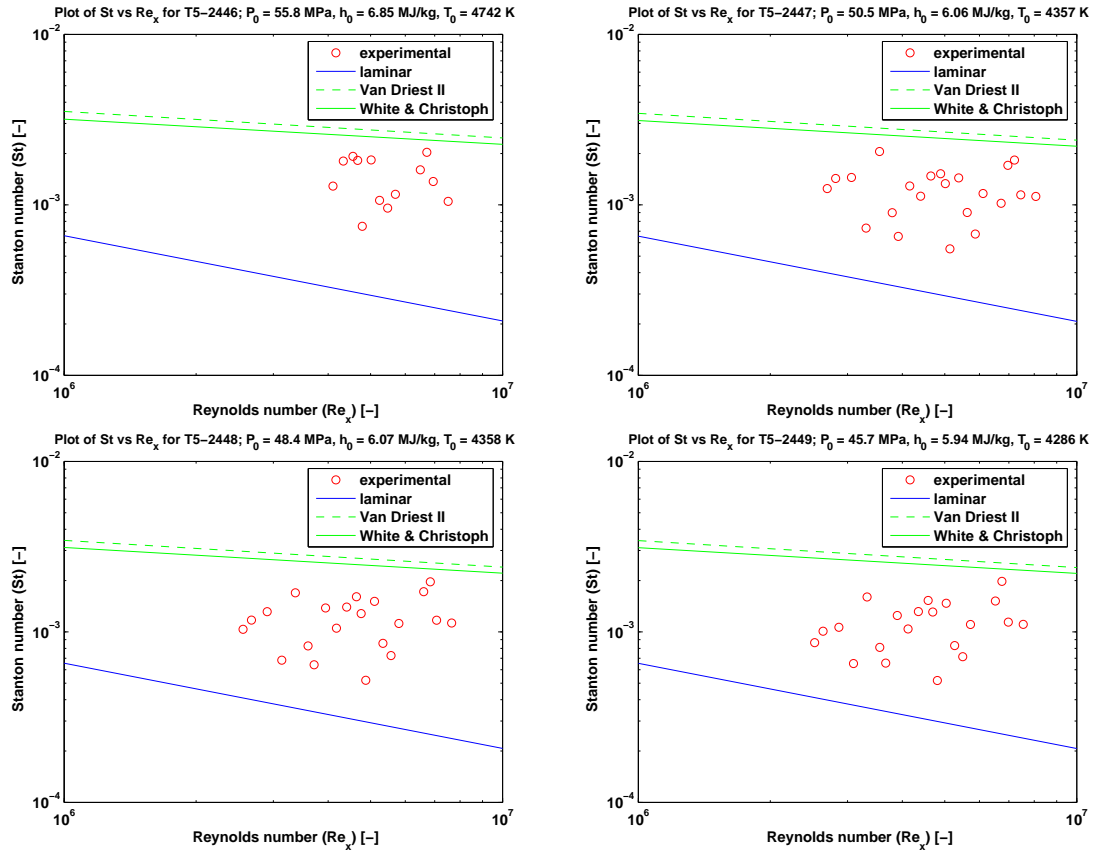


Figure A.4: Heat flux profiles from series 4 experiments.



## Appendix B

# Matlab Scripts

This appendix contains the Matlab scripts and function files used to calculate the flow from the nozzle through to the conditions at the edge of the cone boundary layer. Comments have been added throughout where appropriate.

### B.0.1 Xscriptnozflow.m

```
%
% SCRIPT: Xscriptnozflow.m
% This script runs nozflowfun.m recursively for all the shot numbers indicated

clear all;

index = [2446 2447 2448 2449];
[a b] = size(index);

for i = 1:b
    input_file = ['Xshot', num2str(index(i)), '.dat'];
    nozflowfun(input_file);
end
```

### B.0.2 nozflowfun.m

```
%
% SCRIPT: nozflowfun.m
% This script creates arrays for P-v Curves to the sonic point, then solves
% for quasi 1-D flow down a nozzle with area change
%
% Calls non-Cantera functions - nonideal_soundspeed.m, isenfun.m,
% nonideal_eq_soundspeed.m, oneDflow.m

function nozflowfun(inp)

% read in # of species
AA = textread(inp,'%d',1,'commentstyle','matlab');
n = AA(1);
N = n + 4;

% read in species concentrations
BB = textread(inp,'%s',N,'commentstyle','matlab');
```

```

mech = BB{N-2}; % N.B. curly braces to read inside cell
fname = BB{N-1}; % (to read them in as string)
nozzle = BB{N}; % parantheses for entire cell

% read in initial temperature and pressure
CC = textread(inp, '', 'headerlines', N, 'commentstyle', 'matlab');

T0 = CC(1);
P0 = CC(2);
outfile = CC(3);
plotfns = CC(4);
xfinal = CC(5);

% reads the species concentrations into a string

for i = 1:n
    Q{i} = BB{i+1};
end

q = Q{1};

if n >= 2
    for i = 2:n
        q = [q, ' ', Q{i}];
    end
end

% this gets rid of the concentrations and leaves a string
% with just the species
for i = 1:n
    S = sscanf(Q{i}, '%c');
    j = 1;
    while (S(j) ~= ':' && (j < 8))
        SS(j) = S(j);
        j=j+1;
    end
    spec{i} = SS;
    clear SS S
end

species = spec.';

%%%%%%%%%%%%%%%%%%%%%%%%%%%%%%%%%%%%%%%%%%%%%%%%%%%%%%%%%%%%%%%%%%%%%%%%
% ISENTROPE CURVE ON P-V DIAGRAM
%%%%%%%%%%%%%%%%%%%%%%%%%%%%%%%%%%%%%%%%%%%%%%%%%%%%%%%%%%%%%%%%%%%%%%%%

% GET FIRST POINT ON ISENTROPE

gas = importPhase(mech);
set(gas, 'T', T0, 'P', P0, 'X', q); % sets the state of the gas
r0 = density(gas); % initial density
st = entropy_mass(gas); % total entropy
ht = enthalpy_mass(gas); % total enthalpy

i = 1;
va = 1/r0; % specific volume

```



[illegible]

```
warning off MATLAB:ode15s:IntegrationTolNotMet:
```

```
out = ode15s(@oneDflow,xel,y0,options,gas,Ps,nozzle);
```

[illegible]

```
% Species profile for current iteration
yy = zeros(nsp,1);
```

[illegible]

```

throat = areafun(0,nozzle);

for i = 1:b
    for m = 4:a
        yy(m-3,1) = abs(out.y(m,i));
    end
    rho(i) = out.y(2,i);

    set(gas,'Rho',rho(i),'Y',transpose(yy));
    wt(i) = meanMolecularWeight(gas);
    R(i) = gasconstant/wt(i);
    T(i) = out.y(1,i)*Ps/(out.y(2,i)*R(i));

    pos(i) = out.x(i);
    area = areafun(pos(i),nozzle);
    AR(i) = area/throat;
    Pr(i) = out.y(1,i)*Ps; % pressure [Pa]

    set(gas,'T',T(i),'Rho',rho(i),'Y',transpose(yy));

    % Vectors
    wdot = netProdRates(gas);
    mw = molecularWeights(gas);

    % Scalars
    cp = cp_mass(gas);
    cv = cv_mass(gas);
    g(i) = cp/cv;
    c(i) = nonideal_soundspeed(gas,mech);

    U(i) = out.y(3,i);
    M(i) = U(i)/c(i); % Mach Number
    mF(i,1:nsp) = moleFractions(gas);
end

Pexit = Pr(b);
rexit = rho(b);
xexit = pos(b);
Texit = T(b);
Rexit = R(b);
wtexit = wt(b);

Uexit = U(b);
Mexit = M(b);
cexit = c(b);
gexit = g(b);
mFexit = mF(b,1:nsp);

%%%%%%%%%%%%%%%%%%%%%%%%%%%%%%%%%%%%%%%%%%%%%%%%%%%%%%%%%%%%%%%%%%%%%%%%%%%%%%
% APPEND TO OUTPUT TEXT FILE
%%%%%%%%%%%%%%%%%%%%%%%%%%%%%%%%%%%%%%%%%%%%%%%%%%%%%%%%%%%%%%%%%%%%%%%%%%%%%%

if(outfile == 0)
    disp('No output files created (script_nozzle)')
else
    fid = fopen(fn, 'a');
    fprintf(fid, ...);...

```

```

y = [pos; rho; Pr; T; U];
fprintf(fid, '%1.6e \t %1.6e \t %1.6e \t %1.6e \t %1.6e \n', y);

fprintf(fid, ...);...
fclose(fid);
end

%%%%%%%%%%%%%%%%%%%%%%%%%%%%%%%%%%%%%%%%%%%%%%%%%%%%%%%%%%%%%%%%%%%%%%%%%%%%%%
% MAKE PLOTS OF P, T, U, AND CONCENTRATIONS VS AREA RATIO
%%%%%%%%%%%%%%%%%%%%%%%%%%%%%%%%%%%%%%%%%%%%%%%%%%%%%%%%%%%%%%%%%%%%%%%%%%%%%%

if (plotfns == 0) % 0 for no plots, anything else to create plots
    status = 'DONE'
else
    loglog(AR,Pr,'r')
    ...
    figure;
    plot(AR,T,'b')
    ...
    figure;
    plot(AR,U,'r')
    ...
    figure;
    loglog(AR,mF(1:b,1),'or')
    ...
    figure;
    loglog(AR,mF(1:b,2),'b')
    ...
end

```

### B.0.3 isenfun.m

```

function F = isenfun(T1,gas,array)

v1 = array(1);
s1 = array(2);

set(gas,'Density',1/v1,'Temperature',T1);
equilibrate(gas,'TV');
sg1 = entropy_mass(gas);
sg2 = s1;
F = sg2-sg1;

```

### B.0.4 nonideal\_eq\_soundspeed.m

```

function b = nonideal_soundspeed_eq(a,mech)
% SOUNDSPEED - Speed of sound (m/s).

rho0 = density(a);
V0 = 1/rho0;
t0 = temperature(a);
p0 = pressure(a);
s0 = entropy_mass(a);
q0 = moleFractions(a);

temp_gas = importPhase(mech);
set(temp_gas,'T',t0,'P',p0,'X',q0);

```

```

p1 = 1.001*p0;
set(temp_gas, 'P', p1, 'S', s0, 'X', q0);
equilibrate(temp_gas, 'SP');
rho1 = density(temp_gas);

dpdrho_s = (p1 - p0)/(rho1 - rho0);
b = sqrt(dpdrho_s);

```

### B.0.5 nonideal\_soundspeed.m

```

function b = nonideal_soundspeed(a, mech)
% SOUNDSPEED - Speed of sound (m/s).

rho0 = density(a);
t0 = temperature(a);
p0 = pressure(a);
s0 = entropy_mass(a);
q0 = moleFractions(a);

temp_gas = importPhase(mech);
set(temp_gas, 'T', t0, 'P', p0, 'X', q0);

rho1 = 1.001*rho0;
set(temp_gas, 'Density', rho1, 'Entropy', s0, 'X', q0);
p1 = pressure(temp_gas);

dpdrho_s = (p1 - p0)/(rho1 - rho0);
b = sqrt(dpdrho_s);

```

### B.0.6 oneDflow.m

```

% oneDflow.m
% Set of ODEs to solve quasi 1-D flow with area change
%
% FUNCTION SYNTAX
% =====
% dydx = oneDflow(x, y, gas, P1, nfile)
% ALWAYS called by an ODE solver, in this case
%   out = ode15s(@oneDflow, xel, y0, options, gas, Ps, nozzle)
%   where:
%       xel = distance span
%       y0 = initial conditions array (pressure, density, velocity)
%       options = specified in program that calls oneDflow.m
%       gas = Cantera gas object
%       Ps = Pressure at throat
%       nozzle = conical, contour or constant
%
% INPUT
% =====
% pos = position
% y = solution array
% gas = Cantera gas object
% P1 = pressure at throat
% nfile = filename of contoured nozzle data
%
% OUTPUT
% =====
% dydx = Array of ODEs to be solved by ode15s

```



```

    uprime
    zeros(nsp,1) ];

% species equations
rrho = 1.0/density(gas);

for i = 1:nsp
    dydx(i+3) = rrho*molwt(i)*wdot(i)/U;
end

```

### B.0.7 areafun.m

This function takes the distance downstream, 'x', and the name of the file containing the nozzle area function data, 'nozfile', as inputs and returns the appropriate  $Area(x)$  and  $\frac{dArea}{dx}(x)$ . The input file format can be found in subsection B.1.1, in section B.1.

```

%
% x = position in the x direction
% nozfile = name of the file containing the nozzle area function data
%
% INPUT FILE :nozfile.dat
%
% To use this function, x must be non-dimensionalized by 1 cm.
% i.e. x* = x/0.01
% The area coming out has been non-dimensionalized by the throat area.
% i.e. A* = A/A_throat => A = A* x A_throat
% The change in area coming out has been non-dimensionalized by both.
% i.e. dA*/dx* = (0.01 x dA/dx)/A_throat
% => dA/dx = 100 x A_throat x dA*/dx*

function [area,dAdx] = areafun(xpos,nozfile)

filnam = [nozfile,'.dat'];

fid = fopen(filnam,'r');
fscanf(fid,'%s',2);      % only two strings allowed in line 1
ATP = fscanf(fid,'%14e',5); % there must be 5 ATP coeffs
fscanf(fid,'%s',2);      % only two strings allowed in line 3
A = fscanf(fid,'%14e',10); % there must be 10 A coeffs
fscanf(fid,'%s',2);      % only two strings allowed in line 6
B = fscanf(fid,'%14e',31); % there must be 31 B coeffs
fclose(fid);

xstar = 100*xpos;

delta = 0;
delta2 = 0;

if xstar < ATP(1)
    coef = flipud(A(1:3));
    astar = polyval(coef,xstar);
    for j=2:3
        delta = delta + A(j)*(j-1)*xstar^(j-2);
    end
elseif xstar < 0
    coef = flipud(A(4:10));

```

```

    astar = polyval(coef,xstar);
    for j=5:10
        delta = delta + A(j)*(j-4)*xstar^(j-5);
    end
elseif xstar < ATP(2)
    coef = flipud(B(1:3));
    astar = polyval(coef,xstar);
    for j=2:3
        delta = delta + B(j)*(j-1)*xstar^(j-2);
    end
elseif xstar < ATP(3)
    coef = flipud(B(4:10));
    astar = polyval(coef,xstar);
    for j=5:10
        delta = delta + B(j)*(j-4)*xstar^(j-5);
    end
elseif xstar < ATP(4)
    coef = flipud(B(11:17));
    astar = polyval(coef,xstar);
    for j=12:17
        delta = delta + B(j)*(j-11)*xstar^(j-12);
    end
elseif xstar < ATP(5)
    coef = flipud(B(18:24));
    astar = polyval(coef,xstar);
    for j=19:24
        delta = delta + B(j)*(j-18)*xstar^(j-19);
    end
elseif (ATP(2) == 0)
    coef = flipud(B(1:3));
    astar = polyval(coef,xstar);
    for j=2:3
        delta = delta + B(j)*(j-1)*xstar^(j-2);
    end
else
    coef = flipud(B(25:31));
    astar = polyval(coef,xstar);
    for j=26:31
        delta = delta + B(j)*(j-25)*xstar^(j-26);
    end
end

throat = pi*(0.015)^2;

area = astar*throat;
dAdx = delta*100*throat;

```

## B.0.8 NASA2Chemkin.m

```

% FORMAT
% Rec 1: species name A24, col 1-24
%       : comments (data source) A56, col 25-80
% Rec 2: number of T intervals I2, col 2
%       : optional identification code A6, col 4-9
%       : chem formulas, sym, nos 5(A2,F6.2), col 11-50
%       : zero for gas and nonzero for condensed phases I1, col 52
%       : molecular weight F13.5 col 53-65
%       : heat of formation at 298.15 K [J/mol] F13.5 col 66-80

```

```

% Rec 3: temp range 2F10.3 col 2-21
%      : no of coeff for Cp^o/R I1 col 23
%      : T exponents in empirical eqn for Cp^o/R 8F5.1 col 24-63
%      : H^o(298.15) - H^o(0) [J/mol] F15.3 col 66-80
% Rec 4: first 5 coeffs for Cp^o/R 5D16.8 col 1-80
% Rec 5: last three coeffs for Cp^o/R 3D16.8 col 1-48
%      : integration consts B1 & B2 2D16.8 col 49-80
% repeat 3, 4, and 5 for each interval
%
%
% C      Hf:CJP v33 1955 p125. NSRDS-NBS 3 sec3 1970.
% 3 g 7/97 C 1.00 0.00 0.00 0.00 0.00 0 12.0107000 716680.000
% 200.000 1000.0007 -2.0 -1.0 0.0 1.0 2.0 3.0 4.0 0.0 6535.895
% 6.495031470e+02-9.649010860e-01 2.504675479e+00-1.281448025e-05 1.980133654e-08
%-1.606144025e-11 5.314483411e-15 8.545763110e+04 4.747924288e+00
% 1000.000 6000.0007 -2.0 -1.0 0.0 1.0 2.0 3.0 4.0 0.0 6535.895
%-1.289136472e+05 1.719528572e+02 2.646044387e+00-3.353068950e-04 1.742092740e-07
%-2.902817829e-11 1.642182385e-15 8.410597850e+04 4.130047418e+00
% 6000.000 20000.0007 -2.0 -1.0 0.0 1.0 2.0 3.0 4.0 0.0 6535.895
% 4.432528010e+08-2.886018412e+05 7.737108320e+01-9.715281890e-03 6.649595330e-07
%-2.230078776e-11 2.899388702e-16 2.355273444e+06-6.405123160e+02
%
% need to change fname & coefficients Axx & Bxx

clear all;

hp = 'N2';
NASAfile = [hp, '_highT.inp'];
writetxt = 1;

%*****
%
% READ IN NASA HIGH TEMP COEFFS
%
%*****

fid2 = fopen(NASAfile, 'r');

for m = 1:3
    tline = fgets(fid2);
    temp2(m) = sscanf(tline(2:11), '%d');
    k = sscanf(tline(23), '%d');
    for n = 1:k
        b = 23 + 5*n;
        a = b - 4;
        EX = sscanf(tline(a:b), '%e');
        ex(m,n) = EX;
    end

    hf = sscanf(tline(66:80), '%e');
    for z = 1:2
        txtline = fgets(fid2);
        for x = 1:5
            d = 16*x;
            a = d - 15;
            b = a + 11;
            c = d - 2;
            n = 5*(z-1) + x;

```

```

        num = sscanf(txtline(a:b), '%e');
        alpha = class(num);
        if (alpha(1:4) == 'char')
            coeff(m,n) = 0;
        else
            EX2 = sscanf(txtline(c:d), '%d');
            coeff(m,n) = num*10^EX2;
        end
    end
end
end

temp2(4) = sscanf(tline(12:22), '%d');    % end of range 3 [K]

fclose(fid2);

plotfns = 1;    % 0 for no plots, anything else for plots

T1 = temp2(1);    % start of range 1 [K]
T2 = temp2(2);    % start of range 2 [K]
T3 = temp2(3);    % start of range 3 [K]
T4 = temp2(4);    % end of range 3 [K]

Tstart = T1;
Tbreak = 5000;    % mid temperature between two temp ranges
Tend = 10000;

T1plot = T1;    % start temperature for plots
T2plot = Tend;    % end temperature for plots

Nstart = 1;
Nbreak = Tbreak - Tstart + 1;    % corresponding index number
Nend = Tend - Tstart + 1;

N1plot = T1plot - Tstart + 1;    % corresponding index number for plots
N2plot = T2plot - Tstart + 1;

ex1 = ex(1);    % exponents of T
ex2 = ex(2);
ex3 = ex(3);
ex4 = ex(4);
ex5 = ex(5);
ex6 = ex(6);
ex7 = ex(7);

A11 = coeff(1,1);
A12 = coeff(1,2);
A13 = coeff(1,3);
A14 = coeff(1,4);
A15 = coeff(1,5);
A16 = coeff(1,6);
A17 = coeff(1,7);
B11 = coeff(1,9);
B12 = coeff(1,10);

A21 = coeff(2,1);
A22 = coeff(2,2);
A23 = coeff(2,3);

```

```

A24 = coeff(2,4);
A25 = coeff(2,5);
A26 = coeff(2,6);
A27 = coeff(2,7);
B21 = coeff(2,9);
B22 = coeff(2,10);

A31 = coeff(3,1);
A32 = coeff(3,2);
A33 = coeff(3,3);
A34 = coeff(3,4);
A35 = coeff(3,5);
A36 = coeff(3,6);
A37 = coeff(3,7);
B31 = coeff(3,9);
B32 = coeff(3,10);

i = 1;
T = Tstart;

while T < T2
    CpR(i) = A11*(T^ex1) + A12*(T^ex2) + A13*(T^ex3) + A14*(T^ex4) +
    A15*(T^ex5) + A16*(T^ex6) + A17*(T^ex7);
    HRT(i) = -A11*(T^ex1) + A12*(T^ex2)*log(T) + A13*(T^ex3) + A14*(T^ex4)/2 +
    A15*(T^ex5)/3 + A16*(T^ex6)/4 + A17*(T^ex7)/5 + B11/T;
    SR(i) = -A11*(T^ex1)/2 - A12*(T^ex2) + A13*(T^ex3)*log(T) + A14*(T^ex4) +
    A15*(T^ex5)/2 + A16*(T^ex6)/3 + A17*(T^ex7)/4 + B12;
    X(i) = T;
    i = i + 1;
    T = T + 1;
end

while T < T3
    CpR(i) = A21*(T^ex1) + A22*(T^ex2) + A23*(T^ex3) + A24*(T^ex4) +
    A25*(T^ex5) + A26*(T^ex6) + A27*(T^ex7);
    HRT(i) = -A21*(T^ex1) + A22*(T^ex2)*log(T) + A23*(T^ex3) + A24*(T^ex4)/2 +
    A25*(T^ex5)/3 + A26*(T^ex6)/4 + A27*(T^ex7)/5 + B21/T;
    SR(i) = -A21*(T^ex1)/2 - A22*(T^ex2) + A23*(T^ex3)*log(T) + A24*(T^ex4) +
    A25*(T^ex5)/2 + A26*(T^ex6)/3 + A27*(T^ex7)/4 + B22;
    X(i) = T;
    i = i + 1;
    T = T + 1;
end

while T < T4
    CpR(i) = A31*(T^ex1) + A32*(T^ex2) + A33*(T^ex3) + A34*(T^ex4) +
    A35*(T^ex5) + A36*(T^ex6) + A37*(T^ex7);
    HRT(i) = -A31*(T^ex1) + A32*(T^ex2)*log(T) + A33*(T^ex3) + A34*(T^ex4)/2 +
    A35*(T^ex5)/3 + A36*(T^ex6)/4 + A37*(T^ex7)/5 + B31/T;
    SR(i) = -A31*(T^ex1)/2 - A32*(T^ex2) + A33*(T^ex3)*log(T) + A34*(T^ex4) +
    A35*(T^ex5)/2 + A36*(T^ex6)/3 + A37*(T^ex7)/4 + B32;
    X(i) = T;
    i = i + 1;
    T = T + 1;
end

X3 = X(Nstart:Nbreak).^2;
X4 = X(Nstart:Nbreak);

```

```

X5 = ones(size(X3));

AA = [ X3' X4' X5' ];
[i1,j1] = size(AA);

Y2 = X(Nbreak+1:Nend).^3;
Y3 = X(Nbreak+1:Nend).^2;
Y4 = X(Nbreak+1:Nend);
Y5 = ones(size(Y3));

DD = [ Y2' Y3' Y4' Y5' ];
[i2,j2] = size(DD);

BB = zeros([i1,j2]);
CC = zeros([i2,j1]);

alpha1 = [AA, BB; CC, DD]; % solving alpha1*P = xx

xx1 = CpR(Nstart:Nend);

P = (alpha1'*alpha1)\(alpha1'*xx1'); % P(1:3) for CpR1
                                     % P(4:7) for CpR2

coef2 = -P(4);
coef3 = P(1)-P(5);
coef4 = P(2)-P(6);
coef5 = P(3)-P(7);

alpha2 = [Tbreak^4 -Tbreak^4 Tbreak^3;
          4*Tbreak^3 -4*Tbreak^3 3*Tbreak^2;
          12*Tbreak^2 -12*Tbreak^2 6*Tbreak];
xx2 = [-coef2*Tbreak^3-coef3*Tbreak^2-coef4*Tbreak-coef5;
        -3*coef2*Tbreak^2-2*coef3*Tbreak-coef4;
        -6*coef2*Tbreak-2*coef3];
c_hat = (alpha2'*alpha2)\(alpha2'*xx2);

P1(1) = c_hat(1); % P1 for CpR1, HRT1, SR1
P1(2) = c_hat(3);
P2(1) = c_hat(2); % P2 for CpR2, HRT2, SR2
P2(2) = P(4);

for n = 1:3
    P1(n+2)=P(n);
    P2(n+2)=P(n+4);
end

Tatm = 298;
Natm = Tatm - Tstart + 1;

HHatm = 0;
HH1 = 0;
HH2 = 0;

for j=1:5
    HHatm = HHatm + (P1(j)/(6-j))*Tatm^(5-j);
    HH1 = HH1 + (P1(j)/(6-j))*Tbreak^(5-j);
    HH2 = HH2 + (P2(j)/(6-j))*Tbreak^(5-j);

```

```

end

P1(6) = (HRT(Natm)-HHatm)*Tatm;
P2(6) = (HH1 + P1(6)/Tbreak - HH2)*Tbreak;

SSatm = 0;
SS1 = 0;
SS2 = 0;

for j=1:4
    SSatm = SSatm + (P1(j)/(5-j))*Tatm^(5-j);
    SS1 = SS1 + (P1(j)/(5-j))*Tbreak^(5-j);
    SS2 = SS2 + (P2(j)/(5-j))*Tbreak^(5-j);
end

SSatm = SSatm + P1(5)*log(Tatm);
SS1 = SS1 + P1(5)*log(Tbreak);
SS2 = SS2 + P2(5)*log(Tbreak);

P1(7) = SR(Natm)-SSatm;
P2(7) = SS1 + P1(7) - SS2;

for j = 1:5
    Q1(j) = P1(6-j);
    Q2(j) = P2(6-j);
end

Q1(6:7) = P1(6:7);
Q2(6:7) = P2(6:7);

for n=1:Nbreak
    T = X(n);
    chemCpR(n) = Q1(1) + Q1(2)*T + Q1(3)*T^2 + Q1(4)*T^3 + Q1(5)*T^4;
    chemHRT(n) = Q1(1) + Q1(2)*T/2 + (Q1(3)*T^2)/3 + (Q1(4)*T^3)/4 +
        (Q1(5)*T^4)/5 + Q1(6)/T;
    chemSR(n) = Q1(1)*log(T) + Q1(2)*T + (Q1(3)*T^2)/2 + (Q1(4)*T^3)/3 +
        (Q1(5)*T^4)/4 + Q1(7);
end
for n=Nbreak+1:Nend
    T = X(n);
    chemCpR(n) = Q2(1) + Q2(2)*T + Q2(3)*T^2 + Q2(4)*T^3 + Q2(5)*T^4;
    chemHRT(n) = Q2(1) + Q2(2)*T/2 + (Q2(3)*T^2)/3 + (Q2(4)*T^3)/4 +
        (Q2(5)*T^4)/5 + Q2(6)/T;
    chemSR(n) = Q2(1)*log(T) + Q2(2)*T + (Q2(3)*T^2)/2 + (Q2(4)*T^3)/3 +
        (Q2(5)*T^4)/4 + Q2(7);
end

start = sprintf('%d',Tstart);
endtemp = sprintf('%d',Tend);
brtemp = sprintf('%d',Tbreak);
fn = [hp,'_',start,'-',brtemp,'-',endtemp,'.txt'];
d = date;

fid = fopen(fn,'w');
fprintf(fid, [hp,'\n']);
fprintf(fid, 'CURVE FITTED ON %s\n\n',d);
fprintf(fid, [start, ' ',brtemp,' ',endtemp,'\n']);
fprintf(fid, ' Low range A1-A7: \n');

```

```

fprintf(fid, '%1.8E %1.8E %1.8E %1.8E\n %1.8E %1.8E %1.8E\n\n',Q1);
fprintf(fid, '   High range A1-A7:  \n');
fprintf(fid, '%1.8E %1.8E %1.8E %1.8E\n %1.8E %1.8E %1.8E\n',Q2);
fclose(fid);

midtemp = num2str(Tbreak);

if (plotfns == 0)    % 0 for no plots, anything else to create plots
    status = 'DONE'
else
    plot(X(N1plot:N2plot),CpR(N1plot:N2plot),'r')
    hold on
    plot(X(N1plot:N2plot),chemCpR(N1plot:N2plot),'b')
    hold on
    ...
    figure;
    plot(X(N1plot:N2plot),HRT(N1plot:N2plot),'r')
    hold on
    plot(X(N1plot:N2plot),chemHRT(N1plot:N2plot),'b')
    hold on
    ...
    figure;
    plot(X(N1plot:N2plot),SR(N1plot:N2plot),'r')
    hold on
    plot(X(N1plot:N2plot),chemSR(N1plot:N2plot),'b')
    hold on
    ...
end

```

## B.0.9 Viscosity Files

viscmixCO2.m

```

function mu = viscmixCO2(x,m,mui)
% viscmix Compute the viscosity of a mixture of N species based on
% C.R. Wilke, J.Chem. Phys.,vol.18 pp.517-522, 1950
%
%
% Input:
%   x   = column vector of length N containing the mole fraction of each
%   specie
%   m   = column vector of length N containing the molecular weight of
%   each specie
%   mui = column vector of length N containing the viscosity of each
%   specie
%
% Output:
%   mu = viscosity of the mixture
% Author:
%   Eric Marineau
%   Caltech, T5 Hypervelocity Shock Tunnel Lab, Galcit
%   26 July 2007

% computation of G matrix
N = length(x);
G = zeros(N);
for i=1:N

```

```

    for k=1:N
        if i~=k
            numer = ( 1+(mui(i)/mui(k))^0.5*(m(k)/m(i))^0.25 )^2;
            denom = ( 2^(3/2)*(1+m(i)/m(k))^0.5 );
            G(i,k) = numer/denom;
        end
    end
end
% multiply by 0.1 to get units of kg/m-s
mu = sum(mui./(1+G*x./x));

viscspec.m

function mui = viscspecCO2(chem,T)
% viscspec Compute the viscosity of each specie for the 8 species air
% model using coefficient form NASA Ref 1232 and data from The viscosity
% of argon is taken from M. N. Macrossan and C. R. Lilley,
% Physics of Fluids v 15 (11), Nov 2003
%
%
%
% Input:
%   chem = structure defined in gas_mixture.m containing the curve fits
%   T = temperature of the mixture
% Output:
%   mu = viscosity of the mixture
% Author:
%   Eric Marineau
%   Caltech, T5 Hypervelocity Shock Tunnel Lab, Galcit
%   26 July 2007
% modified to add CO2 by I Leyva, Jan '08
% Original 8 elements: e+, N2, O2, Ar, N, O, NO,NO+
% Additional elements: CO2, CO, C2, C3, CN, C, C+
% Ref: Olynick., D. et al., J of Spacecraft and Rockets,
% Vol. 36, No. 3, May-June 1999

% Viscosity using curve fit
for i = 1:8
    mui(i) = 0.1*exp(chem.spec.MUFC(i))*T^(chem.spec.MUFA(i)*log(T) +
        chem.spec.MUFB(i));
end;

for i = 9:15
    mui(i) = 0.1*exp((chem.spec.MUFA(i)*log(T) +
        chem.spec.MUFB(i))*log(T)+chem.spec.MUFC(i));
end;

% Viscosity of argon T > 1500
Ti = [1500 2000 2230 3000 4000 4360 5000 6000];
muAri = [7.3 8.9 9.6 11.8 14.5 15.4 17.1 19.5]*1E-5;
mui(4) = spline(Ti,muAri,T);

```

## B.1 Input/Output Data Files

### B.1.1 Nozzle Geometry Files

The nozzle geometry files conform to the following guidelines:

[illegible]

### B.1.2 Nozzle Flow I/O Files

#### Sample Input File

```

8                % n = number of species
N:0.001935       % species q{1}
N2:0.680602     % species q{2} (n lines, one for each species)
N0:0.127611
C:0.000000
O:0.111041
CO2:0.000000
CO:0.000000
O2:0.078812
highT_mix_J0.cti % mechanism 'mech' in CTI format
shot2440         % filename for output 'fname', usually shot number
contour30mm      % filename of nozzle area data 'nozzle'
5216             % Stagnation Temperature T0 [K]
53.8e6           % Stagnation Pressure P0 [Pa]
1               % outfile: 1 to print file, 0 to bypass printing
0               % plotfns: 1 to make plots, 0 to bypass
1               % xfinal [m] - position to stop integration

```

Some comments on the previous input file, as taken from the notes in nozflowfun.m:

q = Initial Composition MUST use capital letters - STRING

mech = Mechanism File name in CTI format - STRING (Generally all mechanism files are stored in 'Program Files/Common Files/Cantera/data' on a Windows Machine)

fname = shot number used output file name

nozzle = nozzle geometry - either conical30mm.dat, contour30mm.dat or constantArea.dat

outfile = Output File Name – Enter a non-zero number to generate a .plt file OR enter '0' (the number zero) to bypass generating an output file

plotfns = Plot Functions – Enter a non-zero number to generate plots of Pressure, Temperature, Velocity and Species Concentrations vs Area Ratio OR enter '0' (the number zero) to bypass generating plots

#### Sample Output File

```

#####
#
# ISENTROPE CALCULATION
# CALCULATION RUN ON 29-Mar-2008
#
# INITIAL CONDITIONS
# =====
# STAGNATION TEMPERATURE (K) 5216

```

```

# STAGNATION PRESSURE (Pa) 53800000
# DENSITY (KG/M^3) 3.3768e+001
# SPECIES MOLE FRACTIONS: N:0.001935 N2:0.680602 NO:0.127611 C:0.000000
#                               O:0.111041 CO2:0.000000 CO:0.000000 O2:0.078812
#
#####
THE OUTPUT DATA COLUMNS ARE:
Volume    Pres    Sound    Vel
[m^3/kg]  [Pa]     [m/s]   [m/s]

0.0296    53800000    1434.04    0.00
0.0306    51697603    1390.84    356.00
0.0316    49706735    1385.44    500.60
0.0326    47852200    1380.24    608.02
.
.
.
#####
#
# NOZZLE CALCULATION
# THROAT CONDITIONS
# =====
# TEMPERATURE (K) 4758
# PRESSURE (Pa) 30205328
# DENSITY (KG/M^3) 2.1002e+001
# SOUND SPEED [m/s] 1.3589e+003
# SPECIES MOLE FRACTIONS: N:0.000845 N2:0.695317 NO:0.114866 C:0.000000
#                               O:0.092391 CO2:0.000000 CO:0.000000 O2:0.096582
#
#####
THE OUTPUT DATA COLUMNS ARE:
Position    Density    Pressure    Temperature    Velocity
[m]          [kg/m^3]    [Pa]        [K]            [m/s]
1.000000e-003    2.100242e+001    3.020533e+007    4.757985e+003    1.359930e+003
1.000016e-003    2.100143e+001    3.020351e+007    4.757921e+003    1.359993e+003
1.000033e-003    2.100057e+001    3.020192e+007    4.757866e+003    1.360049e+003
1.000049e-003    2.099983e+001    3.020054e+007    4.757818e+003    1.360097e+003
.
.
.
#####
#
# NOZZLE CALCULATION
# EXIT CONDITIONS
# =====
# PRESSURE [Pa] 24012
# TEMPERATURE [K] 1165
# DENSITY [kg/m^3] 7.1515e-002
# VELOCITY [m/s] 3.6464e+003
# SOUND SPEED [m/s] 6.6856e+002
# MACH [-] 5.4541e+000
# SPECIFIC GAS CONSTANT [J/(kg*K)] 2.8818e+002
# GAMMA [-] 1.3310e+000
# SPECIES MOLE FRACTIONS: N:0.000000 N2:0.753972 NO:0.072055 C:0.000000
#                               O:0.000000 CO2:0.000000 CO:0.000000 O2:0.173973
#
#####

```

Sample \*.cti File

```
#
# Pieced together from highT_co2.cti & highT_n2.cti
# rxn data from Joe Olejniczak
# ref: Mitcheltree 94 CO2-N2 mechanism: 8 species, 12 rxns
#
# originally created Thurs, Nov 2, 2006
# corrected on Fri, Mar 21, 2008
#
units(length = "cm", time = "s", quantity = "mol", act_energy = "cal/mol")
```

```
ideal_gas(name = "gas",
  elements = " N C O ",
  species = "" N N2 NO C O CO2 CO O2 "",
  reactions = "all",
  initial_state = state(temperature = 300.0,
    pressure = OneAtm) )
```

```
#-----
# Species data
#-----
```

```
species(name = "N",
  atoms = " N:1 ",
  thermo = (
    NASA( [ 200.00, 5000.00], [ 2.551359510E+000, -8.707774780E-005,
      2.702513760E-008, -3.855552400E-012, 8.158480060E-016,
      5.609296790E+004, 3.926090980E+000] ),
    NASA( [ 5000.00, 10000.00], [ 3.467587680E-001, 7.155048950E-004,
      -4.985209040E-008, 1.132633460E-012, 0.000000000E+000,
      6.001740740E+004, 1.957078870E+001] )
  )
)
```

```
species(name = "N2",
  atoms = " N:2 ",
  thermo = (
    NASA( [ 200.00, 5000.00], [ 3.367776150E+000, 6.124317000E-004,
      -7.890382710E-008, 5.618762820E-012, -8.265727480E-016,
      -1.030630570E+003, 3.677876810E+000] ),
    NASA( [ 5000.00, 10000.00], [ 8.748225300E+000, -1.609736510E-003,
      1.849739840E-007, -5.446528000E-012, 0.000000000E+000,
      -9.938338770E+003, -3.400417780E+001] )
  )
)
```

```
species(name = "NO",
  atoms = " N:1 O:1 ",
  thermo = (
    NASA( [ 200.00, 5000.00], [ 3.52970451E+000, 5.63745766E-004,
      -7.28596656E-008, -4.51046388E-012, 1.10056467E-015,
      9.90058181E+003, 5.07142356E+000] ),
    NASA( [ 5000.00, 10000.00], [ 6.11917281E+000, -7.30414827E-004,
      1.06554271E-007, -3.83975042E-012, 0.000000000E+000,
      6.23772099E+003, -1.26114326E+001] )
  )
)
```

```

)

species(name = "C",
  atoms = " C:1 ",
  thermo = (
    NASA( [ 200.00, 5000.00], [ 2.492008160E+000, -3.176429740E-006,
      1.230402030E-008, 1.653762660E-012, -3.848031920E-016,
      8.545333520E+004, 4.816987870E+000] ),
    NASA( [ 5000.00, 10000.00], [ 1.897753210E+000, 3.364812680E-004,
      -4.262838170E-008, 1.883958820E-012, 0.000000000E+000,
      8.619126870E+004, 8.797021620E+000] )
  )
)

species(name = "O",
  atoms = " O:1 ",
  thermo = (
    NASA( [ 200.00, 5000.00], [ 2.606288620E+000, -8.921956950E-005,
      1.919984270E-008, 8.465095090E-013, -2.006709720E-016,
      2.919541490E+004, 4.547141860E+000] ),
    NASA( [ 5000.00, 10000.00], [ 2.080292310E+000, 1.544325120E-004,
      -1.012466240E-008, 1.699429180E-013, 0.000000000E+000,
      2.998189400E+004, 8.172285430E+000] )
  )
)

species(name = "CO2",
  atoms = " C:1 O:2 ",
  thermo = (
    NASA( [ 200.00, 5000.00], [ 4.781580110E+000, 1.630974560E-003,
      -2.232868160E-007, -1.652436650E-011, 3.971671770E-015,
      -4.882410360E+004, -2.006776990E+000] ),
    NASA( [ 5000.00, 10000.00], [ 1.158910560E+001, -1.975370230E-003,
      3.030562420E-007, -1.214103190E-011, 0.000000000E+000,
      -5.791598320E+004, -4.809741630E+001] )
  )
)

species(name = "CO",
  atoms = " C:1 O:1 ",
  thermo = (
    NASA( [ 200.00, 5000.00], [ 3.405140110E+000, 6.133646300E-004,
      -8.026241880E-008, -6.763063860E-012, 1.525103350E-015,
      -1.433539910E+004, 4.192231220E+000] ),
    NASA( [ 5000.00, 10000.00], [ 2.641034490E+000, 9.484758230E-004,
      -1.607418360E-007, 9.666733490E-012, 0.000000000E+000,
      -1.296441810E+004, 9.584425660E+000] )
  )
)

species(name = "O2",
  atoms = " O:2 ",
  thermo = (
    NASA( [ 200.00, 5000.00], [ 3.523048030E+000, 6.331510000E-004,
      -6.365018570E-008, -4.741986880E-012, 1.052000240E-015,
      -1.077941160E+003, 4.414943860E+000] ),
    NASA( [ 5000.00, 10000.00], [ 3.243591070E+000, 6.070521740E-004,
      -4.597721320E-008, 2.632995420E-013, -5.421010860E-020,

```

```

-2.153368840E+002, 6.660544630E+000] )
)

#-----
# Reaction data
#-----

# Reaction 1
reaction( "CO2 + CO2 <=> CO + O + CO2", [6.90000E+018, -1.5, 63275])

# Reaction 1
reaction( "CO2 + CO <=> CO + O + CO", [6.90000E+018, -1.5, 63275])

# Reaction 1
reaction( "CO2 + N2 <=> CO + O + N2", [6.90000E+018, -1.5, 63275])

# Reaction 1
reaction( "CO2 + O2 <=> CO + O + O2", [6.90000E+018, -1.5, 63275])

# Reaction 1
reaction( "CO2 + NO <=> CO + O + NO", [6.90000E+018, -1.5, 63275])

# Reaction 1
reaction( "CO2 + C <=> CO + O + C", [1.40000E+019, -1.5, 63275])

# Reaction 1
reaction( "CO2 + N <=> CO + O + N", [1.40000E+019, -1.5, 63275])

# Reaction 1
reaction( "CO2 + O <=> CO + O + O", [1.40000E+019, -1.5, 63275])

# Reaction 2
reaction( "CO + CO2 <=> C + O + CO2", [2.30000E+017, -1.0, 129000])

# Reaction 2
reaction( "CO + CO <=> C + O + CO", [2.30000E+017, -1.0, 129000])

# Reaction 2
reaction( "CO + N2 <=> C + O + N2", [2.30000E+017, -1.0, 129000])

# Reaction 2
reaction( "CO + O2 <=> C + O + O2", [2.30000E+017, -1.0, 129000])

# Reaction 2
reaction( "CO + NO <=> C + O + NO", [2.30000E+017, -1.0, 129000])

# Reaction 2
reaction( "CO + C <=> C + O + C", [3.40000E+017, -1.0, 129000])

# Reaction 2
reaction( "CO + N <=> C + O + N", [3.40000E+017, -1.0, 129000])

# Reaction 2
reaction( "CO + O <=> C + O + O", [3.40000E+017, -1.0, 129000])

```

```

# Reaction 3
reaction( "N2 + CO2 <=> N + N + CO2",    [7.00000E+018, -1.6, 113200])

# Reaction 3
reaction( "N2 + CO <=> N + N + CO",      [7.00000E+018, -1.6, 113200])

# Reaction 3
reaction( "N2 + N2 <=> N + N + N2",      [7.00000E+018, -1.6, 113200])

# Reaction 3
reaction( "N2 + O2 <=> N + N + O2",      [7.00000E+018, -1.6, 113200])

# Reaction 3
reaction( "N2 + NO <=> N + N + NO",      [7.00000E+018, -1.6, 113200])

# Reaction 3
reaction( "N2 + C <=> N + N + C",        [3.00000E+019, -1.6, 113200])

# Reaction 3
reaction( "N2 + N <=> N + N + N",        [3.00000E+019, -1.6, 113200])

# Reaction 3
reaction( "N2 + O <=> N + N + O",        [3.00000E+019, -1.6, 113200])

# Reaction 4
reaction( "O2 + CO2 <=> O + O + CO2",    [2.00000E+018, -1.5, 59750])

# Reaction 4
reaction( "O2 + CO <=> O + O + CO",      [2.00000E+018, -1.5, 59750])

# Reaction 4
reaction( "O2 + N2 <=> O + O + N2",      [2.00000E+018, -1.5, 59750])

# Reaction 4
reaction( "O2 + O2 <=> O + O + O2",      [2.00000E+018, -1.5, 59750])

# Reaction 4
reaction( "O2 + NO <=> O + O + NO",      [2.00000E+018, -1.5, 59750])

# Reaction 4
reaction( "O2 + C <=> O + O + C",        [1.00000E+019, -1.5, 59750])

# Reaction 4
reaction( "O2 + N <=> O + O + N",        [1.00000E+019, -1.5, 59750])

# Reaction 4
reaction( "O2 + O <=> O + O + O",        [1.00000E+019, -1.5, 59750])

# Reaction 5
reaction( "NO + CO2 <=> N + O + CO2",    [1.10000E+014, 0.0, 75500])

# Reaction 5
reaction( "NO + CO <=> N + O + CO",      [5.00000E+012, 0.0, 75500])

# Reaction 5
reaction( "NO + N2 <=> N + O + N2",      [5.00000E+012, 0.0, 75500])

# Reaction 5

```

```

reaction( "NO + O2 <=> N + O + O2",    [5.00000E+012, 0.0, 75500])

# Reaction 5
reaction( "NO + NO <=> N + O + NO",    [1.10000E+014, 0.0, 75500])

# Reaction 5
reaction( "NO + C <=> N + O + C",      [1.10000E+014, 0.0, 75500])

# Reaction 5
reaction( "NO + N <=> N + O + N",      [1.10000E+014, 0.0, 75500])

# Reaction 5
reaction( "NO + O <=> N + O + O",      [1.10000E+014, 0.0, 75500])

# Reaction 6
reaction( "NO + O <=> O2 + N",          [8.40000E+009, 0.0, 19450])

# Reaction 7
reaction( "N2 + O <=> NO + N",          [6.40000E+014, -1.0, 38370])

# Reaction 8
reaction( "CO + O <=> O2 + C",          [3.90000E+010, -0.18, 69200])

# Reaction 9
reaction( "CO2 + O <=> O2 + CO",        [2.10000E+010, 0.0, 27800])

# Reaction 10
reaction( "CO + N <=> NO + C",          [2.86000E+008, 0.5, 53630])

# Reaction 11
reaction( "CO + CO <=> CO2 + C",        [2.33000E+006, 0.5, 65710])

# Reaction 12
reaction( "NO + CO <=> CO2 + N",        [4.59000E+005, 0.5, 12070])

```

### B.1.3 Viscosity Input File

visc\_inputs2440.m

```

% Computation of free stream viscosity in T5 shock tunnel

% Free Stream temperature (K)
% Tinf = 1276.2
Tinf = 1867.5
% Constants for Viscosity Curve Fits (T>=1000 K) taken from
% Nasa Reference 1232 (The constants for viscosity of argon are missing)
% The viscosity of argon is taken from M. N. Macrossan and C. R. Lilley,
% Physics of Fluids v 15 (11), Nov 2003
% Original 8 elements: e+, N2, O2, Ar, N, O, NO,NO+
% Additional elements: CO2, CO, C2, C3, CN, C, C+ added by I Leyva Jan '08
% Ref: Olynick., D. et al., J of Spacecraft and Rockets,
% Vol. 36, No. 3, May-June 1999

chem.spec.MUFA(1)= 0;
chem.spec.MUFA(2)= 0.0203;
chem.spec.MUFA(3)= 0.0484;
chem.spec.MUFA(4)= 0;
chem.spec.MUFA(5)= 0.0120;

```

```
chem.spec.MUFA(6)= 0.0205;
chem.spec.MUFA(7)= 0.0452;
chem.spec.MUFA(8)= 0;
chem.spec.MUFA(9)= -.019527387;
chem.spec.MUFA(10)= -.019527394;
chem.spec.MUFA(11)= -8.4311e-3;
chem.spec.MUFA(12)= -8.4312e-3;
chem.spec.MUFA(13)= -8.3811e-3;
chem.spec.MUFA(14)= -8.3285e-3;
chem.spec.MUFA(15)= -8.3285e-3;
```

```
chem.spec.MUFB(1)= 2.5;
chem.spec.MUFB(2)= 0.4329;
chem.spec.MUFB(3)= -0.1455;
chem.spec.MUFB(4)= 0;
chem.spec.MUFB(5)= 0.5930;
chem.spec.MUFB(6)= 0.4257;
chem.spec.MUFB(7)= -0.0609;
chem.spec.MUFB(8)= 2.5;
chem.spec.MUFB(9)= 1.047818;
chem.spec.MUFB(10)= 1.013295;
chem.spec.MUFB(11)= 0.7876060;
chem.spec.MUFB(12)= 0.7876090;
chem.spec.MUFB(13)= 0.7860330;
chem.spec.MUFB(14)= 0.7703240;
chem.spec.MUFB(15)= 0.7703240;
% additional elements: CO2, CO, C2, C3, CN, C, C+
```

```
chem.spec.MUFC(1)= -37.4475;
chem.spec.MUFC(2)= -11.8153;
chem.spec.MUFC(3)= -8.9231;
chem.spec.MUFC(4)= 0;
chem.spec.MUFC(5)= -12.3805;
chem.spec.MUFC(6)= -11.5803;
chem.spec.MUFC(7)= -9.4596;
chem.spec.MUFC(8)= -32.0453;
chem.spec.MUFC(9)= -14.32212;
chem.spec.MUFC(10)= -13.97873;
chem.spec.MUFC(11)= -13.02680;
chem.spec.MUFC(12)= -12.8240;
chem.spec.MUFC(13)= -12.9406;
chem.spec.MUFC(14)= -12.7378;
chem.spec.MUFC(15)= -12.7378;
```

```
%Number of atoms of j~th element per molecure of the ith species
chem.ALPIJ = [0 0 0 1 0; 2 0 0 0 0; 0 2 0 0 0; 0 0 1 0 0; 1 0 0 0 0; ...
  0 1 0 0 0; 1 1 0 0 0; 1 1 0 -1 0; 0 2 0 0 1; 0 1 0 0 1; ...
  0 0 0 0 2; 0 0 0 0 3; 1 0 0 0 1; 0 0 0 0 1; 0 0 0 -1 1];
```

```
% Element molecular weight
chem.elem.CMW(1) = 14.008;      %N
chem.elem.CMW(2) = 16;         %O
chem.elem.CMW(3) = 39.944;     %Ar
chem.elem.CMW(4) = 0.00054847; %e-
chem.elem.CMW(5) = 12.00;      %C
```

```

% Computation of the molecular weight of species
chem.spec.CGI = chem.ALPIJ*chem.elem.CMW';

% Species concentration (mole fractions) from NENZF

chem.spec.CAPX(1) = 1.e-10;    %e-
chem.spec.CAPX(2) = 0.753972; %N2
chem.spec.CAPX(3) = 0.173973; %O2
chem.spec.CAPX(4) = 1.e-10;    %AR
chem.spec.CAPX(5) = 1.e-10;    %N
chem.spec.CAPX(6) = 1.e-10;    %O
chem.spec.CAPX(7) = 0.072055;  %NO
chem.spec.CAPX(8) = 1.e-10;    %NO+
chem.spec.CAPX(9) = 1.e-10;    %CO2
chem.spec.CAPX(10) = 1.e-10;   %CO
chem.spec.CAPX(11) = 1.e-8;    %C2
chem.spec.CAPX(12) = 1.e-8;    %C3
chem.spec.CAPX(13) = 1.e-8;    %CN
chem.spec.CAPX(14) = 1.e-8;    %C
chem.spec.CAPX(15) = 1.e-8;    %C+

% mixture molecular weight
chem.CMA = chem.spec.CAPX*chem.spec.CGI;

chem.spec.CMU = viscspecCO2(chem,Tinf)
chem.MU = viscmixCO2(chem.spec.CAPX',chem.spec.CGI,chem.spec.CMU')

```



## Appendix C

# Reaction Mechanisms

A number of different mechanisms were considered for the analysis in this work. A summary of the reactions and relevant Arrhenius parameters for each mechanism considered follows in this appendix.

### C.1 Micheltree 94

#### C.1.1 Mixed Gases

Table C.1:  $CO_2$ - $N_2$  Mechanism: 8 species, 12 reactions

Third Body	Reactants		Products	Rxn No.
see #1a	$CO_2 + M$	$\rightleftharpoons$	$CO + O + M$	#1
see #1b	$CO_2 + M$	$\rightleftharpoons$	$CO + O + M$	#1
see #2a	$CO + M$	$\rightleftharpoons$	$C + O + M$	#2
see #2b	$CO + M$	$\rightleftharpoons$	$C + O + M$	#2
see #3a	$N_2 + M$	$\rightleftharpoons$	$N + N + M$	#3
see #3b	$N_2 + M$	$\rightleftharpoons$	$N + N + M$	#3
see #4a	$O_2 + M$	$\rightleftharpoons$	$O + O + M$	#4
see #4b	$O_2 + M$	$\rightleftharpoons$	$O + O + M$	#4
see #5a	$NO + M$	$\rightleftharpoons$	$N + O + M$	#5
see #5b	$NO + M$	$\rightleftharpoons$	$N + O + M$	#5
none	$NO + O$	$\rightleftharpoons$	$O_2 + N$	#6
none	$N_2 + O$	$\rightleftharpoons$	$NO + N$	#7
none	$CO + O$	$\rightleftharpoons$	$O_2 + C$	#8
none	$CO_2 + O$	$\rightleftharpoons$	$O_2 + CO$	#9
none	$CO + N$	$\rightleftharpoons$	$NO + C$	#10
none	$CO + CO$	$\rightleftharpoons$	$CO_2 + C$	#11
none	$NO + CO$	$\rightleftharpoons$	$CO_2 + N$	#12

Table C.2: Arrhenius parameters for each reaction.

Third Body	$C_f$ [ $m^3/(mole \times s)$ ]	$\eta_f$	$\Theta_f$ [ $K$ ]	Rxn No.
$CO_2, CO, N_2, NO, O_2$	$6.900 \times 10^{18}$	-1.50	$6.3275 \times 10^4$	#1a
$C, O, N$	$1.400 \times 10^{19}$	-1.50	$6.3275 \times 10^4$	#1b
$CO_2, CO, N_2, NO, O_2$	$2.300 \times 10^{17}$	-1.0	$1.2900 \times 10^5$	#2a
$C, O, N$	$3.400 \times 10^{17}$	-1.0	$1.2900 \times 10^5$	#2b
$CO_2, CO, N_2, NO, O_2$	$7.000 \times 10^{18}$	-1.6	$1.1320 \times 10^5$	#3a
$C, O, N$	$3.000 \times 10^{19}$	-1.6	$1.1320 \times 10^5$	#3b
$CO_2, CO, N_2, NO, O_2$	$2.000 \times 10^{18}$	-1.5	$5.9750 \times 10^4$	#4a
$C, O, N$	$1.000 \times 10^{19}$	-1.5	$5.9750 \times 10^4$	#4b
$CO_2, CO, N_2, NO, O_2$	$1.100 \times 10^{14}$	0.0	$7.5500 \times 10^4$	#5a
$C, O, N$	$5.000 \times 10^{12}$	0.0	$7.5500 \times 10^4$	#5b
	$8.400 \times 10^9$	0.0	$1.9450 \times 10^4$	#6
	$6.400 \times 10^{14}$	-1.0	$3.8370 \times 10^4$	#7
	$3.900 \times 10^{10}$	-0.18	$6.9200 \times 10^4$	#8
	$2.100 \times 10^{10}$	0.0	$2.7800 \times 10^4$	#9
	$2.860 \times 10^8$	0.5	$5.3630 \times 10^4$	#10
	$2.330 \times 10^6$	0.5	$6.5710 \times 10^4$	#11
	$4.590 \times 10^5$	0.5	$1.2070 \times 10^4$	#12

### C.1.2 Carbon Dioxide

The simplified Mitcheltree mechanism for  $CO_2$  uses 5 species and 6 reactions. They are the same reactions as for the Mixed Gases mechanism (8 species, 12 reactions) without any species containing nitrogen.

## C.2 Various Sources - Carbon Dioxide

Table C.3:  $CO_2$  Mechanism: 5 species, 6 reactions

Third Body	Reactants	Products	Rxn No.
all	$CO_2 + M \rightleftharpoons$	$CO + O + M$	#1
see #2a	$CO + M \rightleftharpoons$	$C + O + M$	#2
$CO$	$CO + M \rightleftharpoons$	$C + O + M$	#2
see #2b	$CO + M \rightleftharpoons$	$C + O + M$	#2
see #3a	$O_2 + M \rightleftharpoons$	$O + O + M$	#3
see #3b	$O_2 + M \rightleftharpoons$	$O + O + M$	#3
see #3c	$O_2 + M \rightleftharpoons$	$O + O + M$	#3
none	$CO + CO \rightleftharpoons$	$CO_2 + C$	#4
none	$CO + O \rightleftharpoons$	$O_2 + C$	#5
none	$O_2 + CO \rightleftharpoons$	$CO_2 + O$	#6

Table C.4: Arrhenius parameters for each reaction from fort.8.new.

Third Body	$C_f$ [ $m^3/(mole \times s)$ ]	$\eta_f$	$\Theta_f$ [K]	Rxn No.
$C, O, CO_2, CO, O_2$	$6.900 \times 10^{18}$	-1.50	$6.3275 \times 10^4$	#1
$CO_2, O_2$	$2.300 \times 10^{17}$	-1.0	$1.2900 \times 10^5$	#2a
$CO$	$3.400 \times 10^{17}$	-1.0	$1.2900 \times 10^5$	#2b
$C, O$	$3.400 \times 10^{17}$	-1.0	$1.2900 \times 10^5$	#2c
$CO_2, CO, N_2, NO, O_2$	$7.000 \times 10^{18}$	-1.6	$1.1320 \times 10^5$	#3a
$C, O, N$	$3.000 \times 10^{19}$	-1.6	$1.1320 \times 10^5$	#3b
$CO_2, CO, N_2, NO, O_2$	$2.000 \times 10^{18}$	-1.5	$5.9750 \times 10^4$	#4a
$C, O, N$	$1.000 \times 10^{19}$	-1.5	$5.9750 \times 10^4$	#4b
$CO_2, CO, N_2, NO, O_2$	$1.100 \times 10^{14}$	0.0	$7.5500 \times 10^4$	#5a
$C, O, N$	$5.000 \times 10^{12}$	0.0	$7.5500 \times 10^4$	#5b
	$8.400 \times 10^9$	0.0	$1.9450 \times 10^4$	#6
	$6.400 \times 10^{14}$	-1.0	$3.8370 \times 10^4$	#7
	$3.900 \times 10^{10}$	-0.18	$6.9200 \times 10^4$	#8
	$2.100 \times 10^{10}$	0.0	$2.7800 \times 10^4$	#9
	$2.860 \times 10^8$	0.5	$5.3630 \times 10^4$	#10
	$2.330 \times 10^6$	0.5	$6.5710 \times 10^4$	#11
	$4.590 \times 10^5$	0.5	$1.2070 \times 10^4$	#12



## Appendix D

# Thermofit data

This appendix contains the thermofit data for each species, together with the Arrhenius parameters for each reaction, used by NENZF to calculate the nozzle flow.

Table D.1: NENZF thermofit data

Species	$a_j$	$b_j$	$c_j$	$d_j$	$e_j$	$k_j$
$E^-$	2.500000	0.000000	0.000000	0.000000	0.000000	-11.73500
$AR$	2.563282	-3.591770 $\times 10^{-5}$	7.469208 $\times 10^{-9}$	-6.747034 $\times 10^{-13}$	2.234019 $\times 10^{-17}$	4.000939
$N_2$	3.451483	3.088332 $\times 10^{-4}$	-4.251428 $\times 10^{-8}$	2.739295 $\times 10^{-12}$	-5.46832 $\times 10^{-17}$	3.071269
$O_2$	3.249473	4.963449 $\times 10^{-4}$	-6.701753 $\times 10^{-8}$	4.443339 $\times 10^{-12}$	-1.000281 $\times 10^{-16}$	5.915022
$N$	3.008922	-3.134625 $\times 10^{-4}$	6.311813 $\times 10^{-8}$	-4.165203 $\times 10^{-12}$	9.334886 $\times 10^{-17}$	1.303476
$O$	2.594143	-5.008914 $\times 10^{-5}$	1.199502 $\times 10^{-8}$	-8.681611 $\times 10^{-13}$	2.148100 $\times 10^{-17}$	4.600615
$NO$	3.756216	2.083961 $\times 10^{-4}$	-2.639548 $\times 10^{-8}$	1.690332 $\times 10^{-12}$	-3.611523 $\times 10^{-17}$	3.611167
$NO^+$	3.397385	3.749384 $\times 10^{-4}$	-6.062030 $\times 10^{-8}$	4.637506 $\times 10^{-12}$	-1.107704 $\times 10^{-16}$	4.200563
$CO_2$	3.025146	2.908230 $\times 10^{-3}$	-9.546056 $\times 10^{-7}$	1.519425 $\times 10^{-10}$	-9.152401 $\times 10^{-15}$	6.890064
$CO$	3.356079	3.247261 $\times 10^{-4}$	-1.396984 $\times 10^{-9}$	-1.091394 $\times 10^{-11}$	1.151856 $\times 10^{-15}$	4.401805
$C$	2.658752	-1.747608 $\times 10^{-4}$	7.555354 $\times 10^{-8}$	-1.224976 $\times 10^{-11}$	7.372575 $\times 10^{-16}$	3.928945

## Appendix E

# Checklists

This appendix contains dummy T5 checklists for both the high enthalpy (normal operating mode) and low enthalpy shots. All facility data recorded on the checklists from this project are also included.

### E.1 High Enthalpy Shots

T5 Checklist, Version 21, October 28, 2008

Signature: \_\_\_\_\_

Operators: \_\_\_\_\_ Date: \_\_\_\_\_ Time: \_\_\_\_\_ Shot#: \_\_\_\_\_

Researcher: \_\_\_\_\_ Name of Test: \_\_\_\_\_

Action	Check	Signal
--------	-------	--------

Piston Mass: \_\_\_\_\_ kg

Diaphragm Thickness: \_\_\_\_\_

Expected burst pressure: \_\_\_\_\_ MPa Value: \_\_\_\_\_ MPa

Position Tunnel correctly	LVDT1: setting: _____ value: _____	<input type="radio"/>
	LVDT2: setting: _____ value: _____	<input type="radio"/> A
Turn off blower		<input type="radio"/>
Open SV-24 (DT pressure gage)		<input type="radio"/>
SV-23 (DT vacuum gage)		<input type="radio"/>
HS-20 (DT vacuum pump isolation valve)		<input type="radio"/>
Close HS-19 (DT vacuum pump vent)		<input type="radio"/>
HS-21 (DT vent)		<input type="radio"/>
Turn on cooling water for DT pump		<input type="radio"/>
Turn on PO/3 (DT vacuum pump)		<input type="radio"/>

Open V-17 (ST vacuum valve)		<input type="radio"/>
Close V-18 (ST vacuum pump vent valve)		<input type="radio"/>
Turn on PO/2 (ST vacuum pump)		<input type="radio"/>
Open SV-25A (ST pressure gage)		<input type="radio"/>
SV-25B (ST pressure gage)		<input type="radio"/>
SV-26 (ST vacuum gage)		<input type="radio"/>
V-14 (ST Pressure Isolation valve)		<input type="radio"/>
<hr/>		
Close 2R pressure isolation valve (near P1)		<input type="radio"/>
Open V-11 (High pressure CT isolation)		<input type="radio"/>
V-8 (CT vacuum)		<input type="radio"/>
V-7 (CT/2R vacuum valve)		<input type="radio"/>
V-12 (CT/2R/PS vacuum valve)		<input type="radio"/>
Close ZS-4 manual and remote (emergency 2R vent)		<input type="radio"/>
ZS-13 (CT vacuum pump vent valve)		<input type="radio"/>
Turn on PO/1 (2R, Piston Space and CT vacuum pump)		<input type="radio"/>
Open SV-29 (CT vacuum gage)		<input type="radio"/>
SV-27 (2R vacuum gage)		<input type="radio"/>
SV-31 (PS vacuum gage)		<input type="radio"/> D
Open CT gauge(s)		<input type="radio"/>
Open Flex hose isolation valve		<input type="radio"/>
<hr/>		
Wait 30 - 60 minutes for vacuum		<input type="radio"/>
<hr/>		
Check vacuum levels	DT: _____ mmHg	<input type="radio"/>
	ST: _____ mmHg	<input type="radio"/>
	CT: _____ mmHg	<input type="radio"/>
	2R: _____ mmHg	<input type="radio"/>
	PS: _____ mmHg	<input type="radio"/>
<hr/>		
Disconnect nozzle support trolley		<input type="radio"/>
Isolate ST vacuum valve (V-17)		<input type="radio"/>
Turn off ST vacuum pump (PO/2)		<input type="radio"/>
Open ST vacuum pump vent valve (V18)		<input type="radio"/>
Isolate ST vacuum gauge (SV-26)		<input type="radio"/>
<hr/>		

Fill ST	gas: _____	setting: _____ kPa abs	<input type="radio"/>
	(multiply setting by 20)	thumbwheel: _____	<input type="radio"/>
		value: _____	<input type="radio"/>
Press hand switch HS-C3 to confirm ST pressure			<input type="radio"/>
<u>Close V-14 (ST isolation)</u>			<input type="radio"/>
Isolate DT pressure gauge, HS-24			<input type="radio"/>
Close ZS-20 (DT vacuum isolation)			<input type="radio"/>
Turn off HS-3 (dump tank vacuum pump)			<input type="radio"/>
Open vent HS-19 (DT vacuum pump vent)			<input type="radio"/>
Close V-8 (CT isolation)			<input type="radio"/> E
Close (ST gages):                SV-25A     &     SV-25B			<input type="radio"/> F
<u>Close SV-29 (CT vacuum gage)</u>			<input type="radio"/> G
Fill CT	gas: _____	vacuum: _____ kPa gage	
		setting: _____ kPa abs	
		thumbwheel: _____ kPa gage	
		value: _____ kPa gage	<input type="radio"/>
Absolute pressure desired: _____			
	gas: _____		
		setting: _____ kPa abs	
		thumbwheel: _____ kPa gage	
		value: _____ kPa gage	<input type="radio"/>
<u>Close V-11 (CT high pressure isolation valve)</u>			<input type="radio"/> H
Close V-7 (CT/2R vacuum)			<input type="radio"/>
<u>Close SV-23 (DT vacuum gage)</u>			<input type="radio"/> I,J
WARNING LIGHTS ON (P1).		Verify door is closed	<input type="radio"/>
Close SV-27 (2R vacuum gage)			<input type="radio"/>
2R Temperature before _____ °C			<input type="radio"/>
Fill 2R:		setting: _____ PSI gage	
		thumbwheel: _____ PSI gage	
		value: _____ PSI gage	<input type="radio"/>
Check for changes in tunnel position CT: _____ CT-2R: _____			<input type="radio"/>

Toggle Dry Run Relay box to “Experiment”	<input type="radio"/>
Arm “T5 das”	<input type="radio"/>
Isolate flex hose	<input type="radio"/>
Confirm 2R pressure, Hand switch HS-C1	<input type="radio"/>
Isolate 2R gage	<input type="radio"/>
Confirm isolation, Hand switch HS-28	<input type="radio"/> K,L
Close SV-31 (PS vacuum gage)	<input type="radio"/> M
Confirm CT pressure, Hand switch HS-C2                      value: _____ kPa gage	<input type="radio"/> N
Isolate CT gage	<input type="radio"/>
Confirm isolation, Hand Switch HS-30	<input type="radio"/> O
2R Temperature after _____ °C	<input type="radio"/>
Close V-12 (2R vacuum)	<input type="radio"/> P
Open V-13 to vent CT vacuum pump	<input type="radio"/>
Turn off CT vacuum pump (PO/1)	<input type="radio"/>
READY TO FIRE    Time: _____	<input type="radio"/>
Press and hold down firing buttons	<input type="radio"/>

## E.2 Low Enthalpy Shots

T5 Checklist - Low  $h_0$ , Vers.21b, October 28, 2008

Signature: \_\_\_\_\_

Operators: \_\_\_\_\_ Date: \_\_\_\_\_ Time: \_\_\_\_\_ Shot#: \_\_\_\_\_

Researcher: \_\_\_\_\_ Name of Test: \_\_\_\_\_

Action	Check	Signal
Piston Mass: _____ kg		

Diaphragm Thickness: \_\_\_\_\_

Expected burst pressure: \_\_\_\_\_ MPa Value: \_\_\_\_\_ MPa

Position Tunnel correctly	LVDT1: setting: _____ value: _____	<input type="radio"/>
	LVDT2: setting: _____ value: _____	<input type="radio"/> A
Turn off blower		<input type="radio"/>
Open SV-24 (DT pressure gage)		<input type="radio"/>
SV-23 (DT vacuum gage)		<input type="radio"/>
HS-20 (DT vacuum pump isolation valve)		<input type="radio"/>
Close HS-19 (DT vacuum pump vent)		<input type="radio"/>
HS-21 (DT vent)		<input type="radio"/>
Turn on cooling water for DT pump		<input type="radio"/>
Turn on PO/3 (DT vacuum pump)		<input type="radio"/>
Open V-17 (ST vacuum valve)		<input type="radio"/>
Close V-18 (ST vacuum pump vent valve)		<input type="radio"/>
Turn on PO/2 (ST vacuum pump)		<input type="radio"/>
Open SV-25A (ST pressure gage)		<input type="radio"/>
SV-25B (ST pressure gage)		<input type="radio"/>
SV-26 (ST vacuum gage)		<input type="radio"/>
V-14 (ST Pressure Isolation valve)		<input type="radio"/>
Close 2R pressure isolation valve (near P1)		<input type="radio"/>
Open V-11 (High pressure CT isolation)		<input type="radio"/>
V-8 (CT vacuum)		<input type="radio"/>
V-7 (CT/2R vacuum valve)		<input type="radio"/>
V-12 (CT/2R/PS vacuum valve)		<input type="radio"/>

Close ZS-4 manual and remote (emergency 2R vent)		<input type="radio"/>
ZS-13 (CT vacuum pump vent valve)		<input type="radio"/>
Turn on PO/1 (2R, Piston Space and CT vacuum pump)		<input type="radio"/>
Open SV-29 (CT vacuum gage)		<input type="radio"/>
SV-27 (2R vacuum gage)		<input type="radio"/>
SV-31 (PS vacuum gage)		<input type="radio"/> D
Open CT gauge(s)		<input type="radio"/>
Open Flex hose isolation valve		<input type="radio"/>
<hr/>		
Wait 30 - 60 minutes for vacuum		<input type="radio"/>
<hr/>		
Check vacuum levels	DT: _____ mmHg	<input type="radio"/>
	ST: _____ mmHg	<input type="radio"/>
	CT: _____ mmHg	<input type="radio"/>
	2R: _____ mmHg	<input type="radio"/>
	PS: _____ mmHg	<input type="radio"/>
<hr/>		
Disconnect nozzle support trolley		<input type="radio"/>
Isolate ST vacuum valve (V-17)		<input type="radio"/>
Turn off ST vacuum pump (PO/2)		<input type="radio"/>
Open ST vacuum pump vent valve (V18)		<input type="radio"/>
Isolate ST vacuum gauge (SV-26)		<input type="radio"/>
Close V-8 (CT isolation)		<input type="radio"/>
Close SV-29 (CT vacuum gage)		<input type="radio"/>
<hr/>		
Fill ST & CT	gas: _____ setting: _____ kPa abs	<input type="radio"/>
(multiply setting by 20)	thumbwheel: _____	<input type="radio"/>
	value: _____	<input type="radio"/>
Press hand switch HS-C3 to confirm ST pressure		<input type="radio"/>
Close V-14 (ST isolation)		<input type="radio"/>
<hr/>		
Isolate DT pressure gauge, HS-24		<input type="radio"/>
Close ZS-20 (DT vacuum isolation)		<input type="radio"/>
Turn off HS-3 (dump tank vacuum pump)		<input type="radio"/>
Open vent HS-19 (DT vacuum pump vent)		<input type="radio"/>
Close (ST gages):	SV-25A & SV-25B	<input type="radio"/> E,F,G

<u>Close V-11 (CT high pressure isolation valve)</u>	<input type="radio"/> H
Close V-7 (CT/2R vacuum)	<input type="radio"/>
<u>Close SV-23 (DT vacuum gage)</u>	<input type="radio"/> I,J
WARNING LIGHTS ON (P1). Verify door is closed	<input type="radio"/>
Close SV-27 (2R vacuum gage)	<input type="radio"/>
2R Temperature before _____ °C	<input type="radio"/>
Close vent HS-19 (DT vacuum pump vent)	<input type="radio"/> →D
Turn on HS-3 (dump tank vacuum pump)	<input type="radio"/>
Open ZS-20 (DT vacuum isolation)	<input type="radio"/>
Fill 2R: setting: _____ PSI gage	
thumbwheel: _____ PSI gage	
value: _____ PSI gage	<input type="radio"/>
<u>Close ZS-20 (DT vacuum isolation)</u>	<input type="radio"/>
Turn off HS-3 (dump tank vacuum pump)	<input type="radio"/>
Open vent HS-19 (DT vacuum pump vent)	<input type="radio"/> →J
Check for changes in tunnel position CT: _____ CT-2R: _____	<input type="radio"/>
Toggle Dry Run Relay box to “Experiment”	<input type="radio"/>
Arm “T5 das”	<input type="radio"/>
<u>Arm oscilloscope</u>	<input type="radio"/>
Isolate flex hose	<input type="radio"/>
Confirm 2R pressure, Hand switch HS-C1	<input type="radio"/>
Isolate 2R gage	<input type="radio"/>
<u>Confirm isolation, Hand switch HS-28</u>	<input type="radio"/> K,L
<u>Close SV-31 (PS vacuum gage)</u>	<input type="radio"/> M
<u>Confirm CT pressure, Hand switch HS-C2</u> value: _____ kPa gage	<input type="radio"/> N
Isolate CT gage	<input type="radio"/>
Confirm isolation, Hand Switch HS-30	<input type="radio"/> O
<u>2R Temperature after _____ °C</u>	<input type="radio"/>
Close V-12 (2R vacuum)	<input type="radio"/> P
Open V-13 to vent CT vacuum pump	<input type="radio"/>
Turn off CT vacuum pump (PO/1)	<input type="radio"/>

READY TO FIRE

Time: \_\_\_\_\_



Press and hold down firing buttons



## E.3 Checklist data

### E.3.1 Series 1

Table E.1: Series 1 Checklist data

Shot#	Date [y/m/d]	ref Shot#	oper	diaphm [10 <sup>-3</sup> "]	$P_4$ [MPa]	LVDT <sub>1</sub>	LVDT <sub>2</sub>	DT	ST	CT	PS
2331	2006/02/28	1999	BA	242/185	95.4	+52	+505	0.2	0.25	0.2	0.2
2332	2006/03/02	1999	BA	249/197	107.7	+48	+503	0.15	0.22	0.07	0.06
2333	2006/03/06	1999	BA	250/197	104.5	+39	+504	0.15	0.15	0.07	0.055
2334	2006/03/07	1999	BA	249/197	102.6	+45	+498	0.2	0.2	0.08	0.06
2335	2006/03/09	1993	BA	251/178	77.5	+190	+705	0.2	0.18	0.075	0.065
2336	2006/05/17	1993	BA	251/179	78.0	+193	+719	0.2	0.3	0.5	0.55
2337	2006/05/18	1999	BA	251/199	110.2	+53	+487	0.2	0.7	0.07	0.06

Table E.2: Series 1 Checklist data (cont'd)

Shot#	$N_2$ [%]	$P_{part'l}$ [kPa <sub>a</sub> ]	$CO_2$ [%]	$P_{ST}$ [kPa <sub>a</sub> ]	He [%]	$P_{part'l}$ [kPa <sub>a</sub> ]	Ar [%]	$P_{part'l}$ [kPa <sub>a</sub> ]	$P_{CT}$ [kPa <sub>g</sub> ]	$T_1$ [K]	$P_{2R}$ [psi]	$T_2$ [K]
2331	100			85	85	98.5	15	17.5	+16.0	23.9	1100	25.4
2332	95	80.75	5	85	85	98.5	15	17.5	+16.0	24.8	1100	26.8
2333			100	54.09	85	98.5	15	17.5	+16.0	24.3	1100	26.1
2334	50	42.5	50	69.55	85	98.5	15	17.5	+16.0	24.1	1100	25.8
2335			100	100	82	76.0	18	17.0	-7.0	23.8	800	24.8
2336			100	100	82	76.0	18	17.0	-7.0	25.4	800	26.7
2337	95	80.75	5	83.45	85	98.5	15	17.5	+16.0	26.6	1100	28.7

### E.3.2 Series 2

Table E.3: Series 2 Checklist data

Shot#	Date [y/m/d]	ref Shot#	oper	diaphm [10 <sup>-3</sup> "]	$P_4$ [MPa]	LVDT <sub>1</sub>	LVDT <sub>2</sub>	DT	ST	CT	PS
2433	2007/10/10	2331	BA	247/197	63.6	+55	+498	0.2	0.25	0.2	0.08
2434	2007/10/11	2331	BA	247/197	72.7	+50	+499	0.15	0.3	0.3	0.2
2435	2007/10/12	2331	EA	246/204	88.9	+47	+516	0.18	0.2	0.18	0.07
2436	2007/10/16	2331	BEA	252/206	105.8	+53	+496	0.35	0.2	0.2	0.09
2437	2007/10/17	2331	BIA	252/207	106.2	+53	+504	0.25	0.23	0.18	0.07
2438	2007/10/25	2331	BA	248/204	107.3	+55	+303	0.2	0.23	0.17	0.05
2439	2007/11/14	2364	BEA	246/188	98.6	+56	+402	0.2	0.3	0.3	0.2

Table E.4: Series 2 Checklist data (cont'd)

Shot#	air [%]	$P_{part'l}$ [kPa <sub>a</sub> ]	$CO_2$ [%]	$P_{ST}$ [kPa <sub>a</sub> ]	He [%]	$P_{part'l}$ [kPa <sub>a</sub> ]	Ar [%]	$P_{part'l}$ [kPa <sub>a</sub> ]	$P_{CT}$ [kPa <sub>g</sub> ]	$T_1$ [K]	$P_{2R}$ [psi]	$T_2$ [K]
2433	100			85	85	98.5	15	17.5	+16	22.2	1100	24.1
2434	100			85	85	98.5	15	17.5	+16	22.6	1100	24.6
2435	100			85	85	98.5	15	17.5	+16	22.1	1100	24.1
2436	100			85	85	98.5	15	17.5	+16	21.0	1100	23.3
2437	100			60	85	98.5	15	17.5	+16	21.9	1100	23.8
2438	100			85	85	98.5	15	17.5	+16	24.1	1100	26.3
2439	100			98	82	80.4	18	17.6	-2.0	22.4	1150	24.7

### E.3.3 Series 3

Table E.5: Series 3 Checklist data

Shot#	Date [y/m/d]	ref Shot#	oper	diaphm [10 <sup>-3</sup> "]	$P_4$ [MPa]	LVDT <sub>1</sub>	LVDT <sub>2</sub>	DT	ST	CT	PS
2440	2007/11/19	2365	BA	246/185	104.0	-46	+398	0.5	0.2	0.2	0.09
2441	2007/11/20	2365	BA	246/189	94.0	-53	+391	0.3	0.2	0.2	0.08
2442	2007/11/21	2365	BA	245/188	93.6	-52	+406	0.3	0.28	0.18	0.06
2443	2007/11/21	2365	BA	246/189	92.5	-49	+404	0.3	0.25	0.18	0.06
2444	2007/11/30	2365	EA	245/188	90.2	-49	+411	0.3	0.2	0.09	0.07
2445	2007/12/03	2365	BA	246/185	103.8	-60	+404	0.2	0.25	0.6	0.7

Table E.6: Series 3 Checklist data (cont'd)

Shot#	air [%]	$P_{part'l}$ [kPa <sub>a</sub> ]	$CO_2$ [%]	$P_{ST}$ [kPa <sub>a</sub> ]	He [%]	$P_{part'l}$ [kPa <sub>a</sub> ]	Ar [%]	$P_{part'l}$ [kPa <sub>a</sub> ]	$P_{CT}$ [kPa <sub>g</sub> ]	$T_1$ [K]	$P_{2R}$ [psi]	$T_2$ [K]
2440	100			117	74	72.5	26	25.5	-2	21.0	1150	22.7
2441	80	93.6	20	108.94	74	72.5	26	25.5	-2	21.6	1150	23.4
2442	60	70.2	40	100.88	74	72.5	26	25.5	-2	22.2	1150	24.2
2443	30	35.1	70	88.78	74	72.5	26	25.5	-2	21.8	1150	24.1
2444			100	76.69	74	72.5	26	25.5	-2	21.9	1150	23.8
2445			100	76.69	74	72.5	26	25.5	-2	21.9	1150	24.1

### E.3.4 Series 4

Table E.7: Series 4 Checklist data

Shot#	Date [y/m/d]	ref Shot#	oper	diaphm [10 <sup>-3</sup> "]	$P_4$ [MPa]	LVDT <sub>1</sub>	LVDT <sub>2</sub>	DT	ST	CT	PS
2446	2008/01/11	2365	IA	245/187	94.2	-47	+391	0.3	0.25	0.2	0.07
2447	2008/01/16	2365	SA	223/191	90.0	-47	+399	0.2	0.15	0.15	0.06
2448	2008/01/17	2365	SA	225/196	92.1	-50	+395	0.2	0.2	0.2	0.06
2449	2008/01/18	2365	BISA	223/201	89.0	-61	+403	0.2	0.2	0.25	0.23

Table E.8: Series 4 Checklist data (cont'd)

Shot#	air [%]	$P_{part'l}$ [kPa <sub>a</sub> ]	CO <sub>2</sub> [%]	$P_{ST}$ [kPa <sub>a</sub> ]	He [%]	$P_{part'l}$ [kPa <sub>a</sub> ]	Ar [%]	$P_{part'l}$ [kPa <sub>a</sub> ]	$P_{CT}$ [kPa <sub>g</sub> ]	$T_1$ [K]	$P_{2R}$ [psi]	$T_2$ [K]
2446	100			117	74	72.5	26	25.5	-2	22.8	1150	24.4
2447	100			117	74	72.5	26	25.5	-2	23.4	1150	25.3
2448	100			117	74	72.5	26	25.5	-2	23.2	1150	24.9
2449	100			117	74	72.5	26	25.5	-2	23.3	1150	24.8

### E.3.5 Series 5

Table E.9: Series 5 Checklist data

Shot#	Date [y/m/d]	ref Shot#	oper	diaphm [10 <sup>-3</sup> "]	LVDT <sub>1</sub> [MPa]	LVDT <sub>2</sub>	DT	ST	CT	PS
2452	2008/02/14	1198	BSA	none	+208	+990	0.15	0.75	0.35	0.15
2453	2008/02/20	1198	SA	none	+199	+983	0.13	0.3	0.3	0.08
2454	2008/02/22	1198	SA	none	+210	+998	0.3	0.3	0.18	0.06
2455	2008/02/26	1198	SA	none	+206	+990	0.2	0.3	0.2	0.1
2456	2008/02/27	1198	SA	none	+203	+1014	0.2	0.4	0.3	0.3

Table E.10: Series 5 Checklist data (cont'd)

Shot#	$N_2$ [%]	$P_{ST/CT}$ [kPa <sub>a</sub> ]	$T_1$ [K]	$P_{2R}$ [psi]	$T_2$ [K]	$P_{RT0}$ [psig]	$P_{RTF}$ [psig]
2452	100	122	22.7	170	23.0	360.9	294.3
2453	100	122	22.7	170	22.6	162.26	85.2
2454	100	122	22.5	170	22.5	50.24	26.28
2455	100	122	24.0	170	24.2	15.57	6.01
2456	100	122	24.3	170	24.6		



# References

- [1] ADAM, P. *Enthalpy Effects on Hypervelocity Boundary Layers*. PhD thesis, California Institute of Technology, 1997.
- [2] ANDERSON, J. *Hypersonic and High Temperature Gas Dynamics*. McGraw-Hill, 1989.
- [3] ANDERSON, J. *Hypersonic and high-temperature gas dynamics*, 2 ed. AIAA Education Series, 2006.
- [4] BUNKER, R. A review of shaped hole turbine film-cooling technology. *Journal of Heat Transfer* 127 (April 2005), 441–453.
- [5] DEMETRIADES, A. Laminar boundary layer stability measurements at Mach 7 including wall temperature effects. AFOSR Technical Report 77-1311, Air Force Office of Scientific Research (AFOSR), Washington, D.C., 1977.
- [6] DICRISTINA, V. Three-dimensional laminar boundary-layer transition on a sharp  $8^\circ$  cone at Mach 10. *AIAA Journal* 8, 5 (May 1970), 852–856.
- [7] DORRANCE, W. *Viscous hypersonic flow*. McGraw-Hill Series in Missile and Space Technology, 1962.
- [8] ECKERT, E. Engineering relations for friction and heat transfer to surfaces in high velocity flow. *Journal of the Aeronautical Sciences* 22 (August 1955), 585–587.
- [9] FUJII, K., AND HORNING, H. An experiment of high-enthalpy effect on attachment line transition. AIAA Paper 2001-2779, 2001. (31st AIAA Fluid Dynamics Conference and Exhibit, June 11-14, Anaheim, CA, USA).
- [10] FUJII, K., AND HORNING, H. Experimental investigation of high-enthalpy effects on attachment line boundary layer transition. *AIAA Journal* 41, 7 (July 2003), 1282–1291.

- [11] GERMAIN, P. *The Boundary Layer on a Sharp Cone in High-Enthalpy Flow*. PhD thesis, California Institute of Technology, 1994.
- [12] HEISER, W., AND PRATT, D. *Hypersonic Airbreathing Propulsion*. AIAA Education Series, 1994.
- [13] HORNUNG, H., ADAM, P., GERMAIN, P., FUJII, K., AND RASHEED, A. On transition and transition control in hypervelocity flows. In *Proceedings of the Ninth Asian Congress of Fluid Mechanics, May 27-31, 2002, Isfahan, Iran* (2002).
- [14] JOHNSON, H., SEIPP, T., AND CANDLER, G. Numerical study of hypersonic reacting boundary layer transition on cones. *Physics of Fluids* 10, 10 (October 1998), 2676–2685.
- [15] KANESHIGE, M., AND HORNUNG, H. Raytheon rtv tests in t5 (revised). Galcit report, California Institute of Technology, 1996.
- [16] MACK, L. Boundary-layer stability theory. In *Special Course on Stability and Transition of Laminar Flow*. 1984. AGARD Report No. 709.
- [17] MORKOVIN, M. Effects of compressibility on turbulent flows. In *Mécanique de la turbulence (A. Favre ed.), CNRS. Paris, France* (1962).
- [18] OLYNICK, D., CHEN, Y.-K., AND TAUBER, M. Aerothermodynamics of the Stardust sample return capsule. *Journal of Spacecraft and Rockets* 36, 3 (1999), 442–462.
- [19] RASHEED, A. *Passive Hypervelocity Boundary Layer Control Using an Ultrasonically Absorptive Surface*. PhD thesis, California Institute of Technology, 2001.
- [20] RESHOTKO, E. Remarks on engineering aspects of transition. In *Transition and Turbulence*. 1981, p. 147. AIAA Education Series.
- [21] SCHLICHTING, H. *Boundary Layer Theory*. McGraw-Hill, 1987.
- [22] SHAPIRO, A. *The dynamics and thermodynamics of compressible fluid flow*, vol. 1. Ronald Press, New York, 1953.
- [23] VAN DRIEST, E. Turbulent boundary layer on a cone in supersonic flow at zero angle of attack. *Journal of the Aeronautical Sciences* 19 (1952), 801–812.

- [24] VAN DRIEST, E. The problem of aerodynamics heating. *Journal of the Aeronautical Sciences* 23 (1956), 1007–1011.
- [25] WHITE, F. *Viscous fluid flow*, 2 ed. McGraw-Hill, New York, 1991.
- [26] WHITE, F., AND CRISTOPH, G. A simple theory for the two-dimensional compressible turbulent boundary layer. *Journal of Basic Engineering* 94 (1972), 636–642.
- [27] WILKE, C. A viscosity equation for gas mixtures. *Journal of Chemical Physics* 18 (April 1950), 517–522.